Estimates of bone elastic constants at sequential hierarchical levels

by

Young June Yoon

A dissertation submitted to the graduate faculty in Engineering in partial fulfillment of the requirements for the degree of Doctor of Philosophy,
The City University of New York.

2005

INFORMATION TO USERS

The quality of this reproduction is dependent upon the quality of the copy submitted. Broken or indistinct print, colored or poor quality illustrations and photographs, print bleed-through, substandard margins, and improper alignment can adversely affect reproduction.

In the unlikely event that the author did not send a complete manuscript and there are missing pages, these will be noted. Also, if unauthorized copyright material had to be removed, a note will indicate the deletion.

ProQuest Information and Learning Company
300 North Zeeb Road
P.O. Box 1346
Ann Arbor, MI 48106-1346

This manuscript has been read and accepted for the Graduate Faculty in Mechanical Engineering in satisfaction of the dissertation requirement for the degree of Doctor of Philosophy

SCCowin

Date

Stephen C. Cowin, PhD
Chair of Examining Committee

4/26/2015

Date

Mumtaz K. Kassir

Mumtaz K. Kassir, PhD
Executive Officer

Feridun Delale, PhD

Susannah P. Fritton, PhD

Ali Sadegh, PhD

Honghui Yu, PhD

Examining Committee

The City University of New York

Abstract

Estimates of bone elastic constants at sequential hierarchical levels

by

Young June Yoon

Advisor: Professor Stephen C. Cowin

Estimates are presented of the elastic constants at the level of a collagen fibril whose diameter is the order of 20 nm, of a collagen fiber whose diameter is the order 80 nm, and a single lamella, which is composed of multiple collagen fibers' layer; the thickness of one collagen fiber layer is the order of 130 nm.

The anisotropic poroelastic constants of an osteon are estimated: The drained elastic constants are the porous medium's elastic constants when the fluid in the osteonal pores easily escapes and the pore fluid can sustain no pore pressure. The drained elastic constants at the lacunar-canalicular porosity tissue level are estimated by using an effective moduli model in which the shape of lacunae is approximated as ellipsoidal cavities. The undrained elastic constants are the porous medium's elastic constants when the medium is fully saturated with pore fluid and the fluid cannot escape, are also estimated.

A method is illustrated for determining the effective transversely isotropic (or isotropic) elastic constants from measured orthotropic elastic constants. This method consists of constructing upper and lower bounds on the effective transversely isotropic (or isotropic) elastic constants using the known orthotropic values. Fortunately, the upper and lower bounds are very close. Thus very good approximations for the effective transversely isotropic (or isotropic) elastic constants for cortical and cancellous bone are obtained from previously published data on the orthotropic elastic constants for those tissue types.

This dissertation is undertaken to build a greater database for the anisotropic elastic constants of bone with the intention of employing them in an anisotropic bone poroelastic model.

To

My parents

In-Yoon and *Wee-Hak*,

My family

Min-ja and *Sung-Eun*,

and

Sung-Hee and *Byung-Chun*

Acknowledgements

Many thanks to committee members, Professors Cowin, Delale, Fritton, Sadegh, and Yu for their valuable time and effort on this dissertation.

Thank to people who were or have been in Tissue Mechanics Laboratory or Bone Journal Club - Drs. Tomi Beno, Lidan You, Liyun Wang, Liyuan Mi, Guoyu Yang, and Mia Mia Thi, and Mrs. Cesare Ciani, Mark Carthy, Steven Tommasini, Yilin Wang, and Yuefeng Han.

Thank to wonderful staffs in the Mechanical Engineering Department- Mr. Louis Hernandez and Robert Kallfa, and Ms. Linda Emedoh and Dahlia Libert.

Thank to Dr. Laurent Mars who was an administrative director in the Biomedical Engineering Department.

Thank to former and current graduate students in both the Mechanical and Biomedical Engineering Departments – Drs. Zhexuan Wang, Abraham Tsacho, Dejan Milentijevic, Xiang Long, and Elizabeth Lawrence, and Mrs. Stewart Russell, Eduardo Hernandez, Minwei Gong, Qianhong Wu, Huapei Wan, and Mohammed Zoghi, and Ms. Veronica Lopez, Xiaobing Zhang, and Annie Shou.

Special thank to Professor Lee in the Chemical Engineering Department, Professors Lee and Chon in the Electrical Engineering Department, and Professor Ro

in the Civil Engineering Department for their sincere care and advices.

Contents

Abstract iv

Acknowledgements vii

List of Tables xiv

List of Figures xviii

Chapter 1

Introduction 1

Chapter 2

The approximate methods of effective moduli **16**

2. 1 Representative Volume Element (RVE) 16

2. 2 The average stress and the average strain of the representative volume element (RVE) 16

2. 3. Boundary conditions at the interface 17

2. 4 The approximation the effective moduli of a two phase composite material 17

2. 4. 1 The Voigt Approximation 19

2. 4. 2 The Reuss Approximation 20

2. 4. 3 Hill's theorem 20

2. 4. 4 The dilute approximation 21

2. 4. 5 The self-consistent method 24

2. 4. 6 The differential scheme 24

2. 4. 7 The Mori-Tanaka theory 26

2. 4. 8 The effective moduli of periodic distribution 27

2. 5 Conclusion 30

Chapter 3

The estimated elastic constants for a single osteonal lamella 31

3. 1. Introduction 31

3. 2 The model description 34

3. 3 Methods 35

3. 3. 1 Calculation of the effective elastic constants of the collagen-water composite and the hydroxyapatite-water composite by using the Voigt and Reuss bounds 35

3. 3. 2 Calculation of the effective elastic constants of the mineralized collagen fibrils 38

3. 3. 3. Calculation of the effective elastic constants of collagen fiber that is

composed of mineralized collagen fibrils 40

3. 3. 4. Calculation of the effective elastic constants of a single lamella that contains collagen fibers 42

3. 4 Steps of calculation 42

3. 5 Results 44

3. 6 Discussion 44

Chapter 4

An estimate of anisotropic poroelastic constants of an osteon 56

4. 1 Introduction 57

4. 2 Method 61

4.2.1 The relationship between Voigt notation and Kelvin notation 61

4.2.2 The bone matrix elastic constants 63

4.2.3 An estimate of the drained elastic constants at the lacunar porosity level 64

4.2.3.1 The case of an isotropic bone matrix 67

4.2.3.2. The case when the bone matrix is anisotropic 68

4.2.4 Estimate of undrained elastic constants at the lacunar porosity level 68

4.2.5 Steps of the calculation 71

4.3. Result 72

4.4. Discussion 72

Chapter 5

Estimation of the effective transversely isotropic elastic constants of a material from known values of the material's orthotropic elastic constants 85

5.1 Introduction 86

5.2 A generalized Hill inequality 86

5.3 Outline of the calculational procedure 89

5.4 Application of the method when the elastic constants data depend on composition 98

5.5 Discussion 99

Chapter 6 Future Study 108

Appendix 115

Appendix 1 The orthotropic, transversely isotropic, and isotropic symmetries 115

Appendix 2 The disturbance strain 119

Appendix 3 The relationship between Voigt notation and Kelvin notation 121

References **124**

List of Tables

Table 1.1 The technical elastic constants for human bone 8

Table 1.2 Summary of the isotropic elastic constants for cortical bone on two levels of porosity 9

Table 1.3 Measured or estimated porosities and permeabilities for the two levels of bone porosity 11

Table 3.1 Compositional volume fraction of the human cortical bone 48

Table 3.2 The technical elastic constants of the collagen and the hydroxyapatite minerals 49

Table 3.3 (a) The effective technical elastic constants of the mineralized collagen fibril (Step 2), the collagen fiber (Step 3), and a single lamella (Step 4) by using the data of Biltz and Pellegrino (1969) 50

Table 3.3 (b) The effective technical elastic constants of the mineralized collagen fibril (Step 2), the collagen fiber (Step 3), and a single lamella (Step 4) by using the data of Gong et al. (1964) 51

Table 3.3 (c) The effective technical elastic constants of the mineralized collagen fibril (Step 2), the collagen fiber (Step 3), and a single lamella (Step 4) by using the data of Gong et al. (1964) that the volume fraction of the volatile inorganic fraction is

excluded from the mineral volume fraction 52

Table 4.1(a). The estimated undrained and drained elastic constants of the type L osteon for the case when the bone matrix is isotropic and the case when it is orthotropic 77

Table 4.1(b). The estimated undrained and drained elastic constants of the type T osteon for the case when the bone matrix is isotropic and the case when it is orthotropic.....78

Table 4.1(c). The estimated undrained and drained elastic constants of the type A osteon for the case when the bone matrix is isotropic and the case when it is orthotropic.....79

Table 4.2 Two estimates of the poroelastic constants assuming the lacunae are ellipsoids and the bone matrix material is isotropic. The estimate on the left side of the table is based on the periodic distribution assumption and that on the right side is based on the dilute distribution assumption, for type L osteon.....80

Table 4.3(a) The estimated Biot effective coefficient $\hat{\mathbf{A}}$ and the estimated Skempton coefficient $\hat{\mathbf{B}}$ in the case where the collagen fibers are oriented in the longitudinal direction (type L osteon). The subscript r, θ, and z indicate the radial direction, the circumferential direction, and the longitudinal direction, respectively.....81

Table 4.3 (b) The estimated Biot effective coefficient $\hat{\mathbf{A}}$ and the estimated Skempton coefficient $\hat{\mathbf{B}}$ in the case where the collagen fibers are oriented in the transverse direction (type T osteon). The subscript r, θ, and z indicate the radial direction, the circumferential direction, and the longitudinal direction, respectively.....82

Table 4.3(c) The estimated Biot effective coefficient $\hat{\mathbf{A}}$ and the estimated Skempton coefficient $\hat{\mathbf{B}}$ in the case where the collagen fibers are oriented in the transverse direction (type A osteon). The subscript r, θ, and z indicate the radial direction, the circumferential direction, and the longitudinal direction, respectively.....83

Table 5.1 Experimental measured orthotropic cortical bone data of Ashman et al (1984) and van Buskirk et al. (1981).....101

Table 5.2 The effective transversely isotropic technical elastic constants calculated from the orthotropic data of Ashman et al. (1984).....102

Table 5.3 The effective transversely isotropic technical elastic constants calculated from the orthotropic data of van Buskirk et al. (1981).....103

Table 5.4 The effective isotropic technical elastic constants calculated from the orthotropic data of Ashman et al. (1984).....104

Table 5.5 The effective transversely isotropic technical elastic constants calculated from the orthotropic data of van Buskirk et al.(1981).....105

Table 5.6 The effective transversely isotropic technical elastic constants calculated from the orthotropic data of Yang et al. (1999).....106

Table 5.7 The effective isotropic technical elastic constants calculated from the orthotropic data of Yang et al. (1999).....107

Table 6.1 The estimated undrained and drained elastic constants of the type L osteon at the vascular porosity level. Both orthotropic and transversely isotropic results are shown.....112

Table 6.2 The estimated undrained and drained elastic constants of the type T osteon

at the vascular porosity level. Both orthotropic and transversely isotropic results are shown.....113

Table 6.3 The estimated undrained and drained elastic constants of the type A osteon at the vascular porosity level. Both orthotropic and transversely isotropic results are shown.....114

Table A1.1 The relationship between the reflective symmetry plane and the transformation tensor.....118

List of Figures

Figure 1.1 A section of an osteon 12

Figure 1.2 The hierarchical levels of bone matrix 13

Figure 1.3 A schematic diagram for why this study is required in the bone mechanics area.....15

Figure 3.1 A combined schematic of the hierarchal development of mineralized bone 53

Figure 3.2 Flow chart of calculation 54

Figure 3.3 The variation of elastic modulus against the water volume fraction.....55

Figure 4.1 The unit of the periodic distribution assumption.....84

Chapter 1

Introduction

This dissertation consists of six chapters. The first one describes the background for this study, especially why this study is required for further development of bone mechanics research. The second chapter explains various methods to estimate the effective moduli of composite materials. In the third chapter, the elastic constants of a single lamella (the thickness of a lamella is approximately 2 to 4 μm for human, Ascenzi et al. 1987) are estimated by using micromechanical models. The poroelastic constants of an osteon (approximately the order of 150 μm, Cowin 1999) are calculated by using micromechanical models and the poroelasticity theory given in the chapter 4. The technique of converting the orthotropic elastic constants to transversely isotropic elastic constants or to isotropic elastic constants is shown in the chapter 5. In chapter 6, suggestions for future studies employing the results obtained in this dissertation are addressed.

The structure of cortical bone

Cortical bone is a dense solid structure and is observed at the diaphyses and the

outer shell of the metaphyses of a long bone. Secondary osteons occur within the cortical bone of human adults. Secondary osteons have a cylindrical shape whose radii are approximately between 100 and 150 μm (Cowin 1999) and those contain the osteonal canal at the center of an osteon. The osteon is generated by a bone remodeling process, in which bone cells remove the old bone and replace it with new bone. The cement line (0.5 to 1 μm, Figure 1.1) separates the secondary osteons from the other interstitial bone that is the previously formed bone matrix. The secondary osteon is composed of a lamella. Many approximately ellipsoidal shaped porous spaces are observed inside the lamella and they are called a lacuna. The lacunae house osteocytes, differentiated bone cells from osteoblasts, which are bone matrix forming cells. The osteocytes are connected to other osteocytes or to osteoblasts by the osteocytic processes in the small tunnels called "canaliculi." In another words, the canaliculi are connected from the osteonal canal to lacunae and lacunae to lacunae (Cowin 1999, Figure 1.1). The space in lacunae and canaliculi is called the lacunar-canalicular porosity, and the space of osteonal and Volkman canals surrounding the vasculature is called the vascular porosity. Both the lacunar-canalicular porosity and the vascular porosity are filled with the bone interstitial fluid, which is considered to be water containing proteins and ions.

The bone fluid fills not only the vascular and the lacunar-canalicular porosities

but also the collagen-mineral porosity. The collagen-mineral porosity is the smallest diameter porosity inside the bone matrix. The water in the collagen-mineral porosity is thought to be bound water. Cowin (1999) noted that the bound water is strongly attracted to the solid and is not moving because the interaction with the ionic crystals in the solid bone matrix (Neuman et al. 1953; Neuman and Neuman, 1958).

The solid bone matrix at the collagen-mineral porosity level has a hierarchical composite structure of collagen molecules and hydroxyapatite mineral crystals. The hydroxyapatite-mineral-crystals start to grow into the space between collagen molecules within the collagen fibril and they fuse into larger and thicker plates (Figure 1.2c). These collagen fibrils are surrounded by the hydroxyapatite-mineral-crystals, and form a collagen fiber (Figure 1.2 d). Collagen fibers establish an array of collagen fibers that are embedded in the hydroxyapatite-mineral-crystals (Figure 1.2 d and f). Note that different levels of porosities, which were explained in Figure 1.1, are not explained in Figure 1.2 and these porosities have to be added between Figure 1.2 f and g.

Why is this study required in the bone mechanics research field?

The anisotropic bone matrix elastic constants at the lacunar-canalicular porosity level and smaller levels need to be estimated : (1) for the mathematical modeling to

elucidate the bone fluid flow through the canalicular network, (2) for the microdamage in the cortical and cancellous bone, and (3) for the tissue engineering (Figure 1.3).

The elastic constants of bone cannot be measured at the lacunar-canalicular porosity level or smaller levels. The elastic constants of the cortical bone were measured experimentally by the ultrasound technique and the mechanical testing (Ashman et al., 1984; Knets et al., 1977; Reilly and Burstein, 1975; Yoon and Katz, 1976; Table 1.1). The specimens for ultrasound and mechanical testing of bone are so large that specimens contain the collagen-hydroxyapatite porosity, the lacunar-canalicular porosity, and the vascular porosity, and thus test results reflect an average of these properties. Because of the size of collagen-hydroxyapatite porosity, all bone matrix elastic constants at the level of collagen-hydroxyapatite porosity can not be measured by the experiment. One possible method to measure some elastic constants at this level is the nanoindentation method, but it can measure only Young's modulus (Fan et al. 2002; Rho et al. 1998; Zysset et al. 1999). Ascenzi et al. (1967, 1968, 1972) measured the elastic constants of an osteon by using tensile, compressive, and torsion tests, (the diameter of an osteon is approximately 300 μm), but the measured values are assumed as isotropic even though elastic constants measured by a nanoindentation (Fan et al. 2002) show anisotropic symmetry (See Appendix 1 for more details of material symmetries).

The elastic constants in bone poroelasticity

The poroelasticity theory has been used to elucidate the bone fluid flow through the lacunar-canalicular network. Osteocytes, differentiated from osteoblasts, are stimulated by the bone fluid flow over their processes due to the deformation of the bone in the lacunar-canalicular network (Cowin 1999; Weinbaum et al. 1994; Zeng et al. 1994). Wang et al. (1999) proposed a theoretical model using poroelasticity to mimic oscillatory four point bending experiments (Starkebaum et al. 1979) of thin bone specimens. Their model showed the local fluid pressure profiles and the fluid pressure response to cyclic loading is not sensitive to the permeability of the osteonal cement lines, but it is sensitive to the applied loading frequency. Zhang et al. (1998) estimated the peak pore pressure due to uniaxial compression for both the vascular porosity and the lacunar-canalicular porosity by using the poroelasticity theory. The peak pore water pressure of vascular porosity is 19 percent of the applied axial stress and 12 percent of the applied axial stress in the lacunar-canalicular porosity. A slight hydraulic stiffening of the bulk modulus at the lacunar-canalicular porosity level was predicted by longer relaxation time of the lacunar-canalicular porosity. All developed poroelastic models for elucidating a bone fluid flow are assumed that the bone matrix is isotropic. Smit et al. (2002) estimated poroelastic constants, the relaxation time, and the permeability, but still all values are isotropic. The

reported isotropic elastic constants and the isotropic permeability for bone are summarized in Table.1.2 and Table 1.3, respectively.

The elastic constants in the bone microdamage

The elastic constants of the bone tissue are degraded when the microdamage is induced in the bone tissue. Currently, the amount of microdamage is quantified by measuring the degradation of the elastic constants of specimens. Chow and Wang (1987) proposed generalized damage variables for the anisotropic elastic medium. However, in the area of bone damage mechanics, the mathematical models are limited by the assumption of isotropy. The model of Fondrk et al. (1999) examined the stress-strain behavior by using the Kelvin-Voigt viscoelastic-element, a element includes elastic elements and a viscous element in parallel. Fondrk et al. (1999) included plasticity and showed the resulting model fits the experimental stress-strain curve. However, it was found that the bone matrix anisotropy strongly influences the anisotropy of the poroelastic constants in Chapter 4. Thus it is clear that the anisotropic bone matrix will play an important role in the bone damage mechanics.

The mechanical properties in tissue engineering

The mechanical properties of the tissue engineered bone matrix grown in vitro have to be similar to those of bone matrix in vivo. Matching will reduce the disparity when the grown tissue in vitro is substituted into the body. Because experiments have been performed for different animals, results may not be able to predict phenomenon in human bones. Rogers et al. (1957) found that the distribution of ash content and composition of the organic matrix in human bone are equal to those in bovine bone, but the structure of human bone is different from the structure of bovine bone because the human cortical bone is mainly composed of secondary osteons. The more accurately estimated elastic constants for human bone structure may help to reduce the disparity of tissue engineered bone matrix with a human bone.

Table 1.1 The technical elastic constants for human bone (Cowin 1989)

Group	Reilly and Burstein (1975)	Yoon and Katz (1976)	Knets et al. (1977)	Ashman et al. (1984)
Bone	Femur	Femur	Tibia	Femur
Symmetry	TI	TI	ORTH	ORTH
Method	M	U	M	U
$E_1(GPa)$	11.5	18.8	6.91	12.0
$E_2(GPa)$	11.5	18.8	8.51	13.4
$E_3(GPa)$	17.0	27.4	18.4	20.0
$G_{12}(GPa)$	3.6[a]	7.17	2.41	4.53
$G_{13}(GPa)$	3.3	8.71	3.56	5.61
$G_{23}(GPa)$	3.3	8.71	4.91	6.23
ν_{12}	0.58	0.312	0.49	0.376
ν_{13}	0.31[a]	0.193	0.12	0.222
ν_{23}	0.31[a]	0.193	0.14	0.235
ν_{21}	0.58	0.312	0.62	0.422
ν_{31}	0.46	0.281	0.32	0.371
ν_{32}	0.46	0.281	0.31	0.350

Note: The three directions are coincident with the long axis of the bone; the one and two directions are radial and circumferential, respectively. Method U is ultrasound and method M is standard machine testing.

[a] Not measured

Table 1.2 Summary of the isotropic elastic constants for cortical bone on two levels of porosity (Zhang *et al.* 1998; Smit *et al.* 2002). * is for the drained case.

	Zhang *et al.* (1998)		Smit *et al.* (2002)	
Properties	Vascular level	Lacuno-canalicular level*	Vascular level	Lacuno-canalicular level
ϕ, porosity	0.04	0.05	0.04	0.05
K_f, bulk modulus of fluid	2.3	2.3	2.3	2.3
E_d, drained Young's modulus	14.595	13.138	14.58	15.75
ν_d, drained Poisson's ratio	0.325	0.316	0.325	0.325
G_d, drained shear modulus	5.5	5	5.50	5.94
K_d, drained bulk modulus	13.9	11.9	13.92	14.99
E_s, solid Young's modulus			15.85	17.51
ν_s, solid Poisson's ratio			0.333	0.335
G_s, solid shear modulus			5.94	6.56
K_s, solid bulk modulus	19.7	13.9	15.82	17.66
E_u, undrained Young's modulus	18.547	13.910	14.65	15.85
ν_u, undrained Poisson's ratio	0.35	0.325	0.332	0.333

Table 1.2 (continued from the previous page)

Summary of the isotropic elastic constants for cortical bone on two levels of porosity (Zhang *et al.* 1998; Smit *et al.* 2002). * is for the drained case.

	Zhang *et al.* (1998)		Smit *et al.* (2002)	
Properties	Vascular level	Lacuno-canalicular level*	Vascular level	Lacuno-canalicular level
K_u, undrained bulk modulus	16.8	12.6	14.56	15.82
A, effective stress coefficient	0.294	0.144	0.120	0.151
B, Skempton pore pressure coefficient	0.58	0.40	0.367	0.344

Table 1.3 Measured or estimated porosities and permeabilities for the two levels of bone porosity

Reference	Porosity	Reference	Permeability (m^2)
a. The vascular porosity (PV)			
Frost (1962)	0.6	Rouhana *et al* (1981)	3.0×10^{-13}
Morris *et al.* (1982)	0.015	Li *et al.* (1987)	5.0×10^{-15}
Schaffler and Burr (1988)	0.04	Zhang *et al.*(1998)	6.35×10^{-13}
Zhang *et al.* (1998)	0.04		
b. The lacunar-canalicular porosity (PLC)			
Frost (1962)	0.023	Zhang *et al.* (1998)	1.47×10^{-20}
Morris *et al.* (1982)	0.042	Smit *et al.* (2002)	2.2×10^{-22}
Baylink and Wergedal (1971)	0.035		
Zhang *et al.* (1998)	0.05		

Figure 1.1 A section of an osteon (Cowin 1999)

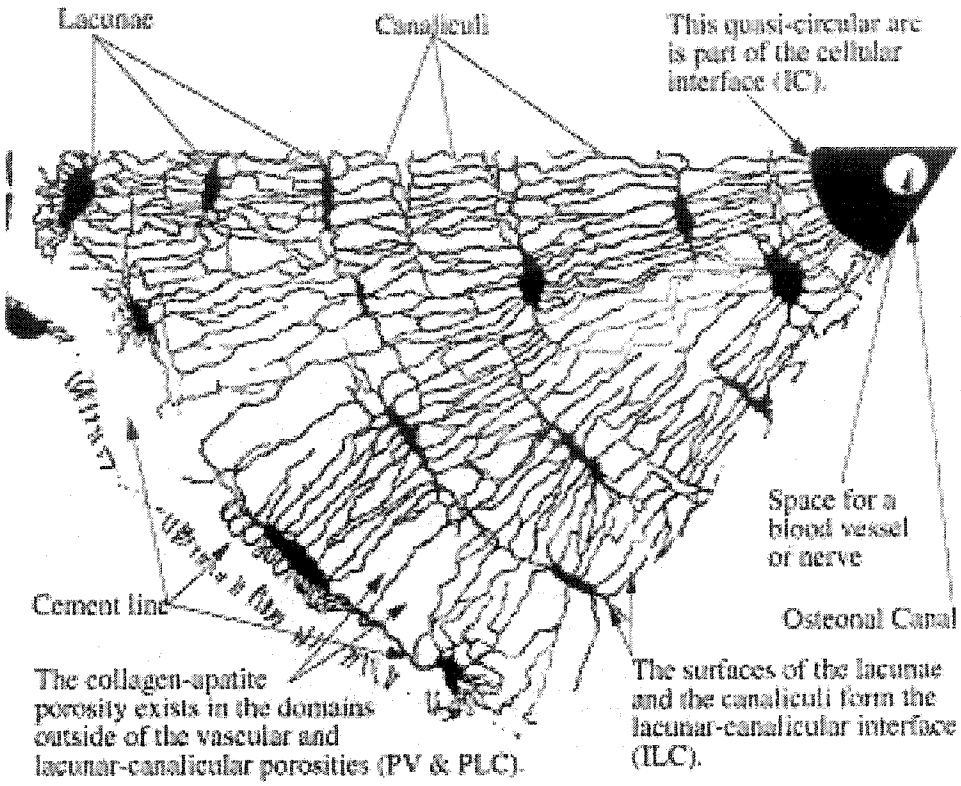

Figure 1.2 The hierarchical levels of bone matrix (Siperko and Landis 2001)

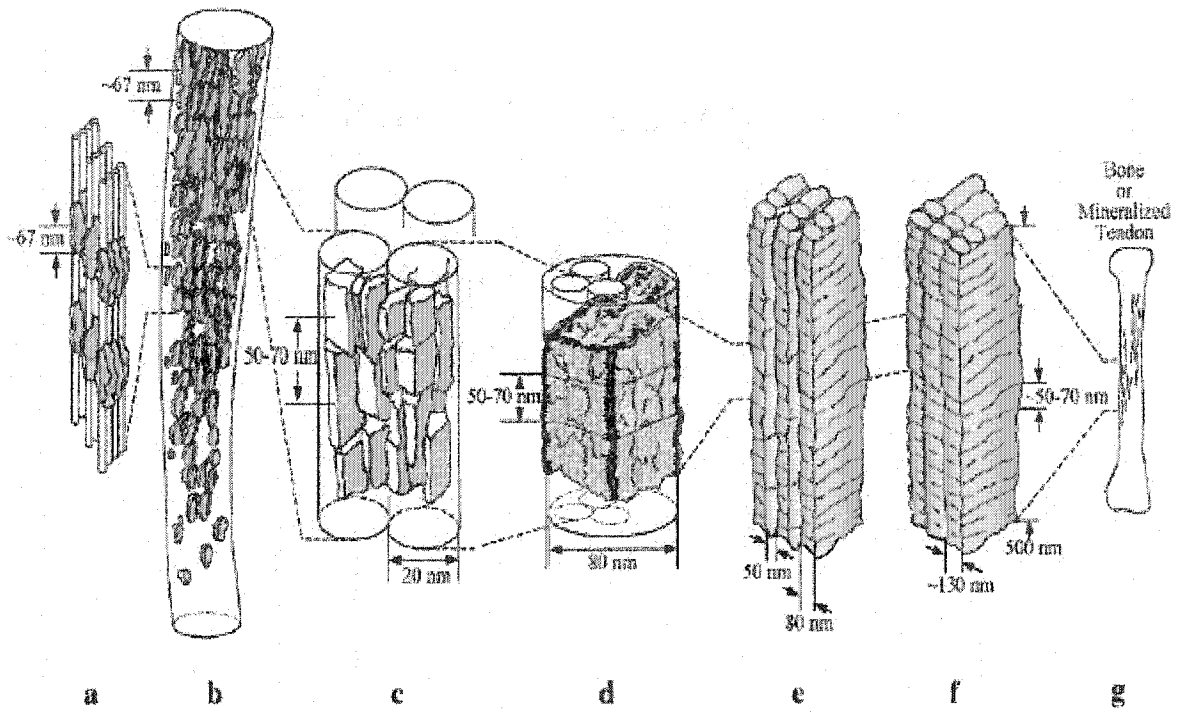

(a) The hydroxyapatite-mineral-crystals are deposited between the 300 nm long collagen molecules. The size 67 nm indicates the overlapped length 27nm with the adjacent collagen molecule and the 40nm gap between collagen molecule ends. (b) the platelet-shape-hydroxyapatite-minerals grow in the gap space within the collagen fibril. (c) the platelet-shape-hydroxyapatite-mineral-crystals grow as large as 50 to 70 nm in length. (d) the platelet-shape-hydroxyapatite-mineral-crystals fuse outside of collagen fibrils and a group of collagen fibrils are surrounded by the hydroxyapatite-mineral-crystals. The space between the platelet-shape-hydroxyapatite-mineral-crystals disappears and collagen

fibrils are embedded in the hydroxyapatite-mineral-crystals. (e) the hydroxyapatite-mineral-crystals fuse outside of collagen fibers. The 50 nm thick hydroxyapatite-mineral-plate is formed between arrays of mineralized collagen fibers of which thickness is approximately 80 nm. (d) the mineralization continues and the mineralized collagen fibers are completely embedded in the hydroxyapatite-mineral-crystals.

Figure 1.3 A schematic diagram for why this study is required in the bone mechanics area

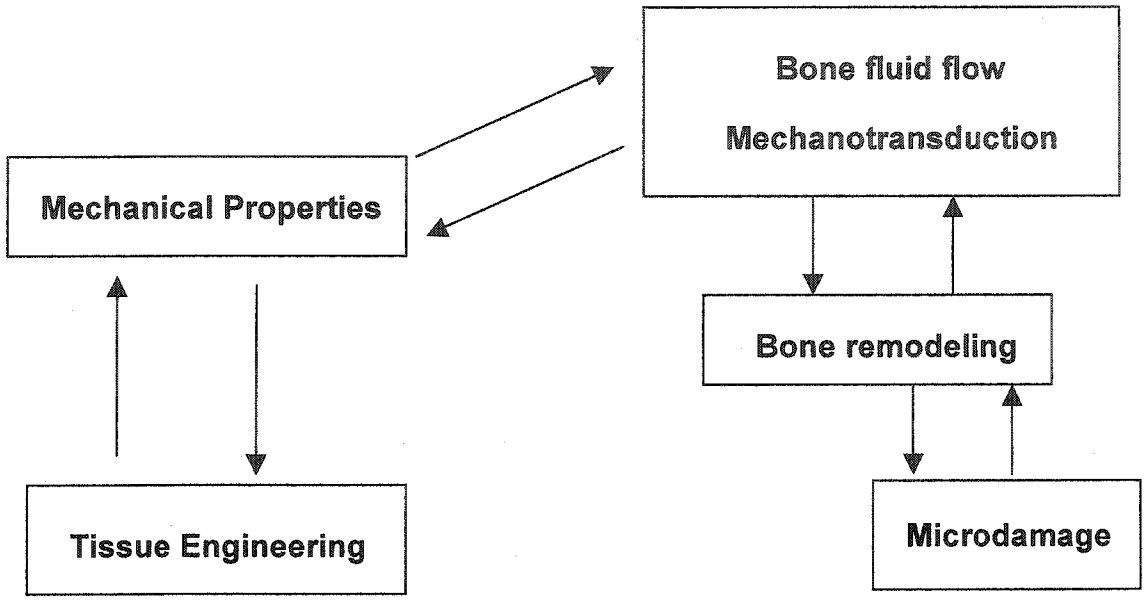

Chapter 2

The approximate methods of effective moduli

2.1. Representative Volume Element (RVE)

The representative volume element (RVE) is the key concept in modeling microstructure for inclusion in a continuum model. An RVE for a volume surrounding a point in a material is a statistically homogeneous representative of the material in the neighborhood of the point. The microstructure of a material, which may not be homogeneous, has to be averaged or homogenized over the RVE to form a point in a continuum model. The effective medium approach, which will be discussed in this chapter, is the traditional averaging process in the solid mechanics.

2.2. The average stress and the average strain of the representative volume element (RVE)

The average stress and the average strain of the representative volume element (RVE) are defined as

$$<\mathbf{T}>=\frac{1}{V}\int_{V}\mathbf{T}dV \quad \text{and} \quad <\mathbf{E}>=\frac{1}{V}\int_{V}\mathbf{E}dV \tag{2.1}$$

where $<\mathbf{T}>$ is the averaged stress in three dimensions, $<\mathbf{E}>$ is the averaged strain in

three dimensions, V is the representative volume element (RVE), $\mathbf{T}$ is the stress in three dimensions, and $\mathbf{E}$ is the strain in three dimensions, respectively.

2.3. Boundary conditions at the interface

The elastic material satisfies the strain-displacement relation, which is given by

$$\frac{\partial \mathbf{u}}{\partial \mathbf{x}} = \mathbf{E} + \mathbf{W}, \tag{2.2}$$

where $\mathbf{u}$ is the displacement on the surface, $\mathbf{E}$ is the strain tensor, and $\mathbf{W}$ is the rotation tensor. By integrating Eq. (2.2) with respect to $\mathbf{x}$ gives

$$\mathbf{u} = (\mathbf{E} + \mathbf{W})\mathbf{x} + C, \tag{2.3}$$

where C is the arbitrary constant. In the case of no rotation, (i.e., $\mathbf{W} = 0$) and constant term, i.e., C is assumed zero, the displacement at the boundary condition is given by

$$\mathbf{u} = \mathbf{E} \cdot \mathbf{x}, \tag{2.4}$$

and the traction force at the boundary condition is given by

$$\mathbf{t} = \mathbf{T} \cdot \mathbf{n}, \tag{2.5}$$

respectively, where $\mathbf{n}$ is the unit outward normal vector on the surface S of the boundary.

2.4. The approximation of the effective moduli of a two phase composite

material

The average stress and the average strain of a two phase composite in six dimensions are expressed in a linear way as

$$<\hat{\mathbf{T}}>=(1-\phi)<\hat{\mathbf{T}}^{M}>+\phi<\hat{\mathbf{T}}^{I}>, \tag{2.6}$$

and

$$<\hat{\mathbf{E}}>=(1-\phi)<\hat{\mathbf{E}}^{M}>+\phi<\hat{\mathbf{E}}^{I}>, \tag{2.7}$$

where ϕ is the volume fraction of the inclusion. Note that the letter with a hat indicates the six dimensions. The averaged strain of the matrix $<\hat{\mathbf{E}}^{M}>$ and the averaged strain of the inclusion $<\hat{\mathbf{E}}^{I}>$ are calculated by the the tensors $\hat{\mathbf{A}}^{(1)}$ and $\hat{\mathbf{A}}^{(2)}$ from the uniform strain $<\hat{\mathbf{E}}>$ prescribed at the boundary of the RVE,

$$<\hat{\mathbf{E}}^{M}>=\hat{\mathbf{A}}^{(1)}<\hat{\mathbf{E}}> \text{ and } <\hat{\mathbf{E}}^{I}>=\hat{\mathbf{A}}^{(2)}<\hat{\mathbf{E}}>. \tag{2.8}$$

By introducing the Hooke's law for each phase, $<\hat{\mathbf{T}}^{M}>=\hat{\mathbf{C}}^{M}<\hat{\mathbf{E}}^{M}>$ for the matrix and $<\hat{\mathbf{T}}^{I}>=\hat{\mathbf{C}}^{I}<\hat{\mathbf{E}}^{I}>$ for the inclusion, and substituting Eq. (2.8) into Eq. (2.6), the Hooke's law for the two phase composite gives

$$<\hat{\mathbf{T}}>=((1-\phi)\hat{\mathbf{C}}^{M}\hat{\mathbf{A}}^{(1)}+\phi\hat{\mathbf{C}}^{I}\hat{\mathbf{A}}^{(2)})<\hat{\mathbf{E}}>\equiv<\hat{\mathbf{C}}><\hat{\mathbf{E}}>, \tag{2.9}$$

where $\hat{\mathbf{C}}^{M}$ and $\hat{\mathbf{C}}^{I}$ are elasticity tensors of the matrix and the inclusion, respectively, and $<\hat{\mathbf{C}}>$ is the effective elasticity tensor of the two phase composite. Similarly, the inverse form of the Hooke's law will be obtained by introducing the tensors $\hat{\mathbf{B}}^{(1)}$ and

$\hat{\mathbf{B}}^{(2)}$ as

$$<\hat{\mathbf{E}}>=((1-\phi)\hat{\mathbf{S}}^{M}\hat{\mathbf{B}}^{(1)}+\phi\hat{\mathbf{S}}^{I}\hat{\mathbf{B}}^{(2)})<\hat{\mathbf{T}}>\equiv<\hat{\mathbf{S}}><\hat{\mathbf{T}}>. \tag{2.10}$$

where $<\hat{\mathbf{S}}>$ is the effective compliance matrix of the two phases composite and newly defined tensors $\hat{\mathbf{B}}_1$ and $\hat{\mathbf{B}}_2$ are given by

$$<\hat{\mathbf{T}}^{M}>=\hat{\mathbf{B}}^{(1)}<\hat{\mathbf{T}}> \text{ and } <\hat{\mathbf{T}}^{I}>=\hat{\mathbf{B}}^{(2)}<\hat{\mathbf{T}}>. \tag{2.11}$$

The effective elasticity tensor $<\hat{\mathbf{C}}>$ for the two phase composite and the effective compliance tensor $<\hat{\mathbf{S}}>$ are given by

$$<\hat{\mathbf{C}}>=(1-\phi)\hat{\mathbf{C}}^{M}\hat{\mathbf{A}}^{(1)}+\phi\hat{\mathbf{C}}^{I}\hat{\mathbf{A}}^{(2)}, \tag{2.12}$$

and

$$<\hat{\mathbf{S}}>=(1-\phi)\hat{\mathbf{S}}^{M}\hat{\mathbf{B}}^{(1)}+\phi\hat{\mathbf{S}}^{I}\hat{\mathbf{B}}^{(2)}. \tag{2.13}$$

2.4.1. The Voigt Approximation

Voigt (1929) introduced the estimation of the average elastic constants of polycrystals by assuming that the strain over the composite medium is uniform and the effective strain is not influenced by the geometry of phase. Under this assumption, the tensors $\hat{\mathbf{A}}^{(1)}$ and $\hat{\mathbf{A}}^{(2)}$ are equal to the identity tensor $\hat{\mathbf{1}}$. The effective elasticity matrix $<\hat{\mathbf{C}}>$ in Eq. (2.12) is given as the following by replacing the tensors $\hat{\mathbf{A}}^{(1)}$ and $\hat{\mathbf{A}}^{(2)}$ with the identity tensor $\hat{\mathbf{1}}$,

$$<\hat{\mathbf{C}}>=(1-\phi)\hat{\mathbf{C}}^{(1)}+\phi\hat{\mathbf{C}}^{(2)}. \tag{2.14}$$

2.4.2. The Reuss Approximation

Reuss (1929) assumed that the composite is subjected to the uniform stress. Similar to the Voigt approximation, the tensors $\hat{\mathbf{B}}^{(1)}$ and $\hat{\mathbf{B}}^{(2)}$ in Eq. (2.13) are assumed equal to the identity tensor $\hat{\mathbf{1}}$ because it is assumed that the effective compliance tensor is not influenced by the geometry of the inclusion. The effective compliance matrix $<\hat{\mathbf{S}}>$ estimated by Reuss approximation is

$$<\hat{\mathbf{S}}>=(1-\phi)\hat{\mathbf{S}}^{(1)}+\phi\hat{\mathbf{S}}^{(2)}. \tag{2.15}$$

2.4.3. Hill's theorem

Hill (1952, 1963)) showed that the actual overall moduli lie between the Reuss and Voigt estimations (i.e., Hill theorem). Cowin et al. (1999) found that the Hill inequality, or the Reuss and Voigt bounds satisfy for the greater symmetry when components of the greater symmetry are replaced by the components of triclinic symmetry, which is the less symmetry. This technique is used to convert the orthotropic elastic constants to the transversely isotropic elastic constants and the isotropic elastic constants in Chapter 5. Not only the overall moduli but also the eigenvalues and the strain energy satisfy the Reuss and Voigt bounds. The eigenvalues of the elasticity tensor (or

the compliance tensor) satisfy the following characteristic equations,

$$(\hat{\mathbf{C}} - \Lambda\hat{\mathbf{1}})\hat{\mathbf{N}} = 0 \quad (\text{or} \quad (\hat{\mathbf{S}} - \frac{1}{\Lambda}\hat{\mathbf{1}})\hat{\mathbf{N}} = 0), \tag{2.16}$$

where $\hat{\mathbf{C}}$ is the elasticity tensor, Λ is the eigenvalue, $\hat{\mathbf{1}}$ is the identity tensor, and $\hat{\mathbf{N}}$ is the normalized eigenvector, respectively. The elasticity (or the compliance) tensor is decomposed by eigenvalues Λ_k and engentensors $\hat{\mathbf{N}}^{(k)}$ as

$$\hat{\mathbf{C}} = \sum_{k=1}^{6} \Lambda_k \hat{\mathbf{N}}^{(k)} \otimes \hat{\mathbf{N}}^{(k)} \quad (\text{or} \quad \hat{\mathbf{S}} = \sum_{k=1}^{6} \frac{1}{\Lambda_k} \hat{\mathbf{N}}^{(k)} \otimes \hat{\mathbf{N}}^{(k)}), \tag{2.17}$$

where $k = 1, ..., 6$. Also, the strain energy Σ, i.e., $\Sigma = \frac{1}{2}\hat{\mathbf{E}} \cdot \hat{\mathbf{C}} \cdot \hat{\mathbf{E}} = \frac{1}{2}\hat{\mathbf{T}} \cdot \hat{\mathbf{S}} \cdot \hat{\mathbf{T}}$ satisfies the Hill inequalities, the actual overall moduli lie between the Reuss and Voigt estimations. The strain energy by the actual effective elasticity tensor is less than that by the effective elasticity tensor by the Voigt estimation as

$$\hat{\mathbf{E}} \cdot \hat{\mathbf{C}}^{R} \cdot \hat{\mathbf{E}} \le \hat{\mathbf{E}} \cdot \hat{\mathbf{C}}^{eff} \cdot \hat{\mathbf{E}} \le \hat{\mathbf{E}} \cdot \hat{\mathbf{C}}^{V} \cdot \hat{\mathbf{E}} \quad (\text{or} \quad \hat{\mathbf{T}} \cdot \hat{\mathbf{S}}^{V} \cdot \hat{\mathbf{T}} \le \hat{\mathbf{T}} \cdot \hat{\mathbf{S}}^{eff} \cdot \hat{\mathbf{T}} \le \hat{\mathbf{T}} \cdot \hat{\mathbf{S}}^{R} \cdot \hat{\mathbf{T}}), \tag{2.18}$$

which must hold the Hill's inequality for the eigenvalues.

$$\Lambda_k^R \le \Lambda_k^{eff} \le \Lambda_k^V . \tag{2.19}$$

2.4.4. The dilute approximation

The interaction between the particles is neglected in the dilute approximation. Often this approximation is considered similar to the problem of a single particle imbedded in the continuous phase because the no interaction between particles is

involved. If the uniform macrostrain, $\mathbf{E} = \mathbf{E}^0$ is prescribed, the boundary condition for the RVE becomes

$$\mathbf{u} = \mathbf{x} \cdot \mathbf{E}^0 \quad \text{on} \quad \partial V . \tag{2.20}$$

The macrostrain $\mathbf{E}^0$ and the macrostress $\mathbf{T}^0$ satisfy the Hooke's law for the matrix as

$$\mathbf{T}^0 = \mathbf{C}^M \cdot \mathbf{E}^0, (\text{or}\, \hat{\mathbf{T}}^0 = \hat{\mathbf{C}}^M \cdot \hat{\mathbf{E}}^0), \tag{2.21}$$

where $\hat{\mathbf{C}}^M$ (or $\mathbf{C}^M$) is the elasticity tensor of the matrix. Note that the elasticity tensor, stress, and strain with a hat indicate the six dimensions. The Hooke's law in Eq. (2.21) is no longer useful if the matrix contains the inclusion. The strain disturbance $\mathbf{E}^d$ and the stress disturbance $\mathbf{T}^d$ are required to estimate the effective moduli of composite material in three dimensions. The average of the strain in the two phase composite is the average value of the prescribed uniform strain $\hat{\mathbf{E}}^0$ and the disturbed strain $\hat{\mathbf{E}}^d$ by the inclusion in six dimensions, but it has to be equal to the prescribed uniform strain at the boundary of RVE, which is

$$< \hat{\mathbf{E}} > = < \hat{\mathbf{E}}^0 + \hat{\mathbf{E}}^d > = \hat{\mathbf{E}}^0 . \tag{2.22}$$

The Hooke's law shows the relation between the average stress and the average strain as

$$< \hat{\mathbf{T}} > = < \hat{\mathbf{C}} >< \hat{\mathbf{E}} > = < \hat{\mathbf{C}} > \hat{\mathbf{E}}^0, \tag{2.23}$$

and the average stress $< \hat{\mathbf{T}} >$ is modified by two phase composite, matrix and inclusions

$$< \hat{\mathbf{T}} > = (1-\phi) < \hat{\mathbf{T}}^M > + \phi < \hat{\mathbf{T}}^I > = (1-\phi)\hat{\mathbf{C}}^M \hat{\mathbf{E}}^0 + \phi \hat{\mathbf{C}}^I < \hat{\mathbf{E}}^I >, \tag{2.24}$$

where ϕ is the volume fraction of inclusion. The term $(1-\phi)<\hat{\mathbf{T}}^M>$ is expanded by using the Hooke's law as

$$(1-\phi)<\hat{\mathbf{T}}^M>=(1-\phi)\hat{\mathbf{C}}^M<\hat{\mathbf{E}}^M>=\hat{\mathbf{C}}^M(\hat{\mathbf{E}}^0-\phi<\hat{\mathbf{E}}^I>), \tag{2.25}$$

Substituting Eq. (2.25) into Eq. (2.24) gives

$$<\hat{\mathbf{T}}>=\hat{\mathbf{C}}^M\hat{\mathbf{E}}^0-\phi\hat{\mathbf{C}}^M<\hat{\mathbf{E}}^I>+\phi\hat{\mathbf{C}}^I<\hat{\mathbf{E}}^I>=<\hat{\mathbf{C}}><\hat{\mathbf{E}}>. \tag{2.26}$$

By rearranging Eq. (2.26) with Eq. (2.23), it becomes

$$(\hat{\mathbf{C}}^M-<\hat{\mathbf{C}}>)\hat{\mathbf{E}}^0=\phi(\hat{\mathbf{C}}^M-\hat{\mathbf{C}}^I)<\hat{\mathbf{E}}^I>. \tag{2.27}$$

The term $<\hat{\mathbf{E}}^I>$ is defined as (See Appendix 2.A)

$$<\hat{\mathbf{E}}^I>\equiv<\hat{\mathbf{E}}^0+\hat{\mathbf{E}}^d>_I=\hat{\mathbf{A}}^I(\hat{\mathbf{A}}^I-\hat{\mathbf{S}}^I)^{-1}\hat{\mathbf{E}}^0, \tag{2.28}$$

where $\hat{\mathbf{S}}^I$ is the Eshelby tensor and $\hat{\mathbf{A}}^I$ is defined as (See Appendix 2.A)

$$\hat{\mathbf{A}}^I=(\hat{\mathbf{C}}^M-\hat{\mathbf{C}}^I)^{-1}\hat{\mathbf{C}}. \tag{2.29}$$

Substituting (2.28) into (2.27) gives

$$(\hat{\mathbf{C}}^M-<\hat{\mathbf{C}}>)\hat{\mathbf{E}}^0=\phi(\hat{\mathbf{C}}^M-\hat{\mathbf{C}}^I)\hat{\mathbf{A}}^I(\hat{\mathbf{A}}^I-\hat{\mathbf{S}}^I)^{-1}\hat{\mathbf{E}}^0. \tag{2.30}$$

By using the definition of $\hat{\mathbf{A}}^I$ (Eq. 2.29), Eq. (2.30) becomes

$$(\hat{\mathbf{C}}^M-<\hat{\mathbf{C}}>)=\phi(\hat{\mathbf{C}}^M-\hat{\mathbf{C}}^I)\hat{\mathbf{A}}^I(\hat{\mathbf{A}}^I-\hat{\mathbf{S}}^I)^{-1}=\phi\hat{\mathbf{C}}^M(\hat{\mathbf{A}}^I-\hat{\mathbf{S}}^I)^{-1}. \tag{2.31}$$

Then the effective elasticity tensor estimated by the dilute distribution is expressed as

$$<\hat{\mathbf{C}}>=\hat{\mathbf{C}}^M(\hat{\mathbf{1}}-\phi(\hat{\mathbf{A}}^I-\hat{\mathbf{S}}^I)^{-1}). \tag{2.32}$$

2.4.5. The self-consistent method

The self-consistent method is assumed that the inclusion is embedded in the yet-unknown overall elasticity (or compliance) tensor $<\hat{\mathbf{C}}>$ (or $<\hat{\mathbf{S}}>$). Thus Eq. (2.28) is replaced by

$$<\hat{\mathbf{E}}^I>\equiv<\hat{\mathbf{E}}^0+\hat{\mathbf{E}}^d>_I=<\hat{\mathbf{A}}^I>(<\hat{\mathbf{A}}^I>-<\hat{\mathbf{S}}^I>)^{-1}\hat{\mathbf{E}}^0, \tag{2.33}$$

where $<\hat{\mathbf{A}}^I>$ is defined as

$$\hat{\mathbf{A}}^I=(<\hat{\mathbf{C}}>-\hat{\mathbf{C}}^I)^{-1}<\hat{\mathbf{C}}>. \tag{2.34}$$

Substituting Eq. (2.33) into Eq. (2.27) gives

$$(\hat{\mathbf{C}}^M-<\hat{\mathbf{C}}>)\hat{\mathbf{E}}^0=\phi(\hat{\mathbf{C}}^M-\hat{\mathbf{C}}^I)<\hat{\mathbf{A}}^I>(<\hat{\mathbf{A}}^I>-<\hat{\mathbf{S}}^I>)^{-1}\hat{\mathbf{E}}^0. \tag{2.35}$$

Since the prescribed strain $\hat{\mathbf{E}}^0$ is arbitrary, the effective elasticity tensor estimated by the self-consistent method is given by

$$<\hat{\mathbf{C}}>=\hat{\mathbf{C}}^M+\phi(\hat{\mathbf{C}}^I-\hat{\mathbf{C}}^M)<\hat{\mathbf{A}}^I>(<\hat{\mathbf{A}}^I>-<\hat{\mathbf{S}}^I>)^{-1}. \tag{2.36}$$

2.4.6. The differential scheme

The effective moduli of two phase composite are estimated by the differential scheme adding the increments ΔV to the volume of an initial material V_0. The small amount of volume of composite ΔV is added and the portion of the inclusion in the increment ΔV is removed from the added volume of composite ΔV. The total volume

of inclusion after increments are added is that

$$V_0\phi_{i+1} = V_0\phi_i + \Delta V - \Delta V\phi_i, \tag{2.37}$$

where the term on the left side, $V_0\phi_{i+1}$ is the volume of inclusion after the increments are added, the first term on the right side, $V_o\phi_i$ is the volume of inclusion before the increments are added, the second term on the right side, ΔV is the added volume increment that contains both matrix and inclusion, and the last term on the right side, $\Delta V\phi_i$ is the volume fraction of inclusion in the added increment. Eq. (2.37) is simplified as

$$V_0(\phi_{i+1} - \phi_i) = \Delta V(1-\phi_i) \quad \text{or} \quad d\phi = \frac{dV}{V_0}(1-\phi_i). \tag{2.38}$$

The averaged elasticity tensor $<\hat{\mathbf{C}}>$ estimated by the dilute distribution is given by

$$<\hat{\mathbf{C}}> = \hat{\mathbf{C}}^M - \phi(\hat{\mathbf{C}}^I - \hat{\mathbf{C}}^M)\hat{\mathbf{A}}^I(\hat{\mathbf{A}}^I - \hat{\mathbf{S}}^I)^{-1} \equiv \hat{\mathbf{C}}^M - \phi(\hat{\mathbf{C}}^I - \hat{\mathbf{C}}^M)\hat{\mathbf{A}}^{(2)}. \tag{2.39}$$

The localization tensor $\hat{\mathbf{A}}^{(2)}$ is defined as $\hat{\mathbf{A}}^{(2)} \equiv \hat{\mathbf{A}}^I(\hat{\mathbf{A}}^I - \hat{\mathbf{S}}^I)^{-1}$. If the small amount of volume fraction $\Delta\phi$ is added to the volume fraction of inclusion ϕ, Eq. (2.39) will be modified as

$$<\hat{\mathbf{C}}(\phi+\Delta\phi)> = <\hat{\mathbf{C}}(\phi)> - \frac{\Delta V}{V_0}(\hat{\mathbf{C}}^I - <\hat{\mathbf{C}}(\phi)>)\hat{\mathbf{A}}^{(2)}. \tag{2.40}$$

Substituting Eq. (2.38) into Eq. (2.40) gives the differential equation as

$$\frac{d<\hat{\mathbf{C}}>}{d\phi} = \frac{1}{1-\phi}(\hat{\mathbf{C}}^I - <\hat{\mathbf{C}}>)\hat{\mathbf{A}}^{(2)}. \tag{2.41}$$

2.4.7. The Mori-Tanaka theory

The effective moduli in the dilute distribution is given in Eq. (2.32), which is given by

$$<\hat{\mathbf{C}}>=\hat{\mathbf{C}}^{M}+\phi(\hat{\mathbf{C}}^{I}-\hat{\mathbf{C}}^{M})\hat{\mathbf{A}}$$

The localization tensors $\hat{\mathbf{A}}$ and $\hat{\mathbf{B}}$ are explained in Eqs. (2.12) and (2.13), and the strain and stress in the inclusion are given by

$$<\hat{\mathbf{E}}^{I}>=\hat{\mathbf{A}}^{(2)}<\hat{\mathbf{E}}>=\hat{\mathbf{A}}^{(2)}\hat{\mathbf{E}}^{0},$$

and

$$<\hat{\mathbf{T}}^{I}>=\hat{\mathbf{B}}^{(2)}<\hat{\mathbf{T}}>=\hat{\mathbf{B}}^{(2)}\hat{\mathbf{T}}^{0}, \tag{2.42}$$

where $\hat{\mathbf{E}}^{0}$ and $\hat{\mathbf{T}}^{0}$ are the prescribed uniform strain and stress, respectively, at the boundary of surface of inclusion. Let's assume that the RVE contains one inclusion of which the boundary of the inclusion is S' and the boundary of RVE is S. The boundary condition at the inclusion S' is given by

$$\mathbf{u}(S')=\mathbf{E}^{1}\mathbf{x}. \tag{2.43}$$

and the boundary condition at the RVE is given by

$$\mathbf{u}(S)=\mathbf{E}^{0}\mathbf{x}, \tag{2.44}$$

where $\mathbf{E}^{1}$ is the prescribed strain at the boundary of surface of the RVE in three dimensions. Note that the letter with a hat indicates the six dimensions. Assume that the

averaged strain of inclusion $<\hat{\mathbf{E}}^I>$ has the linear dependence to the averaged strain of the matrix $<\hat{\mathbf{E}}^M>$ as

$$<\hat{\mathbf{E}}^I>=T<\hat{\mathbf{E}}^M>. \tag{2.45}$$

The value T can be obtained from boundary conditions, Eqs. (2.43) and (2.44). The overall strain of the RVE $<\hat{\mathbf{E}}>$ is expressed as the following, and at the boundary of the RVE, the overall strain of the RVE $<\hat{\mathbf{E}}>$ is equal to the uniform strain $\hat{\mathbf{E}}^0$,

$$<\hat{\mathbf{E}}>=(1-\phi)<\hat{\mathbf{E}}^M>+\phi<\hat{\mathbf{E}}^I>=\hat{\mathbf{E}}^0. \tag{2.46}$$

Substituting Eq. (2.45) into Eq. (2.46) simplifies,

$$<\hat{\mathbf{E}}^M>=((1-\phi)+\phi T)^{-1}\hat{\mathbf{E}}^0, \tag{2.47}$$

and substituting Eq. (2.47) into Eq. (2.45) and comparing with Eq. (2.42), the tensor $\hat{\mathbf{A}}^{(2)}$ is obtained as

$$\hat{\mathbf{A}}^{(2)}=T((1-\phi)+\phi\cdot T)^{-1}. \tag{2.48}$$

Thus, the overall effective elasticity tensor estimated by Mori-Tanaka method will be

$$<\hat{\mathbf{C}}>=\hat{\mathbf{C}}^M+\phi(\hat{\mathbf{C}}^I-\hat{\mathbf{C}}^M)T((1-\phi)+\phi\cdot T)^{-1}. \tag{2.49}$$

2.4.8. The effective moduli of periodic distribution

The effective moduli of the periodic structure are estimated similarly by replacing the disturbance strain $\hat{\mathbf{E}}^d$ into the periodic strain $\hat{\mathbf{E}}^P$. The periodic strain $\hat{\mathbf{E}}^P$

has the similar physical meaning as the disturbance strain $\hat{\mathbf{E}}^d$ of the dilute distribution, but the relation between the periodic strain $\hat{\mathbf{E}}^P$ and the eigenstrain $\hat{\mathbf{E}}^*$ is defined differently from that between the dilute disturbance strain $\hat{\mathbf{E}}^d$ and the eigenstrain $\hat{\mathbf{E}}^*$. The relation between the periodic strain $\hat{\mathbf{E}}^P$ and the eigenstrain $\hat{\mathbf{E}}^*$ are given by (See Eqs. (12.4.2 a, b), (12.4.10a) and (12.4.22a) in Netmat-Nasser and Hori 1999),

$$F\hat{\mathbf{E}}^P(\xi) = F\hat{\mathbf{S}}^P(\xi) \cdot F\hat{\mathbf{E}}^*(\xi), \tag{2.50}$$

where ξ is the newly defined variable. $F\hat{\mathbf{E}}^P(\xi)$ is the Fourier series expansion of $\hat{\mathbf{E}}^P$ and $F\hat{\mathbf{S}}^P(\xi)$ is the Fourier series expansion of the periodic operator $\hat{\mathbf{S}}^P(\xi)$ that has the similar physical meaning as the Eshelby tensor $\hat{\mathbf{S}}^E$ in the dilute distribution. $F\hat{\mathbf{E}}^*(\xi)$ is the Fourier series expansion of the eigenstrain $\hat{\mathbf{E}}^*(\xi)$. Note that, in the dilute distribution, the disturbance strain, $\hat{\mathbf{E}}^d$, is expressed by the Eshelby tensor $\hat{\mathbf{S}}^E$ and the eigenstrain $\hat{\mathbf{E}}^*(x)$ as

$$\hat{\mathbf{E}}^d(x) = \hat{\mathbf{S}}^E \cdot \hat{\mathbf{E}}^*(x). \tag{2.51}$$

The inverse of Fourier series expansion $F\hat{\mathbf{E}}^P(\xi)$ writes Eq. (2.50) in terms of the eigenstrain $\hat{\mathbf{E}}^*(x)$,

$$F\hat{\mathbf{E}}^P(\xi) = F\hat{\mathbf{S}}^P(\xi) \cdot \frac{1}{V}\int_V \hat{\mathbf{E}}^*(x)\exp(-i\xi x)dV_x, \tag{2.52}$$

where x in the exponential indicates the direction of periodicity of Fourier series. The eigenstrain $\hat{\mathbf{E}}^*(x)$ is not a function of x any longer when x is in the inclusion, The

eigenstrain $\hat{\mathbf{E}}^*(x)$ in Eq. (2.52) is replaced by $\hat{\mathbf{E}}^*$,

$$F\hat{\mathbf{E}}^P(\xi) = F\hat{\mathbf{S}}^P(\xi)\cdot\hat{\mathbf{E}}^*\cdot\frac{\Omega}{V}\frac{1}{\Omega}\int_\Omega \exp(-i\xi x)dV_x . \tag{2.53}$$

The Fourier series, $\hat{\mathbf{E}}(x) = \sum_\xi{}' F\hat{\mathbf{E}}(\xi)\exp(ix\xi)$ is applied to Eq. (2.53) and the volume fraction $\phi = \frac{\Omega}{V}$ is introduced,

$$\hat{\mathbf{E}}^P(x) = \sum_\xi{}' F\hat{\mathbf{S}}^P(\xi)\cdot\hat{\mathbf{E}}^*\cdot\phi\frac{1}{\Omega}\int_\Omega \exp(-i\xi x')dV_{x'}\exp(i\xi x). \tag{2.54}$$

Take the volume average of the periodic strain $\hat{\mathbf{E}}^P(x)$ over the inclusion Ω,

$$\frac{1}{\Omega}\hat{\mathbf{E}}^P(x)dV_x = \sum_\xi{}' F\hat{\mathbf{S}}^P(\xi)\cdot\hat{\mathbf{E}}^*\cdot\phi\frac{1}{\Omega}\int_\Omega \exp(-i\xi x')dV_{x'}\frac{1}{\Omega}\int_\Omega \exp(i\xi x)dV_x . \tag{2.55}$$

We define the g-integral as $g(\xi) \equiv \frac{1}{\Omega}\int_\Omega \exp(i\xi x)dV_x$,

$$\frac{1}{\Omega}\int_\Omega \hat{\mathbf{E}}^P(x)dV_x = \phi\sum_\xi{}' F\hat{\mathbf{S}}^P(\xi)\,g(\xi)\,g(-\xi)\hat{\mathbf{E}}^* . \tag{2.56}$$

The left side of Eq. (2.56) is replaced by the relation $\frac{1}{\Omega}\int_\Omega \hat{\mathbf{E}}^P(x)dV_x \equiv \hat{\mathbf{S}}^P\cdot\hat{\mathbf{E}}^*$,

$$\hat{\mathbf{S}}^P\cdot\hat{\mathbf{E}}^* = \phi\sum_\xi{}' F\hat{\mathbf{S}}^P(\xi)\cdot g(\xi)\cdot g(-\xi)\hat{\mathbf{E}}^* . \tag{2.57}$$

Then the periodic operator $\hat{\mathbf{S}}^P$ is obtained as

$$\hat{\mathbf{S}}^P = \sum_\xi{}' \phi\cdot g(-\xi)\cdot g(\xi)\cdot F\hat{\mathbf{S}}^P(\xi). \tag{2.58}$$

By replacing the Eshelby tensor $\hat{\mathbf{S}}^E$ into the periodic operator $\hat{\mathbf{S}}^P$ in the Eq. (2.32), the effective elasticity tensor for the periodic distribution is given by

$$\hat{\mathbf{C}}^{eff} = \hat{\mathbf{C}}\cdot(\hat{\mathbf{1}} - \phi(\hat{\mathbf{A}}^I - \hat{\mathbf{S}}^P)^{-1}). \tag{2.59}$$

2.5. Conclusion

The reviewed methods to estimate the effective moduli are used to calculate (1)

the elastic constants for three hierarchical levels of bone matrix (Chapter 3), (2) the poroelastic constants for the lacunar-canalicular porosity level in cortical bone (Chapter 4).

Chapter 3

The estimated elastic constants for a single osteonal lamella

Abstract

Estimates are presented here of the elastic constants at the level of a collagen fibril whose diameter is the order of 20 nm, of a collagen fiber whose diameter is the order 80 nm, and a single lamella, which is composed of multiple collagen fibers' layers; the thickness of one collagen fiber layer is the order of 130 nm. These estimates are obtained by using micromechanical models. These results provide the database for building mathematical or computational models for the bone micro-fracture, the bone microdamage, or the bone fluid flow.

3.1. Introduction

A single lamella of osteon is a hierarchical composite of collagens and mineral crystals. The first structural level in a lamella is a collagen fibril, which is composed of collagen molecules. A single collagen molecule is 300 nm long. There is a 40 nm gap between one collagen molecule end and the next collagen molecule end in the longitudinal direction of a collagen fibril, and 27 nm of a 300 nm collagen molecule length is overlapped with the adjacent collagen molecule within a collagen fibril. The length, 67 nm in Figure 3.1(a) indicates both 40 nm gap and 27 nm overlapped length of a collagen molecule within the collagen fibril. Platelet-shape-crystals in the gaps form in the collagen fibril start to grow (Figure 3.1(b)). Platelets fuse into larger and thicker plates as long as 50 to 70 nm, and those are distributed quasi-periodically in the collagen

fibril (Figure 3.1(c)). The collagen fibril containing platelet shape crystals is called the mineralized collagen fibril. The crystals grow to the outside of collagen fibrils in all directions and surround a group of collagen fibrils. A group of collagen fibrils embedded in the mineral crystals forms the next hierarchical structural unit in a lamella, the collagen fiber (Figure 3.1(d)). The crystal plates in the collagen fibers grow as large as 500 nm in length and 80 nm in thickness (Figure 3.1(e)), the space between crystal-platelets gradually disappears. The collagen fibers are fully surrounded by the mineral-crystals. The thickness of the plate, which contains an aggregate of collagen fibers embedded in the mineral-crystals, increases to 130nm (Figure 3.1(f)). This plate is one array of a lamella in the bone (Figure 3.1(g)) (Siperko and Landis 2001).

A single lamella consists of not only collagens and mineral crystals but also water. The volume fraction of water for the human cortical bone is reported as 23.9% and that for the cancellous bone is 27% (Gong et al. 1964). The excess water of the specimen was removed by centrifuging at 8,000 g for 15 minutes and the mass of the specimen was measured in air. The specimen was dried for 72 hours at 80°C and the mass of the specimen was measured. The mass of water is calculated by comparing the mass measured after the specimen was centrifuged and that measured after the specimen was dried, and then the volume of water is calculated from the mass of water divided by the density of the human cortical bone. Biltz and Pellegrino (1969) also measured the volume fractions of each component, which are different from those of Gong et al. (1964). They measured the water content of human cortical bone to be 15.5% by volume (Table 3.1). Gong et al. (1964) measured the mineral fraction including the volatile inorganic fraction (Table 3.1) is approximately 42% by volume, where the organic fraction is 34% by

volume. Biltz and Pellegrino (1969) measured less mineral volume fraction than Gong et al. (1964); the mineral volume fraction determined by Gong et al. (1964) is approximately 39.9% and the volume fraction of organic and CO_2 is 41.8%. Fernandez-Seara et al. (2002) suggested that the bound water may be associated with the mineral phase, or bound to the organic phase, or free. The bound water is not all fluid inside the bone.

Cowin (1999) explained that the bone fluid is filled in three levels of porosity. The largest porosity is the vascular canals (or called the vascular porosity, the radius of the vascular canal is the order of 20 μm) that contain one or two blood vessels, a nerve, and some space occupied by bone fluid. On the wall of the vascular canals, the bone cells form a confluent lining and they are connected to osteocytes (other bone cells) in the lacunae, the ellipsoidal space (approximately 25 μm by 10 μm by 5 μm in shape), by small tunnels (0.2 μm to 0.4 μm in diameter), so called "canaliculi." The space within the canaliculi and lacunae is called the lacunar-canalicular porosity; it is the porosity with the second largest pore diameters in the bone. The smallest pore diameter porosity is the space between the collagen fiber and the mineral, hydroxyapatite. The water in the collagen-hydroxyapatite porosity is bound by interaction with the ionic crystals (Neuman et al. 1953; Neuman and Neuman, 1958), and it is called the bound water.

The elastic constants at the lamellar level were estimated by theoretical models and measured by experimental techniques (Akiva et al. 1997, 1998; Bonfield and Li,1966; Crolet et al. 1993; Currey 1964; Fan et al., 2002; Hellmich and Ulm, 2002; 2004; Katz 1971; Piekarski, 1973; Rho et al., 1993, 1997, 1999a, 1999b, 1999c, 2002; Sasaki et al., 1991; Swadener et al., 2001;Wagner and Weiner, 1992; Zysset et al., 1999), but none of

references provided the full set of the anisotropic elastic constants of a lamella except the work of Hellmich et al. (2002, 2004). Crolet et al. (1993) reported only the anisotropic elastic constants at the level of an osteon, which is the cylindrical lamellar structure in the cortical bone by using the homogenization theory. In early composite models of bone (Bonfield and Li, 1966; Currey 1964; Katz 1971), the elastic constants are calculated by simple composite models, such as the Voigt and Reuss models. The Voigt bounds are obtained by assuming that the boundary of the representative volume element (RVE) is prescribed by the uniform strain and those in the Reuss bounds are obtained by assuming that the uniform stress is prescribed at the boundary of the RVE. The Hirsch model, which combines the Voigt and the Reuss bounds in a linear way, was proposed for a bone by Piekarski (1973). The platelet-shape-mineral reinforced composite model based on the Halpin-Tsai equations (1967) was employed by several investigators (Akiva et al., 1997, 1998; Wagner and Weiner, 1992) based upon the assumption that the mineral is a platelet shaped (Eppell et al. 2001; Currey et al. 1994; Landis et al. 1991, 1993, 1996; Siperko and Landis 2001; Traub et al. 1989; Weiner et al. 1991, 1992). Hellmich et al. (2002, 2004) used the self-consistent method to estimate the elastic constant of bone matrix. However Hellmich et al. (2002, 2004) assumed the shape of hydroxyapatite is spherical, which is not true (Eppell et al. 2001; Currey et al. 1994; Landis et al. 1991, 1993, 1996; Siperko and Landis 2001; Traub et al. 1989; Weiner et al. 1991, 1992).

3.2. The model description

Bound water surrounds both collagen molecules and mineral crystals. The elastic constants of both collagens and minerals with their associated bound water are calculated by averaging of the estimates from the Voigt and Reuss bounds in Step 1 (Figure 3.2).

The elastic constants of the mineralized collagen fibril that is composed of the collagen molecules and the platelet-shape hydroxyapatite-mineral-crystals are calculated in Step 2 (Figure 3.2). The elastic constants of the collagen-water-composite and the hydroxyapatite-mineral-water-composite, estimated in Step 1 of Figure 3.2, are used instead of the elastic constants of collagen molecules and hydroxyapatite-mineral-crystals since the collagen molecule is associated with water as are the hydroxyapatite-minerals. The platelet-shape-hydroxyapatite-mineral-water-composites fuse to the outside of collagen fibrils and the collagen fibrils are surrounded by the hydroxyapatite-mineral-water-composites, which form a collagen fiber, Step 3 (Figure 3.2). Larger aggregates of hydroxyapatite-water composites are formed at the outside of the collagen fibers, and the ensemble constitutes one collagen fibers' array (or layer) in a single lamella in Step 4 (Figure 3.2). The elastic constants estimated at each Step (Steps 2, 3, and 4) are indicated in Table 3.3.

3. 3. Methods

3. 3. 1. Calculation of the effective elastic constants of the collagen-water composite and the hydroxyapatite-water composite by using the Voigt and Reuss bounds (Step 1 in Figure 3.2)

The elastic constants of the collagen-water composite and the hydroxyapatite-mineral-water composite are calculated by the Voigt and Reuss bounds. We adopt here the observation of Fernadez-Seara et al. (2002, 2004) that both the collagen and the minerals are associated with the bound water.

The Young's modulus E_c and Poisson's ratio ν_c for the collagen are 1.2 GPa and 0.35, and those (E_h and ν_h) for hydroxyapatite minerals are 114 GPa and 0.28, respectively (Katz 1971; Crolet et al. 1993). The shear modulus G for both the collagen and the hydroxyapatite is obtained by

$$G = \frac{E}{2(1+\nu)}.$$

The given elastic constants of both collagen and hydroxapatite mineral are tabulated in Table 3.2. Note that the elastic constants of the hydroxyapatite minerals are assumed to be isotropic because the anisotropic elastic constants of the hydroxyapatite minerals in the human bone are not yet known even though the hydroxyapatite-mineral-crystals are known to have the hexagonal symmetry. The volume fractions of each component – water, collagen, and minerals – are taken from Gong et al. (1964) and Biltz and Pellgrino (1969) and the values are shown in Table 3.1.

First, the elastic constants are obtained by using the rule of mixture for the Voigt bound as

$$\hat{\mathbf{C}}_{c.w} = (1-\phi_{wc})\hat{\mathbf{C}}_c + \phi_{wc}\hat{\mathbf{C}}_w$$

and

$$\hat{\mathbf{C}}_{h.w} = (1-\phi_{wh})\hat{\mathbf{C}}_h + \phi_{wh}\hat{\mathbf{C}}_w \tag{3.1}$$

where $\hat{\mathbf{C}}_{c.w}$ is the effective elasticity tensor for the collagen-water composite, $\hat{\mathbf{C}}_{h.w}$ is the effective elasticity tensor for the hydroxyapatite-water composite, $\hat{\mathbf{C}}_c$ is the elasticity tensor for the collagen, $\hat{\mathbf{C}}_h$ is the elasticity tensor for the hydroxyapatite, ϕ_{wc} is the water volume fraction in the collagen-water composite, ϕ_{wh} is the water volume fraction in the

hydroxapatite-water composite, and $\hat{\mathbf{C}}_w$ is the elasticity tensor of the water, respectively. It was assumed that the water volume fraction in the collagen-water composite, ϕ_{wc} is set equal to that in the hydroxyapatite-water composite, ϕ_{wh}. Similarly, the compliance tensor, which is the inverse of the elasticity tensor ($\hat{\mathbf{S}} = \hat{\mathbf{C}}^{-1}$), is obtained by using the rule of mixture for the Reuss model as

$$\hat{\mathbf{S}}_{cw} = (1-\phi_{wc})\hat{\mathbf{S}}_c + \phi_{wc}\hat{\mathbf{S}}_w,$$

and

$$\hat{\mathbf{S}}_{hw} = (1-\phi_{wh})\hat{\mathbf{S}}_h + \phi_{wh}\hat{\mathbf{S}}_w \tag{3.2}$$

where $\hat{\mathbf{S}}_{cw}$ is the effective compliance tensor for the collagen-water composite, $\hat{\mathbf{S}}_{hw}$ is the effective compliance tensor for the hydroxyapatite-water composite, $\hat{\mathbf{S}}_c$ is the compliance tensor for the collagen, $\hat{\mathbf{S}}_h$ is the compliance tensor for the hydroxyapatite, and $\hat{\mathbf{S}}_w$ is the compliance tensor of the water, respectively. A compliance tensor for the bound water was obtained from the known bulk modulus of water K_f (2.3 GPa). To formulate the compliance tensor, we assume that the Poisson's ratio for the bound water is 0.4999. The shear modulus for the bound water obtained with this assumption is 0.9 MPa, which is three orders smaller than the bulk modulus of the water. Similarly, the Young's modulus for the bound water is estimated to be 2.7 MPa, which is also three orders smaller than the bulk modulus of the water. Thus it is believed that increments in both Young's modulus and Shear modulus are not significant compared to the bulk modulus of water.

3. 3. 2. Calculation of the effective elastic constants of the mineralized collagen fibrils

In this section, the elastic constants of collagen fibrils with the platelet-shape-hydroxyapatite-minerals are determined. It is assumed that the platelet-shape-hydroxyapatite-minerals are periodically distributed along the long axes of collagen fibrils. The bound water is assumed to be associated with both the hydroxyapatite-mineral-crystals and the collagen molecules so that the elastic constants of the hydroxyapatite–water composite and those of the collagen–water composite are used instead of the collagen and hydroxyapatite. The effective elasticity tensor for the periodically distributed platelet reinforced composite is calculated by (page 441 in Nemat-Nasser and Hori, 1999),

$$\hat{\mathbf{C}}_{p.c} = \hat{\mathbf{C}}_{c.w} \cdot \{\hat{\mathbf{1}} - \phi_{p.c}((\hat{\mathbf{C}}_{c.w} - \hat{\mathbf{C}}_{h.w})^{-1} \cdot \hat{\mathbf{C}}_{c.w} - \hat{\mathbf{S}}^{P}_{p.c})^{-1}\}, \tag{3.3}$$

where $\hat{\mathbf{C}}_{p.c}$ is the effective elasticity tensor of the platelet-shape-reinforced composite, $\hat{\mathbf{C}}_{c.w}$ is the elasticity tensor of the collagen-water composite obtained in the previous section, $\hat{\mathbf{C}}_{h.w}$ is the elasticity tensor of the hydroxyapatite-water composite obtained in the previous section, $\hat{\mathbf{1}}$ is the identity tensor in six dimensions, $\phi_{p.c}$ is the volume fraction of the platelet-shape-hydroxyapatite-minerals in the mineralized collagen fibril, and $\hat{\mathbf{S}}^{P}_{p.c}$ is the periodic operator for the platelet shape hydroxyapatite-water composite (See Eqs (12.5.6b) and (12.5.9b) on page 440 and 441 in Nemat-Nasser and Hori 1999) , which is given by

$$\hat{\mathbf{S}}^{P}_{ijkl} = \frac{1}{2}\left[\delta_{il}\mathbf{S}_{I(j,k)} + \delta_{ik}\mathbf{S}_{I(j,l)} + \delta_{jl}\mathbf{S}_{I(i,k)} + \delta_{jk}\mathbf{S}_{I(i,l)}\right]$$

$$-\frac{1}{1-\nu}\mathbf{S}_{I(i,j)J(k,l)}+\frac{\nu}{1-\nu}\delta_{kl}\mathbf{S}_{I(i,j)}, \tag{3.4}$$

for the faster numerical calculation, where

$$\mathbf{S}_{I(i,j)}=\sum_{\xi}{}'\phi\, g(\xi)\, g(-\xi)\, h_{I(i,j)}(\xi) \text{ and } \mathbf{S}_{IJ(i,j)}=\sum_{\xi}{}'\phi\, g(\xi)\, g(-\xi)\, h_{IJ(i,j)}(\xi). \tag{3.5}$$

Note that $\mathbf{S}^{P}_{p.c}$ has the dimension of stress. The terms $h_I(\xi)$ and $h_{IJ}(\xi)$ in Eq. (3.5) are defined as (Nemat-Nasser et al. 1982; Iwakuma and Nemat-Nasser 1983; Nemat-Nasser and Hori 1999)

$$h_1(\xi)=(\bar{\xi}_1)^2,\ h_2(\xi)=(\bar{\xi}_2)^2,\ h_3(\xi)=(\bar{\xi}_3)^2,$$

$$h_4(\xi)=\bar{\xi}_2\bar{\xi}_3,\ h_5(\xi)=\bar{\xi}_3\bar{\xi}_1,\ h_6(\xi)=\bar{\xi}_1\bar{\xi}_2,$$

and

$$h_{I(i,j)J(i,j)}(\xi)=h_{I(i,j)}(\xi)\,h_{J(i,j)}(\xi),\ \text{for I, J =1, 2, 3, ... 6,} \tag{3.6}$$

where $\bar{\xi}=\xi/|\xi|$. $I(i,j)$ (or $J(i,j)$) in Eqs. (3.4), (3.5), and (3.6) are replaced by the following relations: $I(1,1)$, $I(2,2)$, $I(3,3)$, $I(2,3)$, $I(1,3)$, and $I(1,2)$ correspond to 1, 2, 3, 4, 5, and 6, respectively. The prime on the summation indicates that $\xi=0$ is excluded, and the new variable ξ is defined as $\xi\equiv\frac{n_i\pi}{a_i}$, where n_i is the number of unit cells in the i-direction and i can be replaced with x, y, z for x-, y-, and z- direction, respectively. The domain of unit cell that contains one platelet is $U=\{x;-a_i<x_i<a_i\ (i=x,y,z)\}$. The g-integral $g(\xi)$ in Eq. (3.5) is the volume average of $\exp(i\xi\cdot x)$ over the inclusion and the g-integral for the platelet shape (or cuboidal) inclusion is given by (Nemat-Nasser et al., 1993; Nemat-Nasser and Hori 1999)

$$g(\xi)=\frac{\sin L_x \sin L_y \sin L_z}{L_x L_y L_z}, \tag{3.7}$$

where L_i is

$$L_i = \xi_i l_i, \tag{3.8}$$

and where the subscript i is replaced by x, y, and z to indicate three perpendicular directions, and l_i is the dimension of the platelet mineral crystals, i.e., l_x=3 nm, l_y=25 nm, and l_z=50 nm (Rho et al. 1998). n_x, n_y, and n_z are the number of platelet mineral crystals in the x, y, and z direction, respectively, and note that the summation in Eq. (3.5) with respect to ξ (or n_x, n_y, and n_z) is generally from 1 to infinity, but in this study, the summation is performed from one to ±50 because the summation up to ± 40 is only 0.7% less than that to ±50 (Nemat-Nasser et al. 1982).

3. 3. 3. Calculation of the effective elastic constants of collagen fiber that is composed of mineralized collagen fibrils

The effective elasticity tensor of the collagen fiber is calculated by using the formula (Nemat-Nasser and Hori, 1999),

$$\hat{\mathbf{C}}_{c.f} = \hat{\mathbf{C}}_{h.w} \cdot \{\hat{\mathbf{1}} - \phi_{c.f}((\hat{\mathbf{C}}_{h.w} - \hat{\mathbf{C}}_{p.c})^{-1} \cdot \hat{\mathbf{C}}_{h.w} - \hat{\mathbf{S}}^{P}_{c.f})^{-1}\}, \tag{3.9}$$

where $\hat{\mathbf{C}}_{c.f}$ is the effective elasticity tensor of the collagen fiber, $\phi_{c.f}$ is the volume fraction of collagen fibrils, and the periodic operator for the mineralized collagen fibers $\hat{\mathbf{S}}^{P}_{c.f}$ are given by

$$\hat{\mathbf{S}}^{\mathrm{P}} = \sum_{\xi}{}' \phi\, g(-\xi)\, g(\xi)\, F\hat{\mathbf{S}}^{\mathrm{P}}(\xi). \tag{3.10}$$

The term $F\hat{\mathbf{S}}^{\mathbf{P}}(\xi)$ in (3.10) above is the Kelvin second rank tensor (See Appendix 3) for the anisotropic symmetry, which will be converted from the fourth rank tensor $F\mathbf{S}^{\mathbf{P}}(\xi)$ that was given in Nemat-Nasser and Hori (1999) (Eq. 12.5.4a on Page 431 in Nemat-Nasser and Hori 1999) as

$$F\mathbf{S}^{P}(\xi) = sym\{\xi \otimes (\xi \cdot C_{h.w} \cdot \xi)^{-1} \otimes \xi) : C_{h.w}, \tag{3.11}$$

where $C_{h.w}$ is the fourth rank elasticity tensor of the hydroxyapatite-water composite obtained in the section 3.3.1. Since the elasticity tensor obtained in the previous section, $\hat{\mathbf{C}}_{p.c}$, reflects the orthotropic symmetry, Eq. (3.10) is used instead of Eq. (3.4). The term $(\xi \cdot C \cdot \xi)$ in Eq. (3.11) is expanded in the index notation as

$$\begin{aligned}(\xi_i C_{ijkl} \xi_l) = {} & \xi_1 C_{1jk1} \xi_1 + \xi_1 C_{1jk2} \xi_2 + \xi_1 C_{1jk3} \xi_3 \\ & + \xi_2 C_{2jk1} \xi_1 + \xi_2 C_{2jk2} \xi_2 + \xi_2 C_{2jk3} \xi_3 \\ & + \xi_3 C_{3jk1} \xi_1 + \xi_3 C_{3jk2} \xi_2 + \xi_3 C_{3jk3} \xi_3 .\end{aligned} \tag{3.12}$$

The inverse of the second rank tensor $(\xi_i C_{ijkl} \xi_l)$ is calculated and another fourth rank tensor, $\xi_i (\xi_p C_{pjkq} \xi_q)^{-1} \xi_l$, is formed. The fourth rank tensor $F\mathbf{S}^{\mathbf{P}}(\xi)$ is obtained by the contraction of this result with the elasticity tensor of the hydroxyapatite-water composite, $C_{h.w}$, and converted into the Kelvin second rank tensor $F\hat{\mathbf{S}}^{\mathbf{P}}(\xi)$ (See Appendix 3 for the relationship between the Kelvin notation and the Voigt notation). The g-integral, $g(\xi)$ for the circular cylindrical shape of the mineralized collagen fibrils, is given by (Nemat-Nasser et al. 1993)

$$g(\xi)=\begin{cases}\dfrac{2}{B}J_1(y) & \text{if } n_3=0\\ 0 & \text{if } n_3\neq 0\end{cases}, \tag{3.13}$$

where J_1 is the order 1 Bessel function of the first kind, and

$$B=2\pi(n_x^2+n_z^2)^{1/2}\sqrt{\frac{\phi_{c.f}}{\pi}}. \tag{3.14}$$

n_x and n_z are the number of cylindrical inclusions in the x and z directions, respectively.

3. 3. 4. Calculation of the effective elastic constants of a single lamella that contains collagen fibers

The effective moduli of a single lamella that contains the cylindrical shape collagen fibers embedded in the hydroxyapatite mineral-water composite are calculated by using the formula (Nemat-Nasser and Hori, 1999),

$$\hat{\mathbf{C}}_l=\hat{\mathbf{C}}_{h.w}\cdot\{\hat{\mathbf{1}}-\phi_l((\hat{\mathbf{C}}_{h.w}-\hat{\mathbf{C}}_{c.f})^{-1}\cdot\hat{\mathbf{C}}_{h.w}-\hat{\mathbf{S}}_l^P)^{-1}\}, \tag{3.15}$$

where $\hat{\mathbf{C}}_l$ is the effective elasticity tensor of a single lamella and ϕ_l is the volume fraction of collagen fibers. The periodic operator $\hat{\mathbf{S}}_l^P$ for a cylindrical shape of collagen fibers is obtained by the same manner in the previous section; all collagen fibers in a lamella are assumed to be aligned in the longitudinal direction. The estimated elastic constants for the mineralized collagen fibril, the collagen fiber, and a single lamella are shown in Table 3.3.

3.4. Steps of calculation

Step 1

Calculate the effective elasticity tensor $\hat{\mathbf{C}}_{c.w}$ for the collagen-water composite, i.e., collagens associated with the water, and that $\hat{\mathbf{C}}_{h.w}$ for the hydroxyapatite mineral – water composite, i.e., hydroxapatite minerals associated with the water. The effective elasticity tensors are estimated by averaging the estimates of the Voigt-Reuss bounds (Eqs.3.1 and 3.2). The compositional volume fractions are taken from Table 3.1 and the elastic constants for the collagen and the hydroxyapatite minerals are selected from Table 3.2. For the elasticity tensor (or the compliance tensor) for the water, it was assumed that the water is elastic material whose Poisson's ratio is very close to 0.5.

Step 2

Calculate the effective elasticity tensor $\hat{\mathbf{C}}_{p.c}$ of the mineralized collagen fibril that has the platelet-shape-hydroxyapatite–water composite by using Eq. (3.3). Both the elasticity tensor of the collagen-water composite, $\hat{\mathbf{C}}_{c.w}$, and that of the hydroxyapatite–water composite, $\hat{\mathbf{C}}_{h.w}$, are obtained in the step 1. The volume fraction of the platelet shape of hydroxyapatite minerals, $\phi_{p.c}$ in Eq. (3.3) is $(0.25\times V_{h.w}/(V_{c.w}+0.25\times V_{h.w})$ because 25% of hydroxyapatite minerals are deposited inside the fibrils (Lucchinetti, 2001; Rho et al. 1998).

Step 3

Calculate the effective elasticity tensor $\hat{\mathbf{C}}_{c.f}$ of the collagen fiber that contains the mineralized collagen fibrils embedded in the hydroxyapatite-water composite by using Eq. (3.9). The elasticity tensor of the mineralized collagen fibrils $\hat{\mathbf{C}}_{p.c}$ was estimated in the step 2. The volume fraction of the collagen fibrils, $\phi_{c.f}$ in Eq. (3.9) is

$(V_{c.w}+0.25\times V_{h.w})/(V_{c.w}+0.25\times V_{h.w}+0.75\times V_{h.w}/2)$ with assuming that the collagen fibrils are surrounded by a half of the extrafibrillar hydroxyapatite mineral-water composite, which is 75% of total hydroxyapatite mineral-water composite (Lucchinetti, 2001; Pidaparti et al. 1996; Rho et al. 1998).

Step 4

Calculate the effective elasticity tensor $\hat{\mathbf{C}}_l$ of a single lamella of which collagen fibers are aligned in the longitudinal direction and embedded in the hydroxyapatite-water composite by using Eq. (3.15). $\hat{\mathbf{C}}_{c.f}$ is the effective elasticity tensor of collagen fibers obtained in the step 3. The volume fraction ϕ_l in Eq. (3.15) is $(V_{c.w}+0.25\times V_{h.w}+0.75\times V_{h.w}/2)/(V_{c.w}+0.25\times V_{h.w}+0.75\times V_{h.w})$ because it is assumed that the rest of the hydroxyapatite mineral-water composite (37.5%) is located outside the collagen fibers (Lucchinetti, 2001; Pidaparti et al. 1996; Rho et al. 1998).

3.5. Results

The elastic constants at levels of a mineralized collagen fibril, a collagen fiber, and a single lamella are estimated by considering the bound water. Based on two sets of experimental data on compositional volume fraction in a human cortical bone (Table 3.1), full sets of orthotropic elastic constants for an osteonal lamella are calculated and shown in Table 3.3.

3.6. Discussion

This is the first study to quantify the elastic constants at three distinct and well recognized hierarchical levels of a mineralized collagen fibril, a collagen fiber, and a

single lamella. Nanoindentation has been used experimentally to determine the Young's modulus the nanoscale, but it is not possible to measure the shear modulus and Poisson's ratio with the nanoindentation method. In theoretical analyses, Akiva et al. (1998) and Wagner and Weiner (1992) calculated elastic constants of a bone matrix by using a platelet reinforced composite model. Their model only considers the mineral deposition inside the collagen fibrils and the model cannot predict the out-of-plane elastic constants. The homogenization method of Crolet et al. (1993) considered the mineral deposition only outside collagen fibers. The present study considers the mineral deposition both inside collagen fibers and outside collagen fibers. Similarly, Hellmich et al. (2002, 2004) estimated the bone matrix elastic constants by using the self-consistent method, but they assumed that the shape of deposited hydroxyapatite minerals to be spherical.

The literature is not unambiguous on the measured volume fraction of water. It was reported that the water volume fraction in the cortical bone matrix is 23.9% (Gong et al. 1964). These authors applied centrifugal acceleration 8,000 g for 15 minutes, but that may remove only the water volume fraction in the Haversian systems (or vascular porosity). Arnold and Tont (1967) suggested that the centrifugal acceleration 25,000 g is adequate to remove the water from Haversian systems and 1,500,000 g is to remove the water from the canaliculi (Ashman 1989). Biltz and Pellgrino (1969) measured the water volume fraction for the human cortical bone is 15.5%, which is less than that measured by Gong et al. (1964). If the water content measured by Gong et al. (1964) and Biltz and Pellgrino (1969) include the water content in the lacunar-canalicular porosity and the vascular porosity, the magnitude of the estimated bone matrix elastic constants will be increased. Figure 3.3 shows that the variation of elastic modulus against the water

volume fraction of the bone matrix, when the water volume fraction is less than 15% in the data of Biltz and Pellgrino (1969).

Even though the water content of Gong et al. (1964) is greater than that of Biltz and Pellgrino (1969), the estimated elastic constants from Gong et al. (1964) are close to those from Biltz and Pellgrino (1969) when the inorganic fraction of Gong et al. (1964) was removed. Table 3.3(a) shows the estimated elastic constants by using the data of Biltz and Pellegrino (1969) in Table 3.1. The water content was 15.5%, mineral content was 39.9%, and organic content with CO2 is 41.8%. The estimated elastic constants E_1, E_2, and E_3 are 16.371 GPa, 18.658 GPa, and 22.773 GPa (Table 3.3a). The data of Gong et al. (1964) have the water fraction, ash fraction, organic fraction, and volatile inorganic fraction. However it was not clear that the inorganic fraction is included in the mineral volume fraction. Thus the two cases are considered: the mineral volume fraction contains both the ash fraction and the volatile inorganic fraction (Table 3.3b), and the mineral volume fraction contains only the ash fraction (Table 3.3c). The estimated elastic constants for the first case are E_1= 19.020 GPa, E_2= 21.343 GPa, and E_3= 24.455 GPa, and those for the last case are E_1=16.883 GPa, E_2=19.021 GPa, and E_3=22.323 GPa, respectively. Interestingly, the estimated elastic constants from the data of Biltz and Pellegrino (1969) are close to those from the data of Gong et al. (1964) if the volatile inorganic volume fraction is not included into the hydroxyapatite mineral volume fraction. The elastic constants from the data of Biltz and Pellgrino (1969) may be reasonable estimation for the bone matrix.

The micromechanical method applied in this study (Iwakuama et al. 1983; Nemat-Nasser 1982; Nemat-Nasser et al. 1993; Nemat-Nasser and Hori 1999) satisfies the

Hashin and Shtrikman bounds. Nemat-Nasser et al. (1982) compared the effective moduli in the periodic distribution assumption to the Hashin and Shtrikman bounds. The bulk modulus of a medium with spherical cavities in the periodic distribution assumption overshoots the upper bound of Hashin and Shtrikman (1963) by about 1%. They explained that it may be the truncation error because the variable ξ was summed from -50 to 50 instead of from – infinity to + infinity because the sum to ± 40 provides an answer only 0.7% less than that to ± 50.

These estimated elastic constants for the bone matrix will provide a dataset for building a mathematical damage models as well as for estimating poroelastic constants for the lacunar-canalicular and the vascular porosity of an osteon (Chapter 4).

Table 3.1 Compositional volume fraction of the human cortical bone (NR: Not reported)

	Water content	Mineral ash	Volatile inorganic fraction	Organic	Organic+CO_2
Biltz and Pellegrino (1969)	15.5	39.9	NR	NR	41.8
Gong et al. (1964)	23.9	37.7	4.6	33.8	NR

Table 3.2 The technical elastic constants of the collagen and the hydroxyapatite minerals

	Collagen	Hydroxyapatite
E[GPa]	1.2	114
v	0.35	0.28
G[GPa]	0.469	44.531

Table 3.3 (a) The effective technical elastic constants of the mineralized collagen fibril (Step 2), the collagen fiber (Step 3), and a single lamella (Step 4) by using the data of Biltz and Pellegrino (1969)

	The mineralized collagen fibril (Step 1)	The collagen fiber (Step 2)	A single lamella (Step 3)
E_1[GPa]	3.351	11.309	16.371
E_2[GPa]	6.190	13.826	18.658
E_3[GPa]	7.687	16.944	22.773
ν_{12}	0.286	0.324	0.334
ν_{13}	0.201	0.230	0.237
ν_{21}	0.528	0.397	0.381
ν_{23}	0.214	0.242	0.247
ν_{31}	0.460	0.345	0.330
ν_{32}	0.266	0.297	0.301
G_{12}[GPa]	1.064	4.770	7.155
G_{13}[GPa]	1.043	4.711	7.064
G_{23}[GPa]	2.960	6.256	8.368

Table 3.3 (b) The effective technical elastic constants of the mineralized collagen fibril (Step 2), the collagen fiber (Step 3), and a single lamella (Step 4) by using the data of Gong et al. (1964)

	The mineralized collagen fibril (Step 1)	The collagen fiber (Step 2)	A single lamella (Step 3)
E_1[GPa]	4.528	13.571	19.020
E_2[GPa]	7.703	16.258	21.343
E_3[GPa]	9.266	18.893	24.455
ν_{12}	0.297	0.315	0.320
ν_{13}	0.214	0.243	0.252
ν_{21}	0.505	0.377	0.359
ν_{23}	0.225	0.255	0.261
ν_{31}	0.437	0.338	0.324
ν_{32}	0.271	0.296	0.299
G_{12}[GPa]	1.403	5.399	7.805
G_{13}[GPa]	1.375	5.379	7.761
G_{23}[GPa]	3.565	7.053	9.120

Table 3.3 (c) The effective technical elastic constants of the mineralized collagen fibril (Step 2), the collagen fiber (Step 3), and a single lamella (Step 4) by using the data of Gong et al. (1964) that the volume fraction of the volatile inorganic fraction is excluded from the mineral volume fraction

	The mineralized collagen fibril (Step 1)	The collagen fiber (Step 2)	A single lamella (Step 3)
E_1[GPa]	3.821	11.880	16.883
E_2[GPa]	6.587	14.299	19.021
E_3[GPa]	8.034	16.962	22.323
v_{12}	0.302	0.320	0.326
v_{13}	0.215	0.239	0.246
v_{21}	0.521	0.386	0.367
v_{23}	0.220	0.249	0.254
v_{31}	0.451	0.341	0.325
v_{32}	0.268	0.296	0.298
G_{12}[GPa]	1.162	4.811	7.081
G_{13}[GPa]	1.138	4.779	7.023
G_{23}[GPa]	3.091	6.308	8.286

Figure 3.1 A combined schematic of the hierarchal development of mineralized bone (Siperko and Landis 2001).

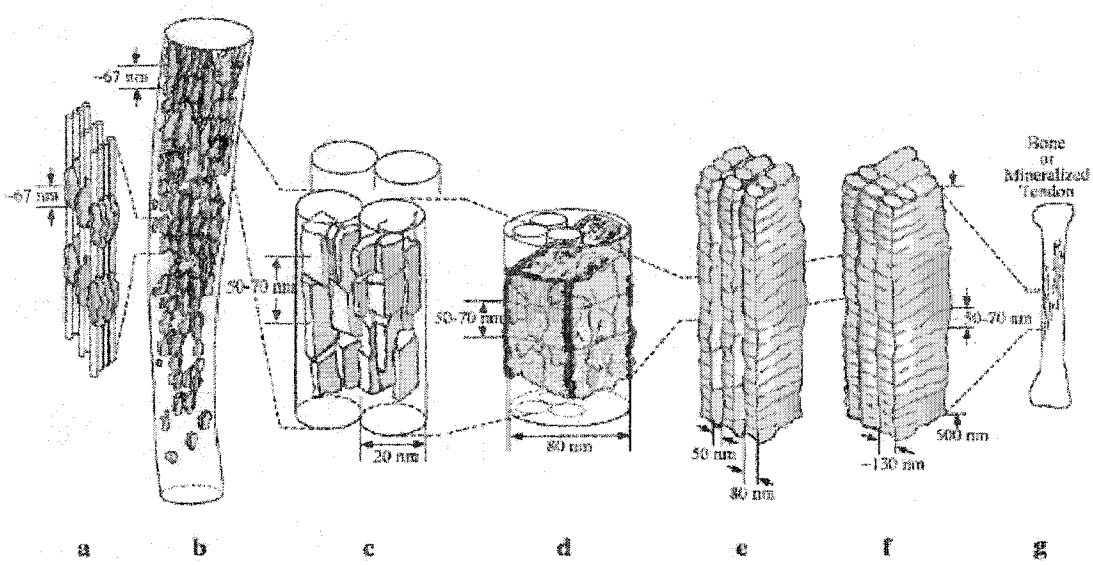

(a) The hydroxyapatite-mineral-crystals are deposited between the 300 nm long collagen molecules. The size 67 nm indicates the overlapped length 27nm with the adjacent collagen molecule and the 40nm gap between collagen molecule ends. (b) the platelet-shape-hydroxyapatite-minerals grow in the gap space within the collagen fibril. (c) the platelet-shape-hydroxyapatite-mineral-crystals grow as large as 50 to 70 nm in length. (d) the platelet-shape-hydroxyapatite-mineral-crystals fuse outside of collagen fibrils and a group of collagen fibrils are surrounded by the hydroxyapatite-mineral-crystals. The space between the platelet-shape-hydroxyapatite-mineral-crystals disappears and collagen fibrils are embedded in the hydroxyapatite-mineral-crystals. (e) the hydroxyapatite-mineral-crystals fuse outside of collagen fibers. The 50 nm thick hydroxyapatite-mineral-plate is formed between arrays of mineralized collagen fibers of which thickness is approximately 80 nm. (d) the mineralization continues and the mineralized collagen fibers are completely embedded in the hydroxyapatite-mineral-crystals.

Figure 3.2 Flow chart of calculation

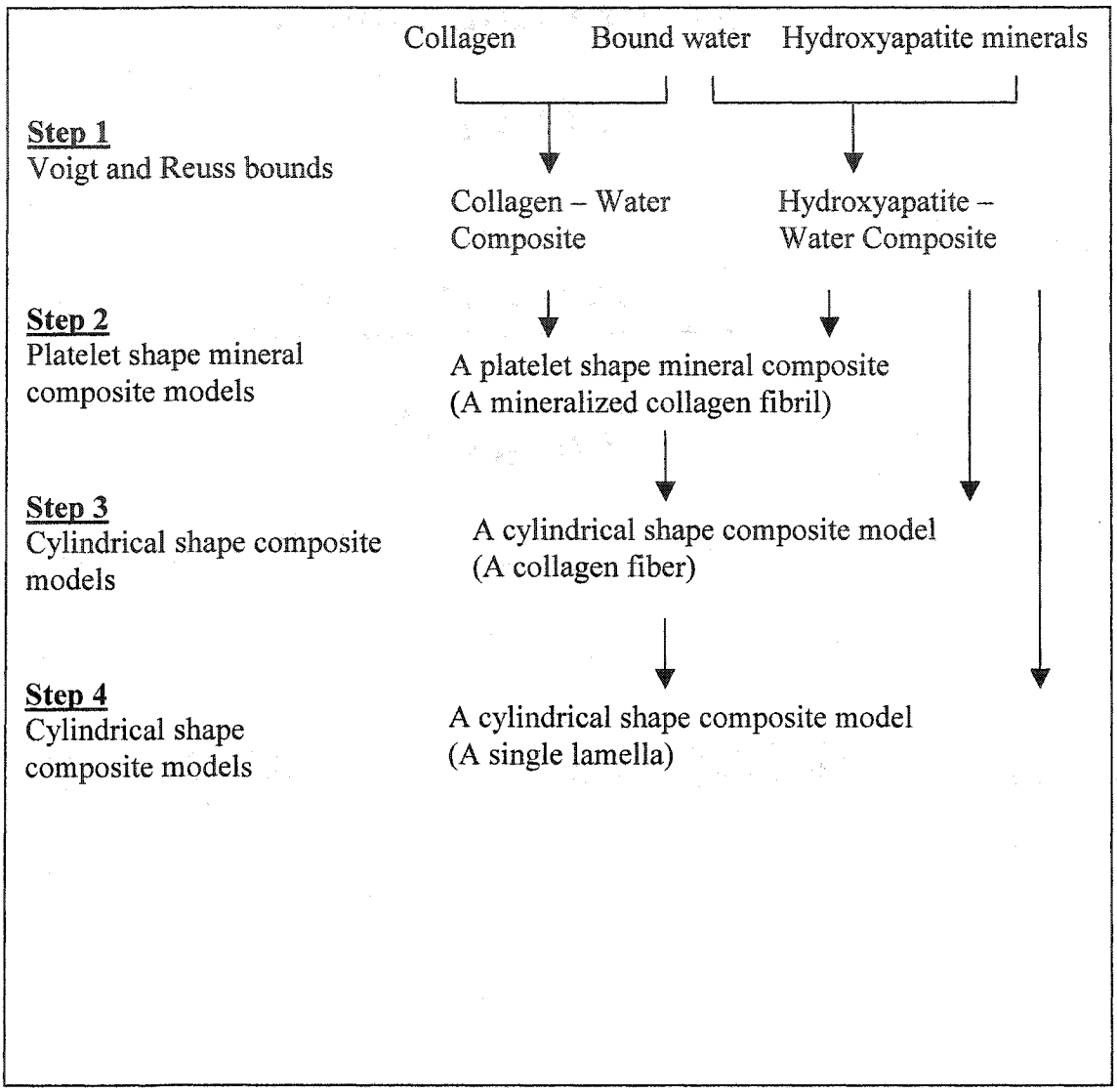

Figure 3.3 The variation of elastic modulus against the water volume fraction

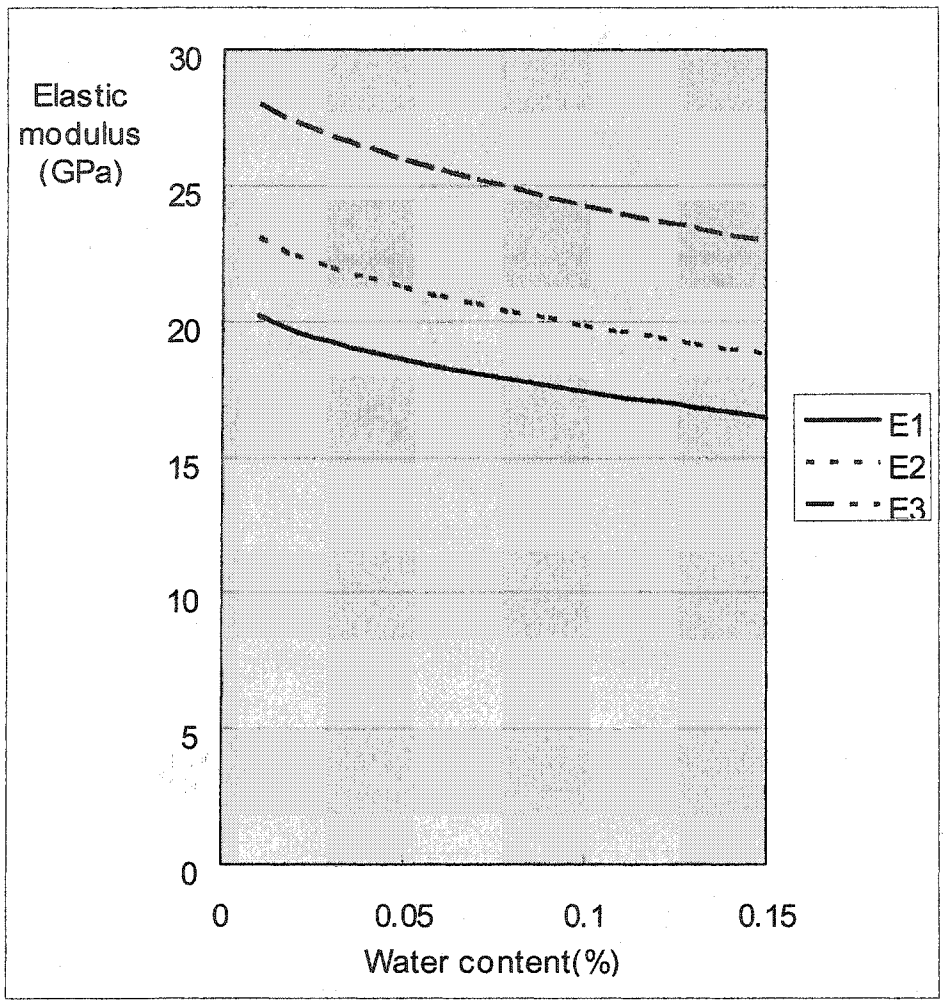

Chapter 4

An estimate of anisotropic poroelastic constants of an osteon

Abstract

The anisotropic poroelastic constants of an osteon are estimated by using a micromechanical analysis. The drained elastic constants are the porous medium's elastic constants when the fluid in the osteonal pores easily escapes and the pore fluid can sustain no pore pressure. The drained elastic constants at the lacunar-canalicular porosity tissue level are estimated by using an effective moduli model in which the shape of lacunae is approximated as ellipsoidal cavities. The undrained elastic constants are the porous medium's elastic constants when the medium is fully saturated with pore fluid and the fluid cannot escape, are also estimated. These estimated anisotropic poroelastic constants will provide a part of a database for the development of an accurate anisotropic poroelastic model of an osteon.

4.1. Introduction

The osteon is a hollow approximately cylindrical structure in the human cortical bone with a radius of roughly 100-150 μm (Cowin 1999). The long axis of the osteon aligns approximately ± 15 degrees with the long axis of a bone. At the center of the osteon is a canal called the osteonal canal or the Haversian canal; it may contain one or two blood vessels, a nerve, and some space occupied by bone fluid. The bone cells form a confluent lining on the wall of osteonal canal. The additional space in the osteonal canal is the vascular porosity; this is the porosity with the largest pore diameters in the osteon and in the osteonal bone. Behind the bone cell layer on the wall of osteonal canal, there are multiple small tunnels (0.2 μm to 0.4 μm in diameter), so called "canaliculi" that connect the osteonal canal to the lacunae and lacunae to other lacunae. The lacunae are approximately ellipsoidal (approximately 25 μm by 10 μm by 5 μm) in shape and contain one ostecyte (Cowin 1999). The space within the canaliculi and lacunae is called the lacunar-canalicular porosity; it is the porosity with the second largest pore diameters in the osteon. The smallest pore diameter porosity is the space between the collagen fiber and the mineral, hydroxyapatite.

The shear stress on the osteocyte due to the bone fluid flow in the canaliculus could be a stimulus of the bone mechanotransduction (Cowin et al. 1991; Cowin et al.

1995; Cowin 1999; Cowin and Moss 2001; Weinbaum et al. 1994). The bone fluid flow through the canaliculi is believed to provide nutrients and remove wastes from osteocytes. Weinbaum et al. (1994) proposed that the osteocytes can be stimulated by relatively small shear stresses acting on the membranes of their osteocytic process. The strain applied to the whole bone (0.04-0.3%) is much smaller than the strain necessary to signal in the deformed cell culture (1-10%) (Burger and Veldhuijen 1993, Williams et al. 1994; You et al. 2000). You et al. (2001) explained a possible mechanism by developing a theoretical model in which the drag force on the fibers attaching the osteocytic process to the canalicular wall amplifies the strain as much as 100 times by intercellular actin cytoskeleton and extracellular fibers in the canalicular process. Poroelasticity theory is used as the theoretical model to determine the bone fluid flow through the canaliculus. The deformation-induced pore fluid pressure gradient causes bone fluid to flow in the pericellular space of the lacunar-canalicular system when a whole bone is deformed. (Cowin 1999; Piekarski and Munro, 1977; Wang et al. 1999, 2000;. Weinbaum et al., 1994; Zhang et al. 1994, 1996, 1998; Zeng et al. 1994). Wang et al. (1999) proposed a theoretical model based on the poroelasticity theory to mimic oscillatory four point bending experiments of thin bone specimens. Their model includes the lacunar-canalicular porosity, osteonal canals, and the osteonal cement lines that is the outer

boundary of the osteon, and shows the local fluid pressure profiles. Their result suggests that the fluid pressure response to cyclic loading is not sensitive to the permeability of the osteonal cement lines, but it is sensitive to the applied loading frequency. Previously, Zhang et al. (1998) estimated the peak pore pressure due to uniaxial compression for both the vascular porosity and the lacunar-canalicular porosity by using the poroelasticity theory. The peak pore water pressure of vascular porosity is 19 percent of the applied axial stress and 12 percent of the applied axial stress in the lacunar-canalicular porosity. A slight hydraulic stiffening of the bulk modulus was predicted by longer relaxation time of the lacunar-canalicular porosity.

Normal human bone matrix outside these porosities consists of the lamellar bone or the osteonal bone. The lamellar bone is highly organized and consists of parallel layers, which is "lamellae," and the osteonal bone is formed by bone remodeling, where bone cells remove the old bone and replace it with the new bone, and consists of cylindrical lamellae. By bone remodeling process, normal human cortical bone consists mostly of osteonal bone matrix.

Three types of osteons are described by Ascenzi and Bonucci (1967, 1968). Type T osteon (bright osteon) has the collagen fibrils aligned in the transverse direction, Type A osteon has the alternative structure of both the longitudinal collagen fibril orientation

and the transverse collagen fibril orientation, and Type L osteon (dark osteon) has the collagen fibrils aligned in the longitudinal direction (Martin et al. 1998). Marotti and Muglia (1988) distinguished the lamellae as the dense lamellae and the loose lamellae, and Weiner and Traub (1992) divided the lamellae structure into the thin and thick lamellae. Marotti et al. (1995) found that the lacunae are located in the loose lamellae and the orientation of lacunae is aligned in the collagen fibril direction. We focus here on type L and type T osteons because the values of the parameters of interest for other types of osteons are bounded by the values of the parameters of the type L and type T osteons. Also type A osteon will be examined by considering the composite of type T osteonal lamellae and type L osteonal lamellae.

The anisotropic poroelastic constants are needed in order to develop the anisotropic (orthotropic or transversely isotropic) poroelastic models of different types of osteons. Early theoretical models (Smit et al. 2002; Wang et al. 1999; Zhang et al. 1996, 1998; Zeng et al. 1994) assumed that the osteonal bone matrix was isotropic, but they expressed the concern that their models were not anisotropic even though the bone matrix is anisotropic. In this study, micromechanical theories will be employed to estimate the drained elastic constants and the undrained elastic constants at the lacuno-canalicular porosity level of the osteon (Cowin 2003; Nemat-Nasser and Hori 1999).

4.2. Method

4.2.1. The relationship between Voigt notation and Kelvin notation

The traditional notation for the anisotropic Hooke's law is the representation of the fourth rank tensor, which is given in indical notation by

$$T_{ij} = C_{ijkm} E_{km} \quad \text{or} \quad E_{ij} = S_{ijkm} T_{km}, \tag{4.1}$$

where T_{ij}, E_{ij}, C_{ijkm}, and S_{ijkm} are the stress tensor, the strain tensor, the elasticity tensor, and the compliance tensor, respectively. Voigt (1910) employed the matrix notation as the coefficients of linearity in the relation between stress and strain,

$$\mathbf{T} = \mathbf{cE} \quad \text{or} \quad \mathbf{E} = \mathbf{sT}, \tag{4.2}$$

where $\mathbf{T}$ and $\mathbf{E}$ are one-by-six column matrices representing stress and strain. $\mathbf{c}$ and $\mathbf{s}$ are the elasticity matrix and the compliance matrix, respectively. The double index notation (or Voigt matrix notation) is important because most of the data on the mechanical properties of anisotropic elastic materials are reported in the double index notation (Hearmon 1961; Cowin and Mehrabadi 1995). The relation between the fourth rank tensor involves factors of 1, 2, and 4. The elements in the upper left hand 3-by-3 matrix have the proportionality factor one, eg, $S_{1111} = s_{11}$; the elements in the upper right hand 3-by-3 matrix (and lower left hand 3-by-3 matrix) have the proportionality factor two, eg, $2S_{2311} = s_{41}$; and the elements in the lower right hand 3-by-3 sub matrix have the

proportionality factor four, eg, $4S_{1212} = s_{66}$ (Hearmon 1961; Cowin and Mehrabadi 1995). However, for the elasticity tensor, no proportionality factors are involved. The proportionality factors do not occur between the Kelvin notation (1856) and the Voigt fourth rank tensor. Kelvin notation equivalent to Eq. (4.2) is

$$\hat{\mathbf{T}} = \hat{\mathbf{C}}\hat{\mathbf{E}} \quad \text{or} \quad \hat{\mathbf{E}} = \hat{\mathbf{S}}\hat{\mathbf{T}}, \tag{4.3}$$

where the stress vector $\hat{\mathbf{T}}$ has components $\{\hat{T}_1, \hat{T}_2, \hat{T}_3, \hat{T}_4, \hat{T}_5, \hat{T}_6\}$, the strain vector $\hat{\mathbf{E}}$ has components $\{\hat{E}_1, \hat{E}_2, \hat{E}_3, \hat{E}_4, \hat{E}_5, \hat{E}_6\}$, $\hat{\mathbf{C}}$ is the elasticity tensor for the orthotropic symmetry and is given as a 6-by-6 matrix of the second rank tensor components in 6 dimensions,

$$\hat{\mathbf{C}} = \begin{Bmatrix} \hat{c}_{11} & \hat{c}_{12} & \hat{c}_{13} & 0 & 0 & 0 \\ \hat{c}_{12} & \hat{c}_{22} & \hat{c}_{23} & 0 & 0 & 0 \\ \hat{c}_{13} & \hat{c}_{23} & \hat{c}_{33} & 0 & 0 & 0 \\ 0 & 0 & 0 & \hat{c}_{44} & 0 & 0 \\ 0 & 0 & 0 & 0 & \hat{c}_{55} & 0 \\ 0 & 0 & 0 & 0 & 0 & \hat{c}_{66} \end{Bmatrix}, \tag{4.4}$$

and $\hat{\mathbf{S}} = \hat{\mathbf{C}}^{-1}$ is the compliance tensor with the same structure. The relationship between the components of the Voigt fourth rank tensor and the components of the Kelvin second rank tensor is as follows: $C_{1111} = \hat{c}_{11}$, $C_{2222} = \hat{c}_{22}$, $C_{3333} = \hat{c}_{33}$, $C_{1122} = \hat{c}_{12}$, $C_{1133} = \hat{c}_{13}$, $C_{2233} = \hat{c}_{23}$, $C_{2323} = \frac{1}{2}\hat{c}_{44}$, $C_{1313} = \frac{1}{2}\hat{c}_{55}$, and $C_{1212} = \frac{1}{2}\hat{c}_{66}$. Similarly, the compliance tensor has the relationship between the components of the Voigt fourth rank tensor and

the components of the Kelvin second rank tensor as

$S_{1111} = \hat{s}_{11}$, $S_{2222} = \hat{s}_{22}$, $S_{3333} = \hat{s}_{33}$, $S_{1122} = \hat{s}_{12}$, $S_{1133} = \hat{s}_{13}$, $S_{2233} = \hat{s}_{23}$, $S_{2323} = \frac{1}{2}\hat{s}_{44}$, $S_{1313} = \frac{1}{2}\hat{s}_{55}$, and $S_{1212} = \frac{1}{2}\hat{s}_{66}$, respectively.

4.2.2. The bone matrix elastic constants

Yoon and Cowin (in preparation) estimated the bone matrix elastic constants by using the micromechanical models that recognized three levels of microstructure: (1) a mineralized collagen fibril, which consists of collagen molecules and platelet-shape-hydroxyapatite-mineral-crystals; (2) a collagen fiber composed of collagen fibrils embedded in the hydroxyapatite-mineral-crystals; and (3) a single lamella, which is a collagen fiber composite structure embedded in the hydroxyapatite-mineral-composite. The bone matrix elastic constants of a single lamella for type L osteon are estimated as: E_1^m =16.371 GPa, E_2^m =18.658 GPa, E_3^m =22.773 GPa, ν_{12}^m =0.334, ν_{13}^m =0.237, ν_{21}^m=0.381, ν_{23}^m=0.247, ν_{31}^m=0.330, ν_{32}^m=0.301, G_{12}^m=7.155 GPa, G_{13}^m=7.064 GPa, and G_{23}^m =8.368 GPa, respectively. Then the bone matrix compliance tensor $\hat{\mathbf{S}}^m$ is constructed by

$$\hat{s}^m = \begin{bmatrix} \frac{1}{E_1^m} & -\frac{\nu_{12}^m}{E_1^m} & -\frac{\nu_{13}^m}{E_1^m} & 0 & 0 & 0 \\ -\frac{\nu_{21}^m}{E_2^m} & \frac{1}{E_2^m} & -\frac{\nu_{23}^m}{E_2^m} & 0 & 0 & 0 \\ -\frac{\nu_{31}^m}{E_3^m} & -\frac{\nu_{31}^m}{E_3^m} & \frac{1}{E_3^m} & 0 & 0 & 0 \\ 0 & 0 & 0 & \frac{1}{2G_{23}^m} & 0 & 0 \\ 0 & 0 & 0 & 0 & \frac{1}{2G_{13}^m} & 0 \\ 0 & 0 & 0 & 0 & 0 & \frac{1}{2G_{12}^m} \end{bmatrix}. \quad (4.5)$$

The elastic constants of type T osteon and type A osteon are determined by the use of tensor transformation laws (Cowin and Mehrabadi 1995) from the orthotropic bone matrix elastic constants of type L osteon. Also, the isotropic bone matrix elastic constants, which are estimated by the averaging method from the orthotropic bone matrix elastic constants (See details in Cowin et al. 1999; Yoon et al. 2002), are obtained to compare to the orthotropic bone matrix elastic constants. These bone matrix elastic constants are considered to represent the elastic constants of the bone matrix without osteonal canals and without lacunae.

4.2.3 An estimate of the drained elastic constants at the lacunar porosity level

The drained elastic constants of a porous medium may be determined by calculating the effective elastic constants of a medium with the appropriately connected

pore structure. The drained elastic constants are elastic constants when the pore fluid pressure is zero. In the lacunar-canalicular porosity, the anisotropy due to cavities or voids is mainly influenced by the distribution of lacunae, which is quasi-periodic, because the size of canaliculi is much smaller than those of lacunae. In this calculation, two assumptions are made. First, the effective moduli of the quasi-periodically distributed lacunae in the circular sector are approximately equal to the effective moduli of periodically distributed lacunae in a rectangle whose dimensions are equal to the circumference of the circle and the radial length of the circular sector. Second, it is assumed that the existence of canaliculi may be ignored in this calculation, but their effect is acknowledged in that the pores are all assumed to have the same pore pressure under a static load. The rationale for this assumption is that the canaliculi, although numerous, are small ($0.2\,\mu m$ to $0.4\,\mu m$) while the lacunae are, by comparison, large ($25\,\mu m$ by $10\,\mu m$ by $5\,\mu m$). The formula for the effective moduli of a medium in the periodically distributed cavities (Nemat-Nasser and Hori, 1999) is given by

$$\hat{\mathbf{C}}^{eff} = \hat{\mathbf{C}}^{m} : \{\hat{\mathbf{1}} - \phi(\hat{\mathbf{1}} - \hat{\mathbf{S}}^{P})^{-1}\}, \tag{4.6}$$

where $\hat{\mathbf{C}}^{eff}$ is the effective elasticity tensor, $\hat{\mathbf{C}}^{m}$ is the elasticity tensor of the matrix material, $\hat{\mathbf{1}}$ is the identity tensor in six dimensions, ϕ is the porosity, and $\hat{\mathbf{S}}^{P}$ is the periodic operator (See Eqs (12.5.6b) and (12.5.9b) on page 440 and 441 in Nemat-Nasser

and Hori 1999) , which is given by

$$\hat{\mathbf{S}}^{\mathrm{P}} = \sum_{\xi}{}' \phi\, g(-\xi)\, g(\xi)\, F\hat{\mathbf{S}}^{\mathrm{P}}(\xi), \tag{4.7}$$

where the prime on the summation indicates that $\xi = 0$ is excluded. $g(\xi)$ is the g-integral, which is the volume average of $\exp(i\xi \cdot x)$ over the cavity. The new variable ξ is defined as $\xi \equiv \frac{n_i \pi}{a_i}$, where n_i is the number of unit cells in the i-direction (Figure 4.1) and i can be replaced with x, y, z for x-, y-, and z- direction, respectively. The unit cell, which contains one osteon, has the domain as $U = \{x; -a_i < x_i < a_i \ (i = x, y, z)\}$. The g-integral, $g(\xi)$ for the ellipsoidal inclusion is given by (Iwakuma and Nemat-Nasser 1983; Nemat-Nasser et al. 1999)

$$g(\xi) = \frac{3}{\eta}(\sin\eta - \eta\cos\eta), \tag{4.8}$$

where η is given by

$$\eta = 2\times\pi\times\left(\frac{3\times\phi}{4\times\pi\times(b_y/b_x)\times(b_z/b_x)}\right)\left[\{n_x\}^2 + \left\{n_y\frac{b_y}{b_x}\right\}^2 + \left\{n_y\frac{b_z}{b_x}\right\}^2\right]^{(1/2)}, \tag{4.9}$$

and where the subscripts x, y, and z indicate three perpendicular directions. n_x, n_y, and n_z are the number of cavities in the x, y, and z direction, respectively. Note that the summation in Eq. (4.7) with respect to ξ (or n_x, n_y, and n_z) is generally from 1 to infinity, but in this study, the summation is from one to ± 50, for which reasons will be explained in the discussion. b_x, b_y, and b_z are the length of principal axes of an

ellipsoidal shape of a lacuna. For the type L osteon, the size of a lacuna (Remaggi et al. 1998) is b_x=25 μm, b_y=10 μm, and b_z=5 μm, respectively, and the value in the y direction is interchanged with that in the z direction for the type T osteon.

4.2.3.1 The case of an isotropic bone matrix

It is assumed that the bone matrix is isotropic in this section. The transversely isotropic case is treated in the next section. Iwakuma and Nemat-Nasser (1983) decomposed the periodic operator $\hat{\mathbf{S}}^P$ as

$$\hat{\mathbf{S}}^P_{ijkl} = \frac{1}{2}\left[\delta_{il}\mathbf{S}_{I(j,k)} + \delta_{ik}\mathbf{S}_{I(j,l)} + \delta_{jl}\mathbf{S}_{I(i,k)} + \delta_{jk}\mathbf{S}_{I(i,l)}\right] - \frac{1}{1-\nu}\mathbf{S}_{I(i,j)J(k,l)} + \frac{\nu}{1-\nu}\delta_{kl}\mathbf{S}_{I(i,j)}, \tag{4.10}$$

for the faster numerical calculation, where

$$\hat{\mathbf{S}}_I = \sum_{\xi} \phi\, g(\xi)\, g(-\xi)\, h_I(\xi) \quad \text{and} \quad \hat{\mathbf{S}}_{IJ} = \sum_{\xi} \phi\, g(\xi)\, g(-\xi)\, h_{IJ}(\xi). \tag{4.11}$$

$h_I(\xi)$ and $h_{IJ}(\xi)$ are given by (Nemat-Nasser et al. 1982; Iwakuma and Nemat-Nasser 1983; Nemat-Nasser and Hori 1999)

$$h_1(\xi) = (\bar{\xi}_1)^2, \quad h_2(\xi) = (\bar{\xi}_2)^2, \quad h_3(\xi) = (\bar{\xi}_3)^2,$$

$$h_4(\xi) = \bar{\xi}_2\bar{\xi}_3, \quad h_5(\xi) = \bar{\xi}_3\bar{\xi}_1, \quad h_6(\xi) = \bar{\xi}_1\bar{\xi}_2,$$

and

$$h_{I(i,j)J(i,j)}(\xi) = h_{I(i,j)}(\xi)\, h_{J(i,j)}(\xi), \text{ for I(i,j) and J(i,j) =1, 2, 3, ... 6.} \tag{4.12}$$

$\bar{\xi} \equiv \xi/|\xi|$ and $I(i,j)$ (or $J(i,j)$) in Eqs. (4.10) and (4.12) are replaced by relations as

$I(1,1)$, $I(2,2)$, $I(3,3)$, $I(2,3)$, $I(1,3)$, and $I(1,2)$ correspond to 1, 2, 3, 4, 5, and 6, respectively.

4.2.3.2. The case when the bone matrix is anisotropic

If it is assumed that the bone matrix is anisotropic, the term, $F\hat{\mathbf{S}}^{\mathrm{P}}(\xi)$ in Eq. (4.7) is determined by (Eq. 12.5.4a on Page 431 in Nemat-Nasser and Hori 1999)

$$F\mathbf{S}^{P}(\xi) = sym\{\xi \otimes (\xi \cdot C^{m} \cdot \xi)^{-1} \otimes \xi) : C^{m}, \tag{4.13}$$

where C^{m} is the fourth rank elasticity tensor of the bone matrix. First, the term $(\xi \cdot C \cdot \xi)$ is expanded in the index notation as

$$\begin{aligned}(\xi_i C_{ijkl} \xi_l) = {} & \xi_1 C_{1jk1} \xi_1 + \xi_1 C_{1jk2} \xi_2 + \xi_1 C_{1jk3} \xi_3 \\ & + \xi_2 C_{2jk1} \xi_1 + \xi_2 C_{2jk2} \xi_2 + \xi_2 C_{2jk3} \xi_3 \\ & + \xi_3 C_{3jk1} \xi_1 + \xi_3 C_{3jk2} \xi_2 + \xi_3 C_{3jk3} \xi_3 .\end{aligned} \tag{4.14}$$

The inverse of the second rank tensor $(\xi_i C_{ijkl} \xi_l)$ is calculated and another fourth rank tensor $\xi_i (\xi_p C_{pjkq} \xi_q)^{-1} \xi_l$ is formed. The quantity $F\hat{\mathbf{S}}^{\mathrm{P}}(\xi)$ in Eq. (4.13) is obtained by the contraction of this result with the fourth rank elasticity tensor of bone matrix, C^{m}.

4.2.4 Estimate of undrained elastic constants at the lacunar porosity level

Three sets of conventional elastic compliance tensors are involved in poroelasticity theory. These are the drained compliance tensor $\hat{\mathbf{S}}^{d}$, the matrix material

compliance tensor $\hat{\mathbf{S}}^m$, and the undrained compliance tensor $\hat{\mathbf{S}}^u$. The matrix material compliance tensor $\hat{\mathbf{S}}^m$ represents the elastic constants of the matrix material in the porous medium (Eq. 4.5). The drained compliance tensor $\hat{\mathbf{S}}^d$ represents the elastic constants of the porous medium when no fluid remains in the pores. The undrained compliance tensor $\hat{\mathbf{S}}^u$ represents the elastic constants of the porous medium when the fluid is not able to escape.

The strain-stress-pore pressure relations for a poroelastic medium are given by (Biot 1941, 1955; Cheng 1997; Cowin 2003; Detournay and Cheng 1993; Thompson and Willis 1991)

$$\hat{\mathbf{E}} = \hat{\mathbf{S}}^d \cdot \hat{\mathbf{T}} + (\hat{\mathbf{S}}^d - \hat{\mathbf{S}}^m) \cdot \hat{\mathbf{U}} p, \tag{4.15}$$

where $\hat{\mathbf{E}}$ is the strain vector in six dimensions, $\hat{\mathbf{T}}$ is the stress vector in six dimensions, $\hat{\mathbf{U}}$ is a six-dimensional vector defined as $\hat{\mathbf{U}} = \{1,1,1,0,0,0\}^T$ and p is the pore fluid pressure. Eq. (4.15) is simplified by introducing the "effective stress", $\Sigma = (\hat{\mathbf{T}} + \hat{\mathbf{A}} p)$ as

$$\hat{\mathbf{E}} = \hat{\mathbf{S}}^d \cdot \Sigma = \hat{\mathbf{S}}^d \cdot (\hat{\mathbf{T}} + \hat{\mathbf{A}} p), \tag{4.16}$$

where the "Biot effective stress coefficient," $\hat{\mathbf{A}}$ is defined as

$$\hat{\mathbf{A}} = (\hat{\mathbf{1}} - (\hat{\mathbf{S}}^d)^{-1} \cdot \hat{\mathbf{S}}^m) \cdot \hat{\mathbf{U}}. \tag{4.17}$$

The variation of fluid volume per unit volume due to diffusive fluid mass transport, ς is given by

$$\varsigma = \hat{\mathbf{S}}^d \cdot \hat{\mathbf{A}} \cdot \hat{\mathbf{T}} + C_{eff}\, p\,, \tag{4.18}$$

where the effective compressibility is

$$C_{eff} = C_d - C_m + \phi(C_f - C_m), \tag{4.19}$$

and where ϕ is the porosity. The compressibility, the inverse of bulk modulus, in Eq. (4.19) is obtained by

$$C_i = \hat{\mathbf{U}} \cdot \hat{\mathbf{S}}^i \cdot \hat{\mathbf{U}}, \tag{4.20}$$

where i in C_i is replaced by d, m, u, f to indicate the compressibility for the drained case, the matrix, the undrained case, and the pore fluid, respectively. Another poroelastic constant is the Skempton compliance difference tensor $\hat{\mathbf{B}}$, which is a measure of the relative compressibility of the fluid and solid phase. It represents the ratio between the pore pressure p and the stress $\hat{\mathbf{T}}$ for the undrained condition when the variation of fluid content is zero ($\varsigma = 0$) as

$$p = -\hat{\mathbf{B}} \cdot \hat{\mathbf{T}}, \tag{4.21}$$

where the "Skempton compliance difference tensor," $\hat{\mathbf{B}}$ is defined as

$$\hat{\mathbf{B}} = \frac{\hat{\mathbf{S}}^d \cdot \hat{\mathbf{A}}}{C_{eff}}. \tag{4.22}$$

By substituting Eqs. (4.21) and (4.22) into Eq. (4.16),

$$\hat{\mathbf{E}} = \hat{\mathbf{S}}^u \cdot \hat{\mathbf{T}} = (\hat{\mathbf{S}}^d - \frac{1}{C_{eff}} \hat{\mathbf{S}}^d \cdot \hat{\mathbf{A}} \otimes \hat{\mathbf{S}}^d \cdot \hat{\mathbf{A}}) \cdot \hat{\mathbf{T}} \tag{4.23}$$

The relation between the undrained compliance tensor $\hat{\mathbf{S}}^u$ and the drained compliance tensor $\hat{\mathbf{S}}^d$ is obtained as

$$\hat{\mathbf{S}}^u = \hat{\mathbf{S}}^d - \frac{1}{C_{eff}} \hat{\mathbf{S}}^d \cdot \hat{\mathbf{A}} \otimes \hat{\mathbf{S}}^d \cdot \hat{\mathbf{A}}. \tag{4.24}$$

4.2.5 Steps of the calculation

For the type L osteon, the following steps are accomplished.

Step 1. Calculate the drained compliance tensor $\hat{\mathbf{S}}^d$ of an osteon by using the inverse of $\hat{\mathbf{C}}^{eff}$ in Eq. (4.6). The compliance tensor of the bone matrix material $\hat{\mathbf{S}}^m$ is constructed by using the elastic constants of bone matrix material (Eq. 4.5). In this calculation, note that the longest principal axis of the lacuna is aligned with the long axis of an osteon.

Step 2. Calculate the Biot effective coefficient $\hat{\mathbf{A}}$ by using Eq. (4.17) and the effective compressibility C_{eff} by using Eq. (4.19).

Step 3. The undrained compliance tensor $\hat{\mathbf{S}}^u$ of an osteon is calculated by using Eq. (4.24). The drained compliance tensor $\hat{\mathbf{S}}^d$ was estimated in step 1, and the effective compressibility C_{eff} was obtained in step 2.

Step 4. Calculate the Skempton coefficient $\hat{\mathbf{B}}$ by using Eq. (4.22)

See Table 4.1 (a) and Table 4.3 (a) for the values of the orthotropic poroelastic constants, the Biot effective coefficient $\hat{\mathbf{A}}$, and the Skempton coefficient $\hat{\mathbf{B}}$. In the similar way, the poroelastic constants for type T osteon and type A osteon are calculated by using the

tensor transformation law (Cowin and Mehrabadi 1995) (Tables 4.1 (b), 4.1(c), 4.3(b), and 4.3(c)).

4.3. Results

Table 4.1(a) shows the drained and undrained orthotropic poroelastic constants at the lacunar-canalicular porosity level of type L osteon for two cases depending on whether the bone matrix material is isotropic or orthotropic. Similarly, those of type T osteon and type A osteon are shown in Tables 4.1(b) and 4.1(c), respectively. The elastic constants estimated by the periodic distribution assumption for type L osteon may be compared to those estimated by the dilute distribution assumption using the data in Table 4.2. Table 4.3(a), 4.3(b), and 4.3(c) show the estimated the Biot effective coefficient and the Skemption coefficient of type L, type T, and type A osteons, respectively, for both orthotropic and the isotropic elastic bone matrix cases.

4.4. Discussion

A major conclusion of this study is that the anisotropy of the bone matrix level elastic constants (or the bone matrix compliance tensor $\hat{\mathbf{S}}^m$) strongly influences the anisotropy of poroelastic constants at the lacunar-canalicular porosity level (or the drained compliance tensor $\hat{\mathbf{S}}^d$ and the undrained compliance tensor $\hat{\mathbf{S}}^u$). Table 4.1 shows that the orthotropic bone matrix generates the higher discrepancy in the elastic

constants, especially between E_1 and E_3 compared to those obtained by assuming that the bone matrix is isotropic. It suggests that the anisotropy of bone matrix itself plays an important role in determining the anisotropic lacunar-canaliculuar porosity level elastic constants no matter what averaging method (Cowin et al. 1999; Yoon et al. 2002) is applied.

The lamellae of type A osteon is composed of successive layers of lamellae in the type L osteon and those in the type T osteon. Ascenzi et al. (1986) observed that another layer, which collagen fibers are aligned 45 degrees with the osteonal axis, lies between the type T osteonal lamella and the type L osteonal lamella. Recently, Ascenzi et al. (2003) observed that the type T osteonal lamellae in the type A osteon is, mostly, oriented 45 degrees with the osteonal axis. Previously the type T osteonal lamellae in the type A osteon is believed to be perpendicular to the type L osteonal lamellae in the type A osteon. The type L osteonal lamellae in the type A osteon observed by Ascenzi et al. (2003) is still aligned along the osteonal axis. Even though the "twisted plywood model" was observed inside the type T osteonal lamellae in the type A osteon, most collagen fiber arrays in the type T osteonal lamellae are oriented 45 degrees with the osteonal axis. Weiner et al. (1999) suggested differently that the different numbers of collagen fiber arrays are rotated 30 degrees with respect to the adjacent group of collagen fiber arrays.

The angle between collagen fiber arrays inside the type A osteon is not clear at this moment. Even though there is reported observation (Ascenzi et al. 2003) that the type T osteonal lamellae in the type A osteon is oriented 45 degrees with the osteonal axis, we will follow the old model that the type T osteonal lamellae in the type A osteon is perpendicular to the osteonal axis. The orthotropic poroelastic constants for type A osteon are shown in Table 4.1(c).

The effective drained elastic constants estimated by using the periodic distribution assumption may be a little suspect because the distribution of lacunae is not perfectly periodic. Table 4.2 shows that the poroelastic constants estimated by the periodic distribution assumption are close to those estimated by the dilute distribution assumption, when the bone matrix is isotropic. The reason is that the orientation of lacunae in the dilute distribution assumption is coincident with those in the periodic distribution assumption. Only distance between lacunae is varied in the dilute distribution assumption.

The values for B_z for the type L, type T, and type A osteons for the two cases listed in Tables 4.3 (a), 4.3 (b), and 4.3(c), the cases when the bone matrix is isotropic and the case when the bone matrix is orthotropic, show something very interesting. If the bone is loaded only axially with a stress T_{zz}, the pore pressure created in the undrained

situation in the type L osteon is, using Eq. (4.22), given by $p = - B_z T_{zz}$; thus, from Table 4.3 (a), $p = - 0.037 T_{zz}$ in the case when the bone matrix is isotropic and $p = - 0.028 T_{zz}$ in the case when the bone matrix is orthotropic. Two aspects of these results are interesting. First the pore pressure p developed in the case of an isotropic matrix material is 1.32 times that developed in the case of orthotropic matrix material. The orthotropic material symmetry in the matrix material effectively shields the pore fluid from the stress in the solid matrix better than the isotropic material symmetry. The pore pressure in the isotropic case is 3.7% of the axial solid matrix stress and the pore pressure in the orthotropic case is 2.8% of the axial solid matrix stress. However for the type T osteon, from Table 4.3 (b), $p = 0.068 T_{zz}$ in the case for the orthotropic bone matrix and $p = 0.070 T_{zz}$ in the case for the isotropic bone matrix. The pore pressure p developed in the case when the bone matrix is isotropic for type T osteon is almost equal to that in the case when the bone matrix is orthotropic. For the type A osteon, from Table 4.3 (c), $p = 0.048 T_{zz}$ in the case for the orthotropic bone matrix and $p = 0.054 T_{zz}$ in the case for the isotropic bone matrix. The pore pressure p developed in the case of an isotropic matrix material is 1.13 times that developed in the case of orthotropic matrix material. The previous estimate (Zhang et al., 1998) of the Skempton coefficient tensor for bone tissue at the lacunar-canalicular level was based on the assumption that pore shape and

distribution were characterized by isotropy as well as the material symmetry of the matrix material. In this case $B_r = B_\theta = B_z = B/3$ and the B was estimated to be 0.4 (Zhang et al., 1998) for the same lacunar-canalicular porosity that is the present subject of discussion. For the type L osteon, the value of B for the isotropic matrix material with ellipsoidal cavities is estimated as 0.380 and that for the orthotropic matrix material is 0.4, which are close to the estimation of Zhang et al. (1998).

Nemat-Nasser et al. (1982) compared the effective moduli in the periodic distribution assumption to the Hashin and Shtrikman bounds. The bulk modulus of a medium with spherical cavities, if the shape of lacuna is assumed spherical, in the periodic distribution assumption overshoots the upper bound of Hashin and Shtrikman (1963) by about 1%. They explained that it may be the truncation error of Eq. (4.7). Eq. (4.7) was summed for the variable ξ from -50 to 50, except when ξ is zero, because the sum to ± 40 provides an answer only 0.7% less than that to ± 50.

The estimated anisotropic poroelastic constants will provide a set of data to develop the more accurate anisotropic poroelastic model than isotropic poroelastic models (Manfredini et al. 1999; Smit et al. 2002; Wang et al. 1999; Zhang et al. 1994, 1996).

Table 4.1(a). The estimated undrained and drained elastic constants of the type L osteon for the case when the bone matrix is isotropic and the case when it is orthotropic

The undrained elastic constants				**The drained elastic constants**			
Bone matrix is **isotropic**		Bone matrix is **orthotropic**		Bone matrix is **isotropic**		Bone matrix is **orthotropic**	
E_1^u	16.174	E_1^u	14.120	E_1^d	15.579	E_1^d	13.551
E_2^u	17.371	E_2^u	17.118	E_2^d	17.324	E_2^d	17.073
E_3^u	17.927	E_3^u	21.571	E_3^d	17.914	E_3^d	21.559
ν_{12}^u	0.298	ν_{12}^u	0.326	ν_{12}^d	0.277	ν_{12}^d	0.304
ν_{13}^u	0.279	ν_{13}^u	0.220	ν_{13}^d	0.264	ν_{13}^d	0.207
ν_{21}^u	0.320	ν_{21}^u	0.396	ν_{21}^d	0.308	ν_{21}^d	0.383
ν_{23}^u	0.295	ν_{23}^u	0.240	ν_{23}^d	0.293	ν_{23}^d	0.238
ν_{31}^u	0.310	ν_{31}^u	0.336	ν_{31}^d	0.304	ν_{31}^d	0.330
ν_{32}^u	0.305	ν_{32}^u	0.303	ν_{32}^d	0.303	ν_{32}^d	0.301
$G_{12}^d = G_{12}^u$	6.927	$G_{12}^d = G_{12}^u$	6.623	$G_{12}^d = G_{12}^u$	6.927	$G_{12}^d = G_{12}^u$	6.623
$G_{13}^d = G_{13}^u$	6.942	$G_{13}^d = G_{13}^u$	6.558	$G_{13}^d = G_{13}^u$	6.942	$G_{13}^d = G_{13}^u$	6.558
$G_{23}^d = G_{23}^u$	7.043	$G_{23}^d = G_{23}^u$	7.869	$G_{23}^d = G_{23}^u$	7.043	$G_{23}^d = G_{23}^u$	7.869

Table 4.1(b). The estimated undrained and drained elastic constants of the type T osteon for the case when the bone matrix is isotropic and the case when it is orthotropic

The undrained elastic constants				**The drained elastic constants**			
Bone matrix is **isotropic**		Bone matrix is **orthotropic**		Bone matrix is **isotropic**		Bone matrix is **orthotropic**	
E_1^u	16.174	E_1^u	14.120	E_1^d	15.579	E_1^d	13.551
E_2^u	17.928	E_2^u	21.571	E_2^d	17.914	E_2^d	21.559
E_3^u	17.371	E_3^u	17.118	E_3^d	17.324	E_3^d	17.073
ν_{12}^u	0.279	ν_{12}^u	0.220	ν_{12}^d	0.264	ν_{12}^d	0.207
ν_{13}^u	0.298	ν_{13}^u	0.326	ν_{13}^d	0.277	ν_{13}^d	0.304
ν_{21}^u	0.310	ν_{21}^u	0.336	ν_{21}^d	0.304	ν_{21}^d	0.330
ν_{23}^u	0.305	ν_{23}^u	0.302	ν_{23}^d	0.303	ν_{23}^d	0.301
ν_{31}^u	0.320	ν_{31}^u	0.396	ν_{31}^d	0.308	ν_{31}^d	0.383
ν_{32}^u	0.295	ν_{32}^u	0.240	ν_{32}^d	0.293	ν_{32}^d	0.238
$G_{12}^d = G_{12}^u$	6.942	$G_{12}^d = G_{12}^u$	6.558	$G_{12}^d = G_{12}^u$	6.942	$G_{12}^d = G_{12}^u$	6.558
$G_{13}^d = G_{13}^u$	6.927	$G_{13}^d = G_{13}^u$	6.623	$G_{13}^d = G_{13}^u$	6.927	$G_{13}^d = G_{13}^u$	6.623
$G_{23}^d = G_{23}^u$	7.042	$G_{23}^d = G_{23}^u$	7.869	$G_{23}^d = G_{23}^u$	7.042	$G_{23}^d = G_{23}^u$	7.869

Table 4.1(c). The estimated undrained and drained elastic constants of the type A osteon for the case when the bone matrix is isotropic and the case when it is orthotropic

The undrained elastic constants				**The drained elastic constants**			
Bone matrix is **isotropic**		Bone matrix is **orthotropic**		Bone matrix is **isotropic**		Bone matrix is **orthotropic**	
E_1^u	16.174	E_1^u	14.120	E_1^d	15.579	E_1^d	13.551
E_2^u	18.070	E_2^u	19.626	E_2^d	18.040	E_2^d	19.597
E_3^u	18.070	E_3^u	19.626	E_3^d	18.040	E_3^d	19.597
ν_{12}^u	0.289	ν_{12}^u	0.273	ν_{12}^d	0.271	ν_{12}^d	0.256
ν_{13}^u	0.289	ν_{13}^u	0.273	ν_{13}^d	0.271	ν_{13}^d	0.256
ν_{21}^u	0.322	ν_{21}^u	0.380	ν_{21}^d	0.314	ν_{21}^d	0.370
ν_{23}^u	0.283	ν_{23}^u	0.247	ν_{23}^d	0.281	ν_{23}^d	0.245
ν_{31}^u	0.322	ν_{31}^u	0.380	ν_{31}^d	0.314	ν_{31}^d	0.370
ν_{32}^u	0.283	ν_{32}^u	0.247	ν_{32}^d	0.281	ν_{32}^d	0.245
$G_{12}^d = G_{12}^u$	6.934	$G_{12}^d = G_{12}^u$	6.590	$G_{12}^d = G_{12}^u$	6.934	$G_{12}^d = G_{12}^u$	6.590
$G_{13}^d = G_{13}^u$	6.934	$G_{13}^d = G_{13}^u$	6.590	$G_{13}^d = G_{13}^u$	6.934	$G_{13}^d = G_{13}^u$	6.590
$G_{23}^d = G_{23}^u$	6.786	$G_{23}^d = G_{23}^u$	7.526	$G_{23}^d = G_{23}^u$	6.786	$G_{23}^d = G_{23}^u$	7.526

Table 4.2. Two estimates of the poroelastic constants assuming the lacunae are ellipsoids and the bone matrix material is isotropic. The estimate on the left side of the table is based on the periodic distribution assumption and that on the right side is based on the dilute distribution assumption, for type L osteon.

The periodic distribution				**The dilute distribution**			
undrained		drained		undrained		drained	
E_1^d	16.174	E_1^d	15.579	E_1^d	15.769	E_1^d	14.968
E_2^d	17.371	E_2^d	17.324	E_2^d	17.246	E_2^d	17.202
E_3^d	17.927	E_3^d	17.914	E_3^d	17.799	E_3^d	17.784
ν_{12}^d	0.298	ν_{12}^d	0.277	ν_{12}^d	0.297	ν_{12}^d	0.271
ν_{13}^d	0.279	ν_{13}^d	0.264	ν_{13}^d	0.278	ν_{13}^d	0.258
ν_{21}^d	0.320	ν_{21}^d	0.308	ν_{21}^d	0.324	ν_{21}^d	0.311
ν_{23}^d	0.295	ν_{23}^d	0.293	ν_{23}^d	0.295	ν_{23}^d	0.293
ν_{31}^d	0.310	ν_{31}^d	0.304	ν_{31}^d	0.313	ν_{31}^d	0.306
ν_{32}^d	0.305	ν_{32}^d	0.303	ν_{32}^d	0.304	ν_{32}^d	0.302
$G_{12}^d = G_{12}^u$	6.927	$G_{12}^d = G_{12}^u$	6.927	$G_{12}^d = G_{12}^u$	6.932	$G_{12}^d = G_{12}^u$	6.932
$G_{13}^d = G_{13}^u$	6.942	$G_{13}^d = G_{13}^u$	6.942	$G_{13}^d = G_{13}^u$	6.945	$G_{13}^d = G_{13}^u$	6.945
$G_{23}^d = G_{23}^u$	7.043	$G_{23}^d = G_{23}^u$	7.043	$G_{23}^d = G_{23}^u$	7.040	$G_{23}^d = G_{23}^u$	7.040

Table 4.3(a). The estimated Biot effective coefficient $\hat{\mathbf{A}}$ and the estimated Skempton coefficient $\hat{\mathbf{B}}$ in the case where the collagen fibers are oriented in the longitudinal direction (type L osteon). The subscript r, θ, and z indicate the radial direction, the circumferential direction, and the longitudinal direction, respectively.

		When the bone matrix is orthotropic	When the bone matrix is isotropic
The Biot effective coefficient $\hat{\mathbf{A}}$	$\hat{\mathbf{A}}_r$	0.206	0.207
	$\hat{\mathbf{A}}_\theta$	0.149	0.139
	$\hat{\mathbf{A}}_z$	0.133	0.126
The Skempton compliance difference tensor $\hat{\mathbf{B}}$	$\hat{\mathbf{B}}_r$	0.302	0.273
	$\hat{\mathbf{B}}_\theta$	0.068	0.070
	$\hat{\mathbf{B}}_z$	0.028	0.037

Table 4.3 (b). The estimated Biot effective coefficient $\hat{\mathbf{A}}$ and the estimated Skempton coefficient $\hat{\mathbf{B}}$ in the case where the collagen fibers are oriented in the transverse direction (type T osteon). The subscript r, θ, and z indicate the radial direction, the circumferential direction, and the longitudinal direction, respectively.

		When the bone matrix is orthotropic	When the bone matrix is isotropic
The Biot effective coefficient $\hat{\mathbf{A}}$	$\hat{\mathbf{A}}_r$	0.206	0.207
	$\hat{\mathbf{A}}_\theta$	0.133	0.126
	$\hat{\mathbf{A}}_z$	0.149	0.139
The Skempton compliance difference tensor $\hat{\mathbf{B}}$	$\hat{\mathbf{B}}_r$	0.302	0.273
	$\hat{\mathbf{B}}_\theta$	0.028	0.037
	$\hat{\mathbf{B}}_z$	0.068	0.070

Table 4.3(c). The estimated Biot effective coefficient $\hat{\mathbf{A}}$ and the estimated Skempton coefficient $\hat{\mathbf{B}}$ in the case where the collagen fibers are oriented in the transverse direction (type A osteon). The subscript r, θ, and z indicate the radial direction, the circumferential direction, and the longitudinal direction, respectively.

		When the bone matrix is orthotropic	When the bone matrix is isotropic
The Biot effective coefficient $\hat{\mathbf{A}}$	$\hat{\mathbf{A}}_r$	0.206	0.207
	$\hat{\mathbf{A}}_\theta$	0.141	0.133
	$\hat{\mathbf{A}}_z$	0.141	0.133
The Skempton compliance difference tensor $\hat{\mathbf{B}}$	$\hat{\mathbf{B}}_r$	0.302	0.273
	$\hat{\mathbf{B}}_\theta$	0.048	0.054
	$\hat{\mathbf{B}}_z$	0.048	0.054

Figure 4.1. The unit of the periodic distribution assumption.

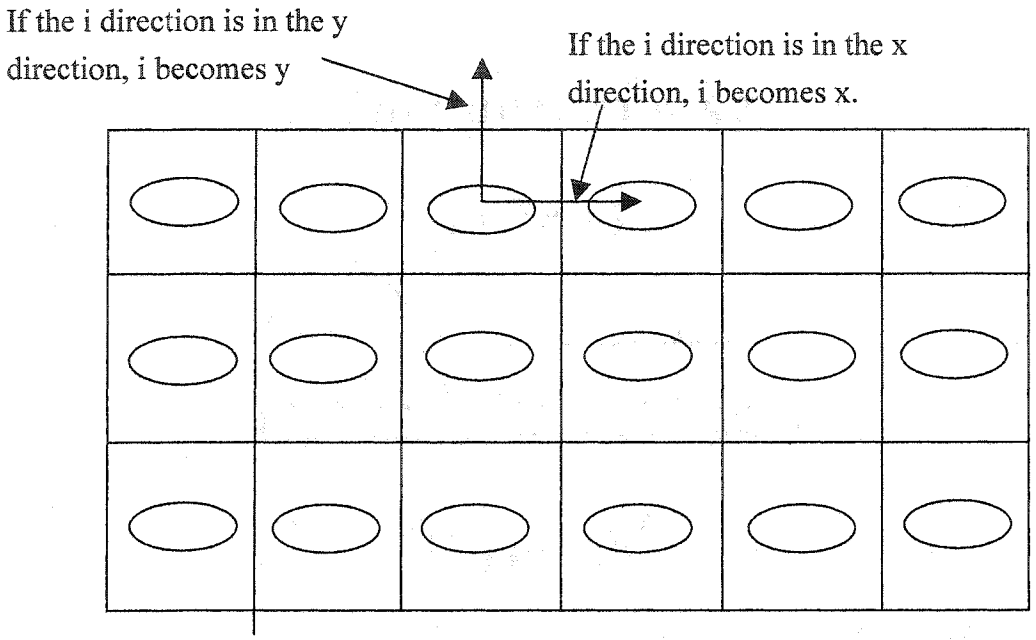

Chapter 5

Estimation of the effective transversely isotropic elastic constants of a material from known values of the material's orthotropic elastic constants

Abstract

A method is illustrated for determining the effective transversely isotropic (or isotropic) elastic constants from measured orthotropic elastic constants. This method consists of constructing upper and lower bounds on the effective transversely isotropic (or isotropic) elastic constants using the known orthotropic values. This method is illustrated using three sets of elastic constants for bone. Fortunately, the upper and lower bounds are very close. Thus very good approximations for the effective transversely isotropic (or isotropic) elastic constants for cortical and cancellous bone are obtained from previously published data on the orthotropic elastic constants for those tissue types. This work is undertaken to build a greater database for the transversely isotropic elastic constants of bone with the intention of employing them in a transversely isotropic model of bone poroelasticity. An interesting aspect of the present result is that the Voigt and Reuss bounds are very tight for these anisotropic materials. This is not always the case for these bounds.

---

* Chapter 5 was published in the Journal: Biomechan. Model. Mechanobiol 1 (2002) 83-93

5.1 Introduction

The type of material symmetry possessed by bone tissue is often ambiguous. Within the accuracy we have to measure the elastic constants of bone, a given specimen may be well represented as, say, orthotropic. However, the orthotropy may not be of high degree in all directions and the specimen may be represented, for all practical purposes, as transversely isotropic or, even, isotropic. The question addressed, and rigorously answered, in this work is the following: Given a set of orthotropic elastic constants for a specific specimen, what bounds do these elastic constants impose on the effective transversely isotropic and the effective isotropic elastic constants of that specimen? In the cases considered thus far for bone, the bounds have been so tight that the effective values of the elastic constants of the higher symmetries have been determined from those of the lower symmetry, as will be illustrated below.

This work is undertaken to build a greater database for the transversely isotropic elastic constants of bone. The longer-term project is to assemble the numerical values of parameters for a transversely isotropic model of bone poroelasticity. A set of numerical values of parameters for an isotropic model of bone poroelasticity is given by Cowin (1999) and Smit et al. (2002).

5.2 A generalized Hill inequality

Hill (1952; 1963) constructed bounds on the effective isotropic elastic coefficients of a material with triclinic symmetry using energy theorems from classical elasticity and the uniform strain and uniform stress bounds of Voigt (1928) and Reuss (1929). It is possible

to extend Hill's results and construct bounds on the effective elastic constants of a material with any anisotropy in terms of triclinic symmetry elastic coefficients (Cowin et al. 1999). As in the case of the bounds found by Hill (1952), it is possible to specialize the triclinic symmetry coefficients appearing in the bounds to those of a greater symmetry. Specific bounds were given by Cowin et al. (1999) for the effective elastic coefficients of cubic, hexagonal (transversely isotropic), tetragonal and trigonal symmetries in terms of the elastic coefficients of triclinic symmetry. In this work, the elastic coefficients of triclinic symmetry are replaced by these of orthotropic symmetry.

The anisotropic form of Hooke's law is often written in indicial notation as $T_{ij} = C_{ijkm} E_{km}$ where the C_{ijkm} are the components of the elasticity tensor in three dimensions, T_{ij} represents the stress tensor and E_{km} the strain tensor. Written as a linear transformation in six dimensions, Hooke's law has the representation $\hat{\mathbf{T}} = \hat{\mathbf{c}}\hat{\mathbf{E}}$ given by

$$\begin{bmatrix} T_{11} \\ T_{22} \\ T_{33} \\ \sqrt{2}T_{23} \\ \sqrt{2}T_{13} \\ \sqrt{2}T_{12} \end{bmatrix} = \begin{bmatrix} c_{11} & c_{12} & c_{13} & \sqrt{2}c_{14} & \sqrt{2}c_{15} & \sqrt{2}c_{16} \\ c_{12} & c_{22} & c_{23} & \sqrt{2}c_{24} & \sqrt{2}c_{25} & \sqrt{2}c_{26} \\ c_{13} & c_{23} & c_{33} & \sqrt{2}c_{34} & \sqrt{2}c_{35} & \sqrt{2}c_{36} \\ \sqrt{2}c_{14} & \sqrt{2}c_{24} & \sqrt{2}c_{34} & c_{44} & c_{45} & c_{46} \\ \sqrt{2}c_{15} & \sqrt{2}c_{25} & \sqrt{2}c_{35} & c_{45} & c_{55} & c_{56} \\ \sqrt{2}c_{16} & \sqrt{2}c_{26} & \sqrt{2}c_{36} & c_{46} & c_{56} & c_{66} \end{bmatrix} \begin{bmatrix} E_{11} \\ E_{22} \\ E_{33} \\ \sqrt{2}E_{23} \\ \sqrt{2}E_{13} \\ \sqrt{2}E_{12} \end{bmatrix}. \tag{5.1}$$

The matrix $\hat{\mathbf{c}}$ is a matrix of *elastic coefficients* and its inverse $\hat{\mathbf{s}}$, $\hat{\mathbf{E}} = \hat{\mathbf{s}}\hat{\mathbf{T}}$, $\hat{\mathbf{s}} = \hat{\mathbf{c}}^{-1}$ is a *compliance* matrix. The symmetric matrices $\hat{\mathbf{c}}$ and $\hat{\mathbf{s}}$ can be shown to represent the matrices of components of second-rank tensors in a 6-dimensional space (Cowin and Mehrabadi 1995; Mehrabadi and Cowin 1990). The eigenvalues of the matrix $\hat{\mathbf{c}}$ ($\hat{\mathbf{s}}$) are the six numbers Λ ($1/\Lambda$) satisfying the equation

$$(\hat{\mathbf{c}} - \Lambda\hat{\mathbf{I}})\hat{\mathbf{N}} = 0 \ \ ((\hat{\mathbf{s}} - (1/\Lambda)\hat{\mathbf{I}})\hat{\mathbf{N}} = 0), \tag{5.2}$$

where the vectors $\hat{\mathbf{N}}$ represent the normalized eigenvectors of $\hat{\mathbf{c}}$ (or $\hat{\mathbf{s}}$). Since $\hat{\mathbf{c}}$ (or $\hat{\mathbf{s}}$) is positive definite, it has six positive real eigenvalues. These eigenvalues are called the *Kelvin moduli* and are denoted by Λ_i, $i = 1, ..., 6$, and are ordered by the inequalities $\Lambda_1 \geq ... \geq \Lambda_6 > 0$. The elastic constants that are not eigenvalues are called *elasticity distributors.* The elasticity distributors specify the ratios of the components for the eigenvectors $\hat{\mathbf{N}}$. Geometrically they represent the ratio of relative extensions in perpendicular directions and/or the amount of shear in an eigenmode; their role is analogous to those of the Poisson's ratios, but they are not related to Poisson's ratios (Cowin and Mehrabadi 1995; Mehrabadi and Cowin 1990).

The results of the preceding paragraphs show that there exist six eigentensors of stress, denoted by $\hat{\mathbf{T}}^{(k)}$ $k = 1,...,6$, in the 6-dimensional space, and six eigentensors of strain, denoted by $\hat{\mathbf{E}}^{(k)}$, $k = 1,...,6$, respectively, which are related by the six equations

$$\hat{\mathbf{T}} = \Lambda_k \hat{\mathbf{E}}^{(k)}, \; k = 1,..., \; 6 . \tag{5.3}$$

It follows that $\hat{\mathbf{c}}$ and $\hat{\mathbf{s}}$ have the representations

$$\hat{\mathbf{c}} = \sum_{k=1}^{6} \Lambda_k \hat{\mathbf{N}}^{(k)} \otimes \hat{\mathbf{N}}^{(k)}, \; \hat{\mathbf{s}} = \sum_{k=1}^{6} \frac{1}{\Lambda_k} \hat{\mathbf{N}}^{(k)} \otimes \hat{\mathbf{N}}^{(k)}, \tag{5.4}$$

and that the strain energy Σ may be expressed as

$$\Sigma = \tfrac{1}{2} \hat{\mathbf{E}}^T \hat{\mathbf{c}} \hat{\mathbf{E}} = \tfrac{1}{2} \hat{\mathbf{T}}^T \hat{\mathbf{s}} \hat{\mathbf{T}} . \tag{5.5}$$

A result based on the stress-strain relation, $\hat{\mathbf{T}} = \hat{\mathbf{c}} \, \hat{\mathbf{E}}$, is easily converted to a result based on the strain-stress relation, $\hat{\mathbf{E}} = \hat{\mathbf{s}} \, \hat{\mathbf{T}}$, simply by interchanging $\hat{\mathbf{T}}$ and $\hat{\mathbf{E}}$ and $\hat{\mathbf{c}}$ and $\hat{\mathbf{s}}$, respectively. Thus, results for stress states or strain states are obtained simply by interchanging the following terms: $\hat{\mathbf{T}}$ and $\hat{\mathbf{E}}$, $\hat{\mathbf{c}}$ and $\hat{\mathbf{s}}$, and Λ_i and $1/\Lambda_i$.

To summarize briefly the development of the generalized Hill bounds, we follow Hill (1963) and note that the average strain energy in any region can be calculated from the assumption of a constant average stress (Reuss, 1929) or from the assumption of a constant average strain (Voigt, 1928). Hence, for the prescribed (constant) strain $\hat{\mathbf{E}}^A$, and the prescribed (constant) stress $\hat{\mathbf{T}}^A$, the average strain energy has the dual representation

$$2\Sigma^A = \hat{\mathbf{E}}^A \cdot \hat{\mathbf{c}}^{eff}\hat{\mathbf{E}}^A = \hat{\mathbf{T}}^A \cdot \hat{\mathbf{s}}^{eff}\hat{\mathbf{T}}^A, \tag{5.6}$$

where the definitions of effective elastic constants $\hat{\mathbf{c}}^{eff}$ and $\hat{\mathbf{s}}^{eff}$ have been employed,

$$\hat{\mathbf{T}}^A = \hat{\mathbf{c}}^{eff}\hat{\mathbf{E}}^A, \ \hat{\mathbf{E}}^A = \hat{\mathbf{s}}^{eff}\hat{\mathbf{T}}^A. \tag{5.7}$$

Now, still following Hill (1963), the principles of minimum potential energy and minimum complementary energy are employed to show that

$$\hat{\mathbf{E}}^A \cdot \hat{\mathbf{c}}^{eff,Grp}\hat{\mathbf{E}}^A \le \hat{\mathbf{E}}^A \cdot \hat{\mathbf{c}}^{V,Grp}\hat{\mathbf{E}}^A \text{ and } \hat{\mathbf{T}}^A \cdot \hat{\mathbf{s}}^{eff,Grp}\hat{\mathbf{T}}^A \le \hat{\mathbf{T}}^A \cdot \hat{\mathbf{s}}^{R,Grp}\hat{\mathbf{T}}^A, \tag{5.8}$$

where V and R stand for Voigt and Reuss and where we have introduced the superscript Grp on $\hat{\mathbf{c}}^{eff}$, $\hat{\mathbf{s}}^{eff}$ to emphasize that the material symmetry groups of $\hat{\mathbf{c}}^{V}$, $\hat{\mathbf{s}}^{R}$, $\hat{\mathbf{c}}^{eff}$ and $\hat{\mathbf{s}}^{eff}$ must be the same. The various symmetry groups (Grp) are denoted by Iso(tropic), Cub(ic), Hex(agonal), Tri(gonal), Tet(ragonal), Ort(hotropic), Mon(oclinic) and T(riclinic) so Grp stands for any one of these. The result (5.8) must hold for each eigenmode thus:

$$\Lambda_k^{eff,Grp} \le \Lambda_k^{V,Grp}, \ \frac{1}{\Lambda_k^{eff,Grp}} \le \frac{1}{\Lambda_k^{R,Grp}}, \text{ for } k = 1, \ldots, 6. \tag{5.9}$$

The two inequalities in (5.9) may be combined in the final result,

$$\Lambda_k^{R,Grp} \le \Lambda_k^{eff,Grp} \le \Lambda_k^{V,Grp}, \text{ for } k = 1, \ldots, 6. \tag{5.10}$$

We refer to the inequalities (5.10) on the eigenvalues as the generalized Hill inequalities.

5.3 Outline of the calculational procedure

Two sets of orthotropic elastic constants for cortical bone (from Ashman et al. 1984; van Buskirk et al.1981) are shown in Table 5.1. These elastic constants are employed to bound and approximate effective transversely isotropic elastic constants for the same material. We present this process as a step-by-step procedure.

(1) Transversely isotropic bounds on orthotropic data

Step 1.

The compliance matrix with given orthotropic data is constructed,

$$\hat{s}^{Ort} = \begin{bmatrix} \hat{s}_{11}^{Ort} & \hat{s}_{12}^{Ort} & \hat{s}_{13}^{Ort} & 0 & 0 & 0 \\ \hat{s}_{12}^{Ort} & \hat{s}_{22}^{Ort} & \hat{s}_{23}^{Ort} & 0 & 0 & 0 \\ \hat{s}_{13}^{Ort} & \hat{s}_{23}^{Ort} & \hat{s}_{33}^{Ort} & 0 & 0 & 0 \\ 0 & 0 & 0 & \hat{s}_{44}^{Ort} & 0 & 0 \\ 0 & 0 & 0 & 0 & \hat{s}_{55}^{Ort} & 0 \\ 0 & 0 & 0 & 0 & 0 & \hat{s}_{66}^{Ort} \end{bmatrix} \tag{5.11}$$

where

$$\hat{s}_{11}^{Ort} = \frac{1}{E_1}\ ,\ \hat{s}_{22}^{Ort} = \frac{1}{E_2}\ ,\ \hat{s}_{33}^{Ort} = \frac{1}{E_3}\ ,\ \hat{s}_{12}^{Ort} = -\frac{\nu_{12}}{E_1}\ ,\ \hat{s}_{13}^{Ort} = -\frac{\nu_{13}}{E_1}\ , \tag{5.12}$$

$$\hat{s}_{23}^{Ort} = -\frac{\nu_{23}}{E_2}\ ,\ \hat{s}_{44}^{Ort} = \frac{1}{2G_{23}}\ ,\ \hat{s}_{55}^{Ort} = \frac{1}{2G_{13}}\ ,\ \hat{s}_{66}^{Ort} = \frac{1}{2G_{12}}\ .$$

The inverse of *compliance matrix* (5.11), $\hat{c}^{Ort} = \left(\hat{s}^{Ort}\right)^{-1}$, the *elasticity matrix*, can be calculated as

$$\hat{c}^{Ort} = \begin{bmatrix} \hat{c}_{11}^{Ort} & \hat{c}_{12}^{Ort} & \hat{c}_{13}^{Ort} & 0 & 0 & 0 \\ \hat{c}_{12}^{Ort} & \hat{c}_{22}^{Ort} & \hat{c}_{23}^{Ort} & 0 & 0 & 0 \\ \hat{c}_{13}^{Ort} & \hat{c}_{23}^{Ort} & \hat{c}_{33}^{Ort} & 0 & 0 & 0 \\ 0 & 0 & 0 & \hat{c}_{44}^{Ort} & 0 & 0 \\ 0 & 0 & 0 & 0 & \hat{c}_{55}^{Ort} & 0 \\ 0 & 0 & 0 & 0 & 0 & \hat{c}_{66}^{Ort} \end{bmatrix}. \tag{5.13}$$

Step 2.

In this step we construct the upper and lower bounds on the effective transversely isotropic elastic constants. The effective elasticity matrix of hexagonal or transversely isotropic symmetry, with the 3 direction as the unique direction and the 1-2 plane as the plane of isotropy, is

$$\hat{c}^{eff,Hex} = \begin{bmatrix} \hat{c}_{11}^{eff,Hex} & \hat{c}_{12}^{eff,Hex} & \hat{c}_{13}^{eff,Hex} & 0 & 0 & 0 \\ \hat{c}_{12}^{eff,Hex} & \hat{c}_{11}^{eff,Hex} & \hat{c}_{13}^{eff,Hex} & 0 & 0 & 0 \\ \hat{c}_{13}^{eff,Hex} & \hat{c}_{13}^{eff,Hex} & \hat{c}_{33}^{eff,Hex} & 0 & 0 & 0 \\ 0 & 0 & 0 & \hat{c}_{44}^{eff,Hex} & 0 & 0 \\ 0 & 0 & 0 & 0 & \hat{c}_{44}^{eff,Hex} & 0 \\ 0 & 0 & 0 & 0 & 0 & \hat{c}_{11}^{eff,Hex} - \hat{c}_{12}^{eff,Hex} \end{bmatrix}. \tag{5.14}$$

Hexagonal (or transversely isotropic) symmetry has four distinct eigenvalues and a single distributor, the angle α. The definition of distributor α for *elasticity matrix* $\hat{c}^{eff,Hex}$ and *compliance matrix* $\hat{s}^{eff,Hex}$ is (See Cowin et al., 1999)

$$\tan 2\alpha^{V} = \frac{(\hat{c}_{11}^{Hex} + \hat{c}_{12}^{Hex} - \hat{c}_{33}^{Hex})}{2\sqrt{2}\hat{c}_{13}^{Hex}} \quad (or \quad \tan 2\alpha^{R} = \frac{(\hat{s}_{11}^{Hex} + \hat{s}_{12}^{Hex} - \hat{s}_{33}^{Hex})}{2\sqrt{2}\hat{s}_{13}^{Hex}}), \tag{5.15}$$

and the effective distributor α^{eff} is selected to satisfy the inequality

$$\tan 2\alpha^{R} \le \tan 2\alpha^{eff} \le \tan 2\alpha^{V}. \tag{5.16}$$

The following inequality is obtained by substituting equation (5.15) into equation (5.16),

$$\frac{\hat{s}_{11}^{Hex} + \hat{s}_{12}^{Hex} - \hat{s}_{33}^{Hex}}{2\sqrt{2}\hat{s}_{13}^{Hex}} \le \frac{\hat{c}_{11}^{eff,Hex} + \hat{c}_{12}^{eff,Hex} - \hat{c}_{33}^{eff,Hex}}{2\sqrt{2}\hat{c}_{13}^{eff,Hex}} \le \frac{\hat{c}_{11}^{Hex} + \hat{c}_{12}^{Hex} - \hat{c}_{33}^{Hex}}{2\sqrt{2}\hat{c}_{13}^{Hex}}. \tag{5.17}$$

The generalized Hill inequality (5.10) requires that the four distinct eigenvalues of the hexagonal symmetry satisfy the following inequalities (See Cowin et al. 1999, especially equations (29) and (30) and section 6),

$$\begin{aligned} &\Lambda_{(1)}^{R,Hex} \le \Lambda_{(1)}^{eff,Hex} \le \Lambda_{(1)}^{V,Hex}, \quad \Lambda_{(2)}^{R,Hex} \le \Lambda_{(2)}^{eff,Hex} \le \Lambda_{(2)}^{V,Hex}, \\ &\Lambda_{(3,6)}^{R,Hex} \le \Lambda_{(3,6)}^{eff,Hex} \le \Lambda_{(3,6)}^{V,Hex}, \quad \Lambda_{(4,5)}^{R,Hex} \le \Lambda_{(4,5)}^{eff,Hex} \le \Lambda_{(4,5)}^{V,Hex} \end{aligned}. \tag{5.18}$$

We now seek expressions for the eigenvalues that are bounded in equation (5.18). The eigenvalues for Reuss (lower) bound are expressed in terms of $\hat{s}^{Hex}$ by

$$\Lambda_{(1)}^{R,Hex} = \frac{2}{\left[(\hat{s}_{11}^{Hex} + \hat{s}_{12}^{Hex} + \hat{s}_{33}^{Hex}) + \sqrt{8(\hat{s}_{13}^{Hex})^2 + (\hat{s}_{11}^{Hex} + \hat{s}_{12}^{Hex} - \hat{s}_{33}^{Hex})}\right]},$$

$$\Lambda_{(2)}^{R,Hex} = \frac{2}{\left[(\hat{s}_{11}^{Hex} + \hat{s}_{12}^{Hex} + \hat{s}_{33}^{Hex}) - \sqrt{8(\hat{s}_{13}^{Hex})^2 + (\hat{s}_{11}^{Hex} + \hat{s}_{12}^{Hex} - \hat{s}_{33}^{Hex})}\right]},$$

$$\Lambda_{(3,6)}^{R,Hex} = \frac{1}{\hat{s}_{11}^{Hex} - \hat{s}_{12}^{Hex}}, \quad \Lambda_{(4,5)}^{R,Hex} = \frac{1}{\hat{s}_{44}^{Hex}}, \tag{5.19}$$

and eigenvalues for Voigt (upper) bound are expressed in terms of $\hat{c}^{Hex}$ by

$$\Lambda_{(1)}^{V,Hex} = \frac{\left[(\hat{c}_{11}^{Hex} + \hat{c}_{12}^{Hex} + \hat{c}_{33}^{Hex}) + \sqrt{8(\hat{c}_{13}^{Hex})^2 + (\hat{c}_{11}^{Hex} + \hat{c}_{12}^{Hex} - \hat{c}_{33}^{Hex})}\right]}{2},$$

$$\Lambda_{(2)}^{V,Hex} = \frac{\left[(\hat{c}_{11}^{Hex} + \hat{c}_{12}^{Hex} + \hat{c}_{33}^{Hex}) - \sqrt{8(\hat{c}_{13}^{Hex})^2 + (\hat{c}_{11}^{Hex} + \hat{c}_{12}^{Hex} - \hat{c}_{33}^{Hex})}\right]}{2},$$

$$\Lambda_{(3,6)}^{V,Hex} = \hat{c}_{11}^{Hex} - \hat{c}_{12}^{Hex}, \quad \Lambda_{(4,5)}^{V,Hex} = \hat{c}_{44}^{Hex}. \tag{5.20}$$

Substituting equations (5.19) and (5.20) into inequalities into equation (5.18) establishes four distinct inequalities that the hexagonal elasticity and compliance components must satisfy. The hexagonal elasticity components $\hat{c}^{Hex}$ and compliance components $\hat{s}^{Hex}$ in the upper and lower bounds of (5.18) are replaced by the orthotropic elasticity components $\hat{c}^{Ort}$ and the orthotropic compliance components $\hat{s}^{Ort}$, respectively, using

$$\hat{s}_{11}^{Hex} = \frac{1}{8}(3\hat{s}_{11}^{Ort} + 2\hat{s}_{12}^{Ort} + 3\hat{s}_{22}^{Ort} + 2\hat{s}_{66}^{Ort}),$$

$$\hat{s}_{12}^{Hex} = \frac{1}{8}(\hat{s}_{11}^{Ort} + 6\hat{s}_{12}^{Ort} + \hat{s}_{22}^{Ort} - 2\hat{s}_{66}^{Ort}),$$

$$\hat{s}_{13}^{Hex} = \frac{1}{2}(\hat{s}_{13}^{Ort} + \hat{s}_{23}^{Ort}),$$

$$\hat{s}_{33}^{Hex} = \hat{s}_{33}^{Ort},$$

$$\hat{s}_{44}^{Hex} = \frac{1}{2}(\hat{s}_{44}^{Ort} + \hat{s}_{55}^{Ort}), \tag{5.21}$$

and

$$\hat{c}_{11}^{Hex} = \frac{1}{8}(3\hat{c}_{11}^{Ort} + 2\hat{c}_{12}^{Ort} + 3\hat{c}_{22}^{Ort} + 2\hat{c}_{66}^{Ort}),$$

$$\hat{c}_{12}^{Hex} = \frac{1}{8}(\hat{c}_{11}^{Ort} + 6\hat{c}_{12}^{Ort} + \hat{c}_{22}^{Ort} - 2\hat{c}_{66}^{Ort}),$$

$$\hat{c}_{13}^{Hex} = \frac{1}{2}(\hat{c}_{13}^{Ort} + \hat{c}_{23}^{Ort}),$$

$$\hat{c}_{33}^{Hex} = \hat{c}_{33}^{Ort},$$

$$\hat{c}_{44}^{Hex} = \frac{1}{2}(\hat{c}_{44}^{Ort} + \hat{c}_{55}^{Ort}). \tag{5.22}$$

These relations were obtained by averaging the orthotropic elastic constants over all orientations permitted by hexagonal symmetry (see Cowin and Mehrabadi 1995; Cowin et al 1999; Hearmon 1946, 1948, 1961).

Then five inequalities from four distinct eigenvalues and one distributor are

$$\frac{\hat{s}_{11}^{Ort} + 2\hat{s}_{12}^{Ort} + \hat{s}_{22}^{Ort} - 2\hat{s}_{33}^{Ort}}{2\sqrt{2}(\hat{s}_{13}^{Ort} + \hat{s}_{23}^{Ort})} \le \frac{\hat{c}_{11}^{eff,Hex} + \hat{c}_{12}^{eff,Hex} - \hat{c}_{33}^{eff,Hex}}{2\sqrt{2}\hat{c}_{13}^{eff,Hex}} \le \frac{\hat{c}_{11}^{Ort} + 2\hat{c}_{12}^{Ort} + \hat{c}_{22}^{Ort} - 2\hat{c}_{33}^{Ort}}{2\sqrt{2}(\hat{c}_{13}^{Ort} + \hat{c}_{23}^{Ort})}, \tag{5.23}$$

$$\frac{4}{\hat{s}_{11}^{Ort} + \hat{s}_{22}^{Ort} + 2\hat{s}_{12}^{Ort} + 2\hat{s}_{33}^{Ort} + 2\sqrt{2}(\hat{s}_{13}^{Ort} + \hat{s}_{23}^{Ort})sec(2\alpha^{R})}$$

$$\le \frac{\hat{c}_{11}^{eff,Hex} + \hat{c}_{12}^{eff,Hex} + \hat{c}_{33}^{eff,Hex} + 2\sqrt{2}\hat{c}_{13}^{eff,Hex}sec(2\alpha^{eff})}{2} \tag{5.24}$$

$$\leq \frac{\hat{c}_{11}^{Ort}+\hat{c}_{22}^{Ort}+2\hat{c}_{12}^{Ort}+2\hat{c}_{33}^{Ort}+2\sqrt{2}(\hat{c}_{13}^{Ort}+\hat{c}_{23}^{Ort})sec(2\alpha^{R})}{4},$$

$$\frac{4}{\hat{s}_{11}^{Ort}+\hat{s}_{22}^{Ort}+2\hat{s}_{12}^{Ort}+2\hat{s}_{33}^{Ort}-2\sqrt{2}(\hat{s}_{13}^{Ort}+\hat{s}_{23}^{Ort})sec(2\alpha^{R})}$$

$$\leq \frac{\hat{c}_{11}^{eff,Hex}+\hat{c}_{12}^{eff,Hex}+\hat{c}_{33}^{eff,Hex}-2\sqrt{2}\hat{c}_{13}^{eff,Hex}sec(2\alpha^{eff})}{2} \qquad (5.25)$$

$$\leq \frac{\hat{c}_{11}^{Ort}+\hat{c}_{22}^{Ort}+2\hat{c}_{12}^{Ort}+2\hat{c}_{33}^{Ort}-2\sqrt{2}(\hat{c}_{13}^{Ort}+\hat{c}_{23}^{Ort})sec(2\alpha^{V})}{4},$$

$$\frac{4}{\hat{s}_{11}^{Ort}+\hat{s}_{22}^{Ort}-2\hat{s}_{12}^{Ort}+2\hat{s}_{66}^{Ort}} \leq \hat{c}_{11}^{eff,Hex}-\hat{c}_{12}^{eff,Hex} \leq \frac{1}{4}(\hat{c}_{11}^{Ort}+\hat{c}_{22}^{Ort}-2\hat{c}_{12}^{Ort}+2\hat{c}_{66}^{Ort}), \qquad (5.26)$$

and,

$$\frac{2}{\hat{s}_{44}^{Ort}+\hat{s}_{55}^{Ort}} \leq \hat{c}_{44}^{eff,Hex} \leq \frac{1}{2}(\hat{c}_{44}^{Ort}+\hat{c}_{55}^{Ort}). \qquad (5.27)$$

Equation (5.23) is obtained from (5.17) by substituting (5.21) and (5.22) into (5.17); equations (5.24) though (5.27) are obtained from the four inequalities (5.18) by substituting (5.19) and (5.20) into (5.18) and then (5.21) and (5.22) into the resulting equations. Five upper bound elasticity components, $\hat{c}_{11}^{eff,Hex+}$, $\hat{c}_{12}^{eff,Hex+}$, $\hat{c}_{13}^{eff,Hex+}$, $\hat{c}_{33}^{eff,Hex+}$, and $\hat{c}_{44}^{eff,Hex+}$ (lower bound elasticity components, $\hat{c}_{11}^{eff,Hex-}$, $\hat{c}_{12}^{eff,Hex-}$, $\hat{c}_{13}^{eff,Hex-}$, $\hat{c}_{33}^{eff,Hex-}$, and $\hat{c}_{44}^{eff,Hex-}$) are obtained from inequalities (5.23) through (5.27) by setting the bounded term equal to its upper bound (lower bound) and solving the resulting equations. Solutions of these equations provide the greatest (least) values for each component of the hexagonal elasticity matrix. The mean values of upper bounds and lower bounds of each component,

$\hat{c}_{11}^{eff,Hex,m}$, $\hat{c}_{12}^{eff,Hex,m}$, $\hat{c}_{13}^{eff,Hex,m}$, $\hat{c}_{33}^{eff,Hex,m}$, and $\hat{c}_{44}^{eff,Hex,m}$ are obtained by summing the upper and lower bounds and dividing by two.

Step 3.

First, from (5.14), the inverse of the effective upper bound *elasticity matrix* for $\hat{c}^{eff,Hex+}$ is

$$\hat{s}^{eff,Hex+} = \begin{bmatrix} \hat{s}_{11}^{eff,Hex+} & \hat{s}_{12}^{eff,Hex+} & \hat{s}_{13}^{eff,Hex+} & 0 & 0 & 0 \\ \hat{s}_{12}^{eff,Hex+} & \hat{s}_{11}^{eff,Hex+} & \hat{s}_{13}^{eff,Hex+} & 0 & 0 & 0 \\ \hat{s}_{13}^{eff,Hex+} & \hat{s}_{13}^{eff,Hex+} & \hat{s}_{33}^{eff,Hex+} & 0 & 0 & 0 \\ 0 & 0 & 0 & \hat{s}_{44}^{eff,Hex+} & 0 & 0 \\ 0 & 0 & 0 & 0 & \hat{s}_{44}^{eff,Hex+} & 0 \\ 0 & 0 & 0 & 0 & 0 & \hat{s}_{11}^{eff,Hex+} - \hat{s}_{12}^{eff,Hex+} \end{bmatrix}, \quad (5.28)$$

and each component of this matrix is converted to an equivalent effective elastic constant by

$$E_1^{eff,Hex} = E_2^{eff,Hex} = \frac{1}{\hat{s}_{11}^{eff,Hex}}, \quad E_3^{eff,Hex} = \frac{1}{\hat{s}_{33}^{eff,Hex}}, \quad G_{12}^{eff,Hex} = \frac{1}{\hat{s}_{11}^{eff,Hex} - \hat{s}_{12}^{eff,Hex}},$$

$$G_{13}^{eff,Hex} = G_{23}^{eff,Hex} = \frac{1}{\hat{s}_{44}^{eff,Hex}}, \quad \nu_{12}^{eff,Hex} = -\frac{\hat{s}_{12}^{eff,Hex}}{\hat{s}_{11}^{eff,Hex}}, \quad \nu_{13}^{eff,Hex} = -\frac{\hat{s}_{13}^{eff,Hex}}{\hat{s}_{11}^{eff,Hex}}, \quad \nu_{21}^{eff,Hex} = -\frac{\hat{s}_{21}^{eff,Hex}}{\hat{s}_{22}^{eff,Hex}},$$

$$\nu_{31}^{eff,Hex} = -\frac{\hat{s}_{31}^{eff,Hex}}{\hat{s}_{33}^{eff,Hex}}, \quad \nu_{23}^{eff,Hex} = -\frac{\hat{s}_{23}^{eff,Hex}}{\hat{s}_{22}^{eff,Hex}}, \quad \nu_{32}^{eff,Hex} = -\frac{\hat{s}_{32}^{eff,Hex}}{\hat{s}_{33}^{eff,Hex}}. \quad (5.29)$$

In the similar way the lower bound $\hat{c}^{eff,Hex-}$ is changed into the effective elastic constants. The mean of the upper bounds and lower bounds $\hat{c}^{eff,Hex,m}$ is then easy to determine in terms of the effective elastic constants. The effective elastic constants for bone based on the orthotropic data sets in Table 5.1 (from Ashman et al 1984; van Buskirk et al.1981), are shown in Tables 5.2 and 5.3.

Example

The orthotropic data set of Ashman et al. (1984), shown in Table 5.1, is used to calculate effective hexagonal elastic constants.

Step 1.

Construct the orthotropic compliance matrix (5.11) using equation (5.12) and the data from Table 5.1, thus

$$\hat{s}^{Ort} = \begin{bmatrix} 0.083 & -0.031 & -0.019 & 0 & 0 & 0 \\ -0.031 & 0.075 & -0.018 & 0 & 0 & 0 \\ -0.019 & -0.018 & 0.05 & 0 & 0 & 0 \\ 0 & 0 & 0 & 0.08 & 0 & 0 \\ 0 & 0 & 0 & 0 & 0.089 & 0 \\ 0 & 0 & 0 & 0 & 0 & 0.11 \end{bmatrix},$$

where each component has the dimensions of $(Pa)^{-1}$.The elasticity matrix is the inverse of the above matrix and has the dimensions of Pa,

$$\hat{c}^{Ort} = \begin{bmatrix} 18.02 & 9.973 & 10.171 & 0 & 0 & 0 \\ 9.973 & 20.12 & 10.745 & 0 & 0 & 0 \\ 10.171 & 10.745 & 27.533 & 0 & 0 & 0 \\ 0 & 0 & 0 & 12.46 & 0 & 0 \\ 0 & 0 & 0 & 0 & 11.22 & 0 \\ 0 & 0 & 0 & 0 & 0 & 9.06 \end{bmatrix}.$$

Step 2.

When the data from Table 5.1 are substituted into equations (5.23) through (5.27), one obtains the following inequalities for the components of $\hat{c}^{eff,Hex}$:

$$0.048 \le \frac{\hat{c}_{11}^{eff,Hex} + \hat{c}_{12}^{eff,Hex} - \hat{c}_{33}^{eff,Hex}}{2\sqrt{2}\hat{c}_{13}^{eff,Hex}} \le 0.051,$$

$$42.978 \le \frac{\hat{c}_{11}^{eff,Hex} + \hat{c}_{12}^{eff,Hex} + \hat{c}_{33}^{eff,Hex} + 2\sqrt{2}\hat{c}_{13}^{eff,Hex}\sec(2\alpha_{eff})}{2} \le 43.097,$$

$$13.459 \le \frac{\hat{c}_{11}^{eff,Hex} + \hat{c}_{12}^{eff,Hex} + \hat{c}_{33}^{eff,Hex} - 2\sqrt{2}\hat{c}_{13}^{eff,Hex}\sec(2\alpha_{eff})}{2} \le 13.479,$$

$$9.059 \le \hat{c}_{11}^{eff,Hex} - \hat{c}_{12}^{eff,Hex} \le 9.079,$$

$$11.808 \le \hat{c}_{44}^{eff,Hex} \le 11.84.$$

The matrices for upper bound, lower bound, and the mean ($\hat{c}^{eff,Hex+}, \hat{c}^{eff,Hex-}, \hat{c}^{eff,Hex,m}$) are constructed. The mean ($\hat{c}^{eff,Hex,m}$) is

$$\hat{c}^{eff,Hex,m} = \begin{bmatrix} 19.026 & 9.957 & 10.441 & 0 & 0 & 0 \\ 9.957 & 19.026 & 10.441 & 0 & 0 & 0 \\ 10.441 & 10.441 & 27.524 & 0 & 0 & 0 \\ 0 & 0 & 0 & 11.824 & 0 & 0 \\ 0 & 0 & 0 & 0 & 11.824 & 0 \\ 0 & 0 & 0 & 0 & 0 & 9.069 \end{bmatrix},$$

and both $\hat{c}^{eff,Hex,+}$ and $\hat{c}^{eff,Hex,-}$ may be calculated in the same way.

Step 3.

The effective transversely isotropic compliance matrix is obtained by inverting the above elasticity matrix, $\hat{c}^{eff,Hex,m}$, thus

$$\hat{s}^{eff,Hex,m} = \begin{bmatrix} 0.079 & -0.031 & -0.018 & 0 & 0 & 0 \\ -0.031 & 0.079 & -0.018 & 0 & 0 & 0 \\ -0.018 & -0.018 & 0.05 & 0 & 0 & 0 \\ 0 & 0 & 0 & 0.085 & 0 & 0 \\ 0 & 0 & 0 & 0 & 0.085 & 0 \\ 0 & 0 & 0 & 0 & 0 & 0.11 \end{bmatrix},$$

where both $\hat{s}^{eff,Hex+}$ and $\hat{s}^{eff,Hex-}$ are calculated as described above. The effective transversely isotropic elastic constants from $\hat{s}^{eff,Hex+}$, $\hat{s}^{eff,Hex-}$, and $\hat{s}^{eff,Hex,m}$ are determined by equation (5.29) and shown in Table 5.2.

(2) Isotropy

The effective isotropic elastic constants are determined using a similar step-by-step procedure. Isotropic symmetry is characterized by two distinct eigenvalues and no distributor. Thus there are two inequalities to satisfy. The data sets of the calculated effective isotropic elastic constants are summarized in Tables 5.4 and 5.5. See Cowin et al. (1999) and Yang et al. (1999) for detailed explanations of the associated eigenvalues, eigenvectors and bounds for isotropy.

5.4 Application of the method when the elastic constants data depend on composition

The method in the previous section is applicable to compositionally dependent materials. The volume fraction dependent orthotropic elastic cancellous bone data set from Yang et al.(1999), valid for $0.05 \le \phi \le 0.35$, is given by

$$E_1 = 528.8E_t\phi^{1.92},\ E_2 = 885E_t\phi^{1.89},\ E_3 = 1240E_t\phi^{1.80}$$

$$2G_{12} = 533.3E_t\phi^{2.04},\ 2G_{13} = 633.3E_t\phi^{1.97},\ 2G_{23} = 972.6E_t\phi^{1.98},$$

$$\nu_{21} = 0.256\phi^{-0.09},\ \nu_{12} = 0.153\phi^{-0.05},\ \nu_{31} = 0.316\phi^{-0.19},$$

$$\nu_{13} = 0.135\phi^{-0.07},\ \nu_{32} = 0.176\phi^{-0.25},\ \nu_{23} = 0.125\phi^{-0.16}. \qquad (5.30)$$

Note that the 1 and 3 coordinate directions of Yang et al. (1999) are interchanged. The dependence of the elastic constants on the volume fraction ϕ makes the conversion to transverse isotropy (or isotropy) more complicated. In order to reduce these analysis to be of the same type as the one described above, seven discrete values of the volume fraction (ϕ = 0.05, 0.1, 0.15, 0.2, 0.25, 0.3, 0.35) are selected and substituted into equation (5.30). There are then seven sets of the elastic constants (5.30), one for each value of the volume fraction from 0.05 to 0.35 in increments of 0.05. The method in the previous section is then applied for each elastic constant on each value of the volume fraction and the associated values of the constants for transverse isotropy (or isotropy) are obtained. A regression against volume fraction for each elastic constant is then accomplished using Statistical software (SPSS 10.1 for Windows). The squared correlation coefficients (R^2) are found to be greater than 0.99 ($R^2 \geq 0.99$). The compositionally dependent effective transversely isotropic and isotropic elastic constants of cancellous bone obtained are listed in Tables 5.6 and 5.7.

5.5 Discussion

A method of bounding the values of the transversely isotropic and isotropic elastic constants of a material using the values of orthotropic elastic constants of the same material was presented. In this study, two compact bone and one compositionally dependent cancellous bone orthotropic data sets were considered.

The bounds on the effective transversely isotropic and isotropic elastic constants obtained from orthotropic elastic constants for compact bone are very tight, and the means of the bounds give a very good approximation to the value of the constant. The

results for cancellous bone contained a several inconsistency. Unhappily, the lower bounds in Table 5.6 for E_3, $\nu_{13}(=\nu_{23})$ and $\nu_{31}(=\nu_{32})$ are slightly greater than the associated upper bounds. For E_3, the lower bound is $1243.61\phi^{1.8}$ while the upper bound is $1242.82\phi^{1.8}$, $0.79\ \phi^{1.8}$ smaller. If one makes the lower and upper bounds equal in this case, taking their value to be the average of the upper and lower bounds, then $E_3 = 1243.215\phi^{1.8}$ inducing an error of 0.03% with respect to the bounds. This error is negligible compared to the potential errors in the experimental and calculational procedures for determining these particular elastic constants. The errors are larger in the case of Poisson's ratio, ν_{31} (or ν_{32}) in Table 5.6. The maximum error in $\nu_{13}(=\nu_{23})$ or $\nu_{31}(=\nu_{32})$ is 6.2 % if the mean value is taken on the upper bound and lower bound. Poisson's ratios are generally prone to more error because they are actually ratios of elastic constants carrying the dimension of stress that carry the basic experimental error which is compounded by the calculation of their ratio. The cancellous bone specimens from which these data were obtained were collected from different anatomical locations of 56 individuals. The data were obtained using reconstructive computer programs coupled to a two-dimensional scanning technique (Kabel et al., 1999a;b). Exact estimates of the errors in the various steps in the primary determination of these elastic constants are not possible retrospectively. It appears, however, that an error of 6.2% in the value of a Poisson ratio is not inconsistent with the complicated experimental technique employed to obtain the basic data and the fact that Poisson's ratios are ratios of stress-dimensioned elastic constants that carry the basic experimental error.

Table 5.1. Experimental measured orthotropic cortical bone data of Ashman et al (1984) and van Buskirk et al. (1981)

	Ashman, *et al.*	Van Buskirk, *et al.*
E_1 [GPa]	12.0	11.6
E_2 [GPa]	13.4	14.6
E_3 [GPa]	20.0	21.7
G_{12} [GPa]	4.53	5.29
G_{23} [GPa]	5.61	6.29
G_{13} [GPa]	6.23	6.99
ν_{12}	0.376	0.302
ν_{13}	0.222	0.109
ν_{23}	0.235	0.205
ν_{21}	0.422	0.380
ν_{31}	0.371	0.206
ν_{32}	0.350	0.307

Table 5.2. The effective transversely isotropic technical elastic constants calculated from the orthotropic data of Ashman et al. (1984).

	Lower	Mean	Upper
$E_1 = E_2$ [GPa]	12.662	12.68	12.695
E_3 [GPa]	20.001	20.001	20.001
G_{12} [GPa]	4.53	4.535	4.539
$G_{23} = G_{13}$ [GPa]	5.904	5.912	5.92
$\nu_{12} = \nu_{21}$	0.398	0.398	0.398
$\nu_{13} = \nu_{23}$	0.228	0.229	0.229
$\nu_{31} = \nu_{32}$	0.36	0.36	0.36

Table 5.3. The effective transversely isotropic technical elastic constants calculated from the orthotropic data of van Buskirk et al. (1981).

	Lower	Mean	Upper
$E_1 = E_2$ [GPa]	13.307	13.404	13.5
E_3 [GPa]	21.892	21.925	21.958
G_{12} [GPa]	5.053	5.088	5.122
$G_{23} = G_{13}$ [GPa]	6.622	6.631	6.64
$\nu_{12} = \nu_{21}$	0.317	0.318	0.318
$\nu_{13} = \nu_{23}$	0.156	0.158	0.16
$\nu_{31} = \nu_{32}$	0.257	0.259	0.261

Table 5.4. The effective isotropic technical elastic constants calculated from the orthotropic data of Ashman et al. (1984).

	Lower	Mean	Upper
E [GPa]	14.228	14.368	14.507
G [GPa]	5.362	5.41	5.457
ν	0.327	0.328	0.329

Table 5.5. The effective transversely isotropic technical elastic constants calculated from the orthotropic data of van Buskirk et al.(1981).

	Lower	Mean	Upper
E [GPa]	15.184	15.288	15.491
G [GPa]	6.109	6.150	6.19
ν	0.243	0.247	0.251

Table 5.6. The effective transversely isotropic technical elastic constants calculated from the orthotropic data of Yang et al. (1999). Note that the values of the lower bounds of E_3, $\nu_{13}=\nu_{23}$ and $\nu_{31}=\nu_{32}$ are greater than the values of the upper bounds. This inconsistency is considered in the Discussion.

	Lower	Mean	Upper
$E_1=E_2$ [GPa]	$656.422\phi^{1.96}$	$670.671\phi^{1.94}$	$685.285\phi^{1.93}$
E_3 [GPa]	$1243.61\phi^{1.80}$	$1243.18\phi^{1.80}$	$1242.82\phi^{1.80}$
G_{12} [GPa]	$273.932\phi^{1.99}$	$276.673\phi^{1.98}$	$279.59\phi^{1.96}$
$G_{23}=G_{13}$ [GPa]	$383.542\phi^{1.96}$	$392.481\phi^{1.96}$	$401.427\phi^{1.96}$
$\nu_{12}=\nu_{21}$	$0.206\phi^{-0.15}$	$0.219\phi^{-0.14}$	$0.233\phi^{-0.13}$
$\nu_{13}=\nu_{23}$	$0.133\phi^{-0.07}$	$0.129\phi^{-0.07}$	$0.124\phi^{-0.08}$
$\nu_{31}=\nu_{32}$	$0.253\phi^{-0.22}$	$0.239\phi^{-0.22}$	$0.225\phi^{-0.22}$

Table 5.7. The effective isotropic technical elastic constants calculated from the orthotropic data of Yang et al. (1999)

	Lower	Mean	Upper
E [GPa]	$794.170\phi^{1.97}$	$822.367\phi^{1.95}$	$851.086\phi^{1.94}$
G [GPa]	$335.617\phi^{2.00}$	$345.540\phi^{1.99}$	$355.621\phi^{1.98}$
ν	$0.190\phi^{-0.15}$	$0.198\phi^{-0.16}$	$0.205\phi^{-0.16}$

Chapter 6

Future Study

The computational anisotropic poroelastic model will be developed by using anisotropic elastic constants estimated in this dissertation. Two steps are needed before constructing a computational model.

Step 1. Verify the location of different types of osteons

Ascenzi et al. (1987) found that type T osteons tend to be located where the cortical bone is thicker and type L osteons are located where the cortical bone is thinner, but exact location of different osteons are still unknown. Thus it is necessary to verify the location of different types of osteons from the histological section of human cortical bone for building a computational anisotropic model of a cortical bone.

Step 2. Estimates of poroelastic constants at the vascular porosity

Only poroelastic constants at the lacunar-canalicular porosity level were estimated in Chapter 4. However, if the poroelastic constants at the vascular porosity level are estimated, the time needed to build a computational model of a cortical bone will be reduced.

Drained elastic constants at the vascular porosity

The drained poroelastic constants at the vascular porosity are calculated by employing the explicit form of Eshelby tensor for a cylindrical void, which is derived by Suvorov and Dvorak (2002). The Eshelby tensor for a cylindrical void is obtained from Hill polarization tensor $\hat{\mathbf{P}}$ as $\hat{\mathbf{S}}^E = \hat{\mathbf{P}}\hat{\mathbf{C}}^M$. Components of Hill polarization tensor $\hat{\mathbf{P}}$ in orthotropic medium, when the cylindrical void is aligned to 3-direction, are given by (Hill 1965; Suvorov and Dvorak 2002).

$$P_{11} = \frac{\rho}{d_1 c_{22} c_{44} c_{66}} \left(c_{55} c_{66} \frac{n_0}{d} + (c_{22} c_{55} + c_{44} c_{66}) n_2 + c_{22} c_{44} n_4 \right),$$

$$P_{12} = \frac{\rho}{d_1 c_{22} c_{44} c_{66}} \left(-c_{55} (c_{12} + c_{66}) n_2 - c_{44} (c_{12} + c_{66}) n_4 \right),$$

$$P_{22} = \frac{\rho}{d_1 c_{44} c_{66}} \left(c_{11} c_{55} n_2 + (c_{55} c_{66} + c_{11} c_{44}) n_4 + c_{44} c_{66} n_6 \right),$$

$$P_{66} = \frac{\rho}{d_1 c_{22} c_{44} c_{66}} \left(c_{11} c_{55} \frac{n_0}{d_2} + (c_{11} c_{44} - 2c_{12} c_{55}) n_2 + (c_{22} c_{55} - 2c_{12} c_{44}) n_4 + c_{22} c_{44} n_6 \right),$$

$$P_{55} = \frac{\rho}{d_1 c_{22} c_{44} c_{66}} \left(c_{11} c_{66} \frac{n_0}{d_2} + \left(c_{11} c_{22} + c_{66}^2 - (c_{12} + c_{66})^2 \right) n_2 + c_{22} c_{66} n_4 \right),$$

$$P_{44} = \frac{\rho}{d_1 c_{22} c_{44} c_{66}} \left(c_{11} c_{66} n_2 + \left(c_{11} c_{22} + c_{66}^2 - (c_{12} + c_{66})^2 \right) n_4 + c_{22} c_{66} n_6 \right),$$

where unknown variables in above equations are defined as

$$d_1 = -g(h + \beta_3 g + \beta_3^2)(\rho^2 + \rho g + h)(\beta_3 + \rho) > 0,$$

$$d_2 = h \beta_3 \rho > 0,$$

$$g = \sqrt{\frac{c_{11} c_{22} - c_{12}^2 + 2c_{66}((c_{11} c_{22})^{1/2} - c_{12})}{c_{22} c_{66}}} > 0,$$

$$\beta_3 = \sqrt{\frac{c_{55}}{c_{44}}},\quad h = \sqrt{\frac{c_{11}}{c_{22}}},\quad \rho = a_1/a_2,\quad s = g^2 - 2h,$$

$$n_0 = 2(h\beta_3 + h\rho + \beta_3\rho g) + \rho^2(g+\beta_3) + \beta_3^2(g+\rho) + hg,$$

$$n_2 = (g + \beta_3 + \rho),$$

$$n_4 = (h\beta_3 + h\rho + \beta_3\rho g),$$

and

$$n_6 = 2\rho h\beta_3(\rho + g + \beta_3) + \rho^2(\beta_3 s + \beta_3^2 g + hg) + \beta_3^2(\rho s + hg) + h^2(\beta_3 + \rho). \quad (6.1)$$

The following equation for the dilute distribution assumption is used to estimate the drained poroelastic constants at the vascular porosity, which is given by

$$\hat{\mathbf{C}}^d = \hat{\mathbf{C}}^{u.l}(\hat{\mathbf{I}} - \phi(\hat{\mathbf{I}} - \hat{\mathbf{S}}^E)^{-1}), \quad (6.2)$$

where $\hat{\mathbf{C}}^d$ is the elasticity tensor for the drained case at the vascular porosity, $\hat{\mathbf{C}}^{u.l}$ is the elasticity tensor for the undrained case at the lacunar-canalicular porosity, $\hat{\mathbf{I}}$ is the identity tensor, ϕ is the vascular porosity ($\phi = 0.04$, Cowin 1999), and $\hat{\mathbf{S}}^E$ is the Eshelby tensor for the vascular porosity estimated from Hill polarization tensor $\hat{\mathbf{P}}$. Note that the elasticity tensor for the undrained case at the lacunar-canalicular porosity ($\hat{\mathbf{C}}^{u.l}$) was used instead of the elasticity tensor of the bone matrix at the vascular porosity level in Eq. (6.2) because the relaxation time of vascular porosity is several orders higher than that of lacunar-canalicular porosity (Smit et al. 2002).

Drained elastic constants at the vascular porosity

The undrained poroelastic constants at the vascular porosity are estimated by

the undrained and drained relation of poroelasticity theory, which is given by

$$\hat{\mathbf{S}}^{u} = \hat{\mathbf{S}}^{d} - \frac{1}{C_{eff}} \hat{\mathbf{S}}^{d} \cdot \hat{\mathbf{A}} \otimes \hat{\mathbf{S}}^{d} \cdot \hat{\mathbf{A}}, \tag{6.3}$$

where $\hat{\mathbf{S}}^{u}$ is the compliance tensor for the undrained case, which is the inverse of the elasticity tensor for the undrained case ($\hat{\mathbf{S}}^{u} = (\hat{\mathbf{C}}^{u})^{-1}$), $\hat{\mathbf{S}}^{d}$ is the compliance tensor for the drained case, which is the inverse of the elasticity tensor for the drained case ($\hat{\mathbf{S}}^{d} = (\hat{\mathbf{C}}^{d})^{-1}$). C_{eff} is the effective compressibility and $\hat{\mathbf{A}}$ is the Biot effective coefficient, which were defined in Chapter 4.

The orthotropic poroelastic constants at the vascular porosity for type L osteon, type T osteon, and type A osteon are calculated and these orthotropic poroelastic constants are converted to transversely isotropic elastic constants by using the technique shown in Chapter 5. The results are shown in Tables 6.1, 6.2, and 6.3, respectively.

Table 6.1 The estimated undrained and drained elastic constants of the type L osteon at the vascular porosity level. Both orthotropic and transversely isotropic results are shown.

Orthotropic results				**Transversely Isotropic results**			
The undrained elastic constants		The drained elastic constants		The undrained elastic constants		The drained elastic constants	
E_1^u	13.571	E_1^d	13.553	$E_1^u = E_2^u$	15.781	$E_1^d = E_2^d$	15.765
E_2^u	16.443	E_2^d	16.431				
E_3^u	20.719	E_3^d	20.708	E_3^u	20.792	E_3^d	20.718
ν_{12}^u	0.327	ν_{12}^d	0.326	$\nu_{12}^u = \nu_{21}^u$	0.327	$\nu_{12}^d = \nu_{21}^d$	0.326
ν_{13}^u	0.221	ν_{13}^d	0.220				
ν_{21}^u	0.397	ν_{21}^d	0.396	$\nu_{13}^u = \nu_{23}^u$	0.243	$\nu_{13}^d = \nu_{23}^d$	0.242
ν_{23}^u	0.241	ν_{23}^d	0.240				
ν_{31}^u	0.337	ν_{31}^d	0.336	$\nu_{31}^u = \nu_{32}^u$	0.319	$\nu_{31}^d = \nu_{32}^d$	0.318
ν_{32}^u	0.304	ν_{32}^d	0.303				
$G_{12}^d = G_{12}^u$	6.354	$G_{12}^d = G_{12}^u$	6.354	$G_{12}^d = G_{12}^u$	5.947	$G_{12}^d = G_{12}^u$	5.947
$G_{13}^d = G_{13}^u$	6.294	$G_{13}^d = G_{13}^u$	6.294	$G_{13}^d = G_{13}^u$	6.923	$G_{13}^d = G_{13}^u$	6.923
$G_{23}^d = G_{23}^u$	7.552	$G_{23}^d = G_{23}^u$	7.552	$G_{23}^d = G_{23}^u$		$G_{23}^d = G_{23}^u$	

Table 6.2 The estimated undrained and drained elastic constants of the type T osteon at the vascular porosity level. Both orthotropic and transversely isotropic results are shown.

Orthotropic results				**Transversely Isotropic results**			
The undrained elastic constants		The drained elastic constants		The undrained elastic constants		The drained elastic constants	
E_1^u	13.572	E_1^d	13.553	$E_1^u = E_2^u$	16.806	$E_1^d = E_2^d$	16.792
E_2^u	20.718	E_2^d	20.706				
E_3^u	16.445	E_3^d	16.433	E_3^u	16.615	E_3^d	16.792
ν_{12}^u	0.221	ν_{12}^d	0.220	$\nu_{12}^u = \nu_{21}^u$	0.285	$\nu_{12}^d = \nu_{21}^d$	0.283
ν_{13}^u	0.327	ν_{13}^d	0.326				
ν_{21}^u	0.303	ν_{21}^d	0.302	$\nu_{13}^u = \nu_{23}^u$	0.312	$\nu_{13}^d = \nu_{23}^d$	0.311
ν_{23}^u	0.337	ν_{23}^d	0.336				
ν_{31}^u	0.397	ν_{31}^d	0.396	$\nu_{31}^u = \nu_{32}^u$	0.309	$\nu_{31}^d = \nu_{32}^d$	0.308
ν_{32}^u	0.241	ν_{32}^d	0.240				
$G_{12}^d = G_{12}^u$	6.293	$G_{12}^d = G_{12}^u$	6.293	$G_{12}^d = G_{12}^u$	6.542	$G_{12}^d = G_{12}^u$	6.542
$G_{13}^d = G_{13}^u$	6.357	$G_{13}^d = G_{13}^u$	6.357	$G_{13}^d = G_{13}^u$	6.954	$G_{13}^d = G_{13}^u$	6.954
$G_{23}^d = G_{23}^u$	7.552	$G_{23}^d = G_{23}^u$	7.552	$G_{23}^d = G_{23}^u$		$G_{23}^d = G_{23}^u$	

Table 6.3 The estimated undrained and drained elastic constants of the type A osteon at the vascular porosity level. Both orthotropic and transversely isotropic results are shown.

Orthotropic results				**Transversely Isotropic results**			
The undrained elastic constants		The drained elastic constants		The undrained elastic constants		The drained elastic constants	
E_1^u	13.571	E_1^d	13.553	$E_1^u = E_2^u$	15.665	$E_1^d = E_2^d$	15.645
E_2^u	15.971	E_2^d	15.959				
E_3^u	15.973	E_3^d	15.961	E_3^u	16.324	E_3^d	16.309
ν_{12}^u	0.274	ν_{12}^d	0.273	$\nu_{12}^u = \nu_{21}^u$	0.277	$\nu_{12}^d = \nu_{21}^d$	0.276
ν_{13}^u	0.274	ν_{13}^d	0.273				
ν_{21}^u	0.381	ν_{21}^d	0.380	$\nu_{13}^u = \nu_{23}^u$	0.280	$\nu_{13}^d = \nu_{23}^d$	0.279
ν_{23}^u	0.248	ν_{23}^d	0.247				
ν_{31}^u	0.381	ν_{31}^d	0.380	$\nu_{31}^u = \nu_{32}^u$	0.292	$\nu_{31}^d = \nu_{32}^d$	0.291
ν_{32}^u	0.248	ν_{32}^d	0.247				
$G_{12}^d = G_{12}^u$	6.323	$G_{12}^d = G_{12}^u$	6.323	$G_{12}^d = G_{12}^u$	6.131	$G_{12}^d = G_{12}^u$	6.131
$G_{13}^d = G_{13}^u$	6.325	$G_{13}^d = G_{13}^u$	6.325	$G_{13}^d = G_{13}^u$	6.774	$G_{13}^d = G_{13}^u$	6.774
$G_{23}^d = G_{23}^u$	7.222	$G_{23}^d = G_{23}^u$	7.222	$G_{23}^d = G_{23}^u$		$G_{23}^d = G_{23}^u$	

Appendix

Appendix 1

The orthotropic, transversely isotropic, and isotropic symmetries

In the biological materials, such as a bone, the material symmetry is determined by the external loading. If the material is subjected to three distinct orthogonal principal stresses, the material will be orthotropic. The transversely isotropic symmetry and isotropic symmetry correspond to two distinct principal directions and three equal principal stresses, respectively (Cowin and Mehrabadi 1987; Mehrabadi and Cowin 1990; Mehrabadi et al. 1994; Cowin and Mehrabadi 1995). Hooke's law is given by

$$\hat{\mathbf{T}} = \hat{\mathbf{C}}\hat{\mathbf{E}}, \tag{A1.1}$$

where the 6-D stress vector $\hat{\mathbf{T}}$ is $\{\hat{\mathbf{T}}_1, \hat{\mathbf{T}}_2, \hat{\mathbf{T}}_3, \hat{\mathbf{T}}_4, \hat{\mathbf{T}}_5, \hat{\mathbf{T}}_6\}$, the 6-D strain vector $\hat{\mathbf{E}}$ is $\{\hat{\mathbf{E}}_1, \hat{\mathbf{E}}_2, \hat{\mathbf{E}}_3, \hat{\mathbf{E}}_4, \hat{\mathbf{E}}_5, \hat{\mathbf{E}}_6\}$, $\hat{\mathbf{C}}$ is the elasticity tensor is given by

$$\hat{\mathbf{C}} = \begin{Bmatrix} \hat{c}_{11} & \hat{c}_{12} & \hat{c}_{13} & \hat{c}_{14} & \hat{c}_{15} & \hat{c}_{16} \\ \hat{c}_{12} & \hat{c}_{22} & \hat{c}_{23} & \hat{c}_{24} & \hat{c}_{25} & \hat{c}_{26} \\ \hat{c}_{13} & \hat{c}_{23} & \hat{c}_{33} & \hat{c}_{34} & \hat{c}_{35} & \hat{c}_{36} \\ \hat{c}_{14} & \hat{c}_{24} & \hat{c}_{34} & \hat{c}_{44} & \hat{c}_{45} & \hat{c}_{46} \\ \hat{c}_{15} & \hat{c}_{25} & \hat{c}_{35} & \hat{c}_{45} & \hat{c}_{55} & \hat{c}_{56} \\ \hat{c}_{16} & \hat{c}_{26} & \hat{c}_{36} & \hat{c}_{46} & \hat{c}_{56} & \hat{c}_{66} \end{Bmatrix}. \tag{A1.2}$$

The orthotropic, transversely isotropic, and isotropic material symmetries are determined by the 6-D transformation tensor $\hat{\mathbf{Q}}$,

$$\hat{\mathbf{C}}' = \hat{\mathbf{Q}}^T \hat{\mathbf{C}} \hat{\mathbf{Q}}, \tag{A1.3}$$

where $\hat{\mathbf{C}}'$ is transformed from the elasticity tensor $\hat{\mathbf{C}}$ by the transformation tensor $\hat{\mathbf{Q}}$. Suppose that the transformation elasticity tensor $\hat{\mathbf{C}}'$ is equivalent to the elasticity tensor $\hat{\mathbf{C}}$, it means that the coordinate transformation tensor $\hat{\mathbf{Q}}$ is possessed by the particular type of symmetry. The transformation tensor $\hat{\mathbf{Q}}$ is determined by the Euler's theorem (Beatthy 1966, 1977; Mehrabadi et al., 1994), and is given in six dimensions by

$$\begin{aligned} \hat{\mathbf{Q}} = \hat{\mathbf{I}} &+ \sin\theta\hat{\mathbf{P}} + (1-\cos\theta)\hat{\mathbf{P}}^2 \\ &+ \frac{1}{3}\sin\theta(1-\cos\theta)(\hat{\mathbf{P}} + \hat{\mathbf{P}}^3) \\ &+ \frac{1}{6}(1-\cos\theta)^2(\hat{\mathbf{P}}^2 + \hat{\mathbf{P}}^4) = e^{\theta P} \end{aligned}, \tag{A1.4}$$

and the second order tensor $\hat{\mathbf{P}}$ in six dimensions is given by

$$\hat{\mathbf{P}} = \begin{bmatrix} 0 & 0 & 0 & 0 & \sqrt{2}p_2 & -\sqrt{2}p_3 \\ 0 & 0 & 0 & -\sqrt{2}p_1 & 0 & \sqrt{2}p_3 \\ 0 & 0 & 0 & \sqrt{2}p_1 & -\sqrt{2}p_2 & 0 \\ 0 & \sqrt{2}p_1 & -\sqrt{2}p_1 & 0 & p_3 & -p_2 \\ -\sqrt{2}p_2 & 0 & \sqrt{2}p_2 & -p_3 & 0 & p_1 \\ \sqrt{2}p_3 & \sqrt{2}p_3 & 0 & p_2 & -p_1 & 0 \end{bmatrix}. \tag{A1.5}$$

The plane of the reflective symmetry $\mathbf{R}^{(a)}$ is defined from the transformation tensor $\hat{\mathbf{Q}}$ and is shown in Table A1.1. For the orthotropic symmetry, three mutually perpendicular planes of symmetry, $\hat{\mathbf{R}}^{(1)}$, $\hat{\mathbf{R}}^{(2)}$, and $\hat{\mathbf{R}}^{(3)}$ (See Table A1.1 for the reflective symmetry plane) are involved and the elasticity tensor will be reduced to

$$\hat{\mathbf{C}}^{Ort} = \begin{Bmatrix} \hat{c}_{11} & \hat{c}_{12} & \hat{c}_{13} & 0 & 0 & 0 \\ \hat{c}_{12} & \hat{c}_{22} & \hat{c}_{23} & 0 & 0 & 0 \\ \hat{c}_{13} & \hat{c}_{23} & \hat{c}_{33} & 0 & 0 & 0 \\ 0 & 0 & 0 & \hat{c}_{44} & 0 & 0 \\ 0 & 0 & 0 & 0 & \hat{c}_{55} & 0 \\ 0 & 0 & 0 & 0 & 0 & \hat{c}_{66} \end{Bmatrix}. \tag{A1.6}$$

The transversely isotropic symmetry is obtained from the hexagonal symmetry. Seven planes of symmetry, $\hat{\mathbf{R}}^{(1)}$, $\hat{\mathbf{R}}^{(2)}$, $\hat{\mathbf{R}}^{(3)}$, $\hat{\mathbf{R}}^{(m)}$, $\hat{\mathbf{R}}^{(n)}$, $\hat{\mathbf{R}}^{(k)}$, and $\hat{\mathbf{R}}^{(p)}$, are involved. The normals to six planes lie in the seventh plane and it becomes the isotropic plane of the the transverse isotropy. The elasticity tensor for the transverse isotropy is given by

$$\hat{C}^{TI} = \begin{pmatrix} \hat{C}_{11} & \hat{C}_{12} & \hat{C}_{13} & 0 & 0 & 0 \\ \hat{C}_{12} & \hat{C}_{11} & \hat{C}_{13} & 0 & 0 & 0 \\ \hat{C}_{13} & \hat{C}_{13} & \hat{C}_{33} & 0 & 0 & 0 \\ 0 & 0 & 0 & \hat{C}_{44} & 0 & 0 \\ 0 & 0 & 0 & 0 & \hat{C}_{44} & 0 \\ 0 & 0 & 0 & 0 & 0 & \hat{C}_{11} - \hat{C}_{12} \end{pmatrix}. \tag{A1.7}$$

Nine planes of the reflective symmetries $\hat{\mathbf{R}}^{(1)}$, $\hat{\mathbf{R}}^{(2)}$, $\hat{\mathbf{R}}^{(3)}$, $\hat{\mathbf{R}}^{(4)}$, $\hat{\mathbf{R}}^{(5)}$, $\hat{\mathbf{R}}^{(6)}$, $\hat{\mathbf{R}}^{(7)}$, $\hat{\mathbf{R}}^{(8)}$, and $\hat{\mathbf{R}}^{(9)}$ characterize cubic symmetry. For isotropic symmetry all planes are planes of isotropic. The elasticity tensor for the isotropic symmetry is given by

$$\hat{C}^{I} = \begin{pmatrix} \hat{C}_{11} & \hat{C}_{12} & \hat{C}_{12} & 0 & 0 & 0 \\ \hat{C}_{12} & \hat{C}_{11} & \hat{C}_{12} & 0 & 0 & 0 \\ \hat{C}_{12} & \hat{C}_{12} & \hat{C}_{11} & 0 & 0 & 0 \\ 0 & 0 & 0 & \hat{C}_{11} - \hat{C}_{12} & 0 & 0 \\ 0 & 0 & 0 & 0 & \hat{C}_{11} - \hat{C}_{12} & 0 \\ 0 & 0 & 0 & 0 & 0 & \hat{C}_{11} - \hat{C}_{12} \end{pmatrix}. \tag{A1.8}$$

Table A1.1 The relationship between the reflective symmetry plane and the transformation tensor

The reflective symmetry plane	The transformation tensor
$\hat{\mathbf{R}}^{(1)}$	$\hat{\mathbf{Q}}(\pi,\mathbf{e}_1)$
$\hat{\mathbf{R}}^{(2)}$	$\hat{\mathbf{Q}}(\pi,\mathbf{e}_2)$
$\hat{\mathbf{R}}^{(3)}$	$\hat{\mathbf{Q}}(\pi,\mathbf{e}_3)$
$\hat{\mathbf{R}}^{(4)}$	$\hat{\mathbf{Q}}(\pi,\frac{1}{\sqrt{2}}(\mathbf{e}_2+\mathbf{e}_3))$
$\hat{\mathbf{R}}^{(5)}$	$\hat{\mathbf{Q}}(\pi,\frac{1}{\sqrt{2}}(\mathbf{e}_1+\mathbf{e}_3))$
$\hat{\mathbf{R}}^{(6)}$	$\hat{\mathbf{Q}}(\pi,\frac{1}{\sqrt{2}}(\mathbf{e}_1+\mathbf{e}_2))$
$\hat{\mathbf{R}}^{(7)}$	$\hat{\mathbf{Q}}(\pi,\frac{1}{\sqrt{2}}(\mathbf{e}_2-\mathbf{e}_3))$
$\hat{\mathbf{R}}^{(8)}$	$\hat{\mathbf{Q}}(\pi,\frac{1}{\sqrt{2}}(\mathbf{e}_1-\mathbf{e}_3))$
$\hat{\mathbf{R}}^{(9)}$	$\hat{\mathbf{Q}}(\pi,\frac{1}{\sqrt{2}}(\mathbf{e}_1-\mathbf{e}_2))$
$\hat{\mathbf{R}}^{(k)}$	$\hat{\mathbf{Q}}(\pi,\frac{1}{2}(\mathbf{e}_1+\sqrt{3}\mathbf{e}_2))$
$\hat{\mathbf{R}}^{(p)}$	$\hat{\mathbf{Q}}(\pi,\frac{1}{2}(\sqrt{3}\mathbf{e}_2-\mathbf{e}_1))$
$\hat{\mathbf{R}}^{(m)}$	$\hat{\mathbf{Q}}(\pi,\frac{1}{2}(\sqrt{3}\mathbf{e}_1+\mathbf{e}_2))$
$\hat{\mathbf{R}}^{(n)}$	$\hat{\mathbf{Q}}(\pi,\frac{1}{2}(\sqrt{3}\mathbf{e}_1-\mathbf{e}_2))$

Appendix 2 The disturbance strain

The disturbance strain, $\hat{\mathbf{E}}^d$ is generated by the existence of the inclusion. It has the relationship with the Eshelby tensor $\hat{\mathbf{S}}^E$ and the eigenstrain $\hat{\mathbf{E}}^*(x)$ that is the uniform strain required for the homogenization,

$$\hat{\mathbf{E}}^d(x) = \hat{\mathbf{S}}^E \cdot \hat{\mathbf{E}}^*(x). \tag{A2.1}$$

The Hooke's law for the matrix and the inclusion is given by

$$\hat{\mathbf{T}}(x) = \begin{cases} \hat{\mathbf{C}} \cdot \hat{\mathbf{E}}(x) = \hat{\mathbf{C}} \cdot (\hat{\mathbf{E}}^0 + \hat{\mathbf{E}}^d) & in\ M \\ \hat{\mathbf{C}}^I \cdot \hat{\mathbf{E}}(x) = \hat{\mathbf{C}}^I \cdot (\hat{\mathbf{E}}^0 + \hat{\mathbf{E}}^d) & in\ \Omega \end{cases}, \tag{A2.2}$$

where $\hat{\mathbf{E}}^0$ is the uniformly prescribed strain at the outer boundary of the RVE. By introducing the eigenstrain $\hat{\mathbf{E}}^*(x)$, the elasticity tensor of the inclusion on the bottom equation of Eq. (A2.2) is replaced by the elasticity tensor of the matrix as

$$\hat{\mathbf{T}}(x) = \hat{\mathbf{C}} \cdot (\hat{\mathbf{E}}(x) - \hat{\mathbf{E}}^*(x)) = \begin{cases} \hat{\mathbf{C}} \cdot (\hat{\mathbf{E}}^0 + \hat{\mathbf{E}}^d(x)) & in\ M \\ \hat{\mathbf{C}} \cdot (\hat{\mathbf{E}}^0 + \hat{\mathbf{E}}^d(x) - \hat{\mathbf{E}}^*(x)) & in\ \Omega \end{cases}. \tag{A2.3}$$

This homogenized method is called the "Eshelby equivalent inclusion method" (Aboudi 1991). The eigenstrain $\hat{\mathbf{E}}^*(x)$ exists only in the inclusion and the Heaviside step function $\mathbf{H}(x;\Omega)$ enables the eigenstrain $\hat{\mathbf{E}}^*(x)$,which is a function of x, to be independent on x,

$$\hat{\mathbf{E}}^*(x) = \mathbf{H}(x;\Omega)\hat{\mathbf{E}}^*, \tag{A2.4}$$

where the Heaviside step function $\mathbf{H}(x;\Omega)$ has the value of 1 in the inclusion Ω and 0 in matrix.

Now we set the Hooke's law of Eq. (A2.2) and Eq. (A2.3) for the inclusion equal. Then the following relation is obtained.

$$\hat{\mathbf{T}}(x) = \hat{\mathbf{C}}^I \cdot \{\hat{\mathbf{E}}^0 + \hat{\mathbf{E}}^d(x)\} = \hat{\mathbf{C}} \cdot \{\hat{\mathbf{E}}^0 + \hat{\mathbf{E}}^d(x) - \hat{\mathbf{E}}^*(x)\}, \tag{A2.5}$$

and it is simplified as

$$\{\hat{\mathbf{E}}^0 + \hat{\mathbf{E}}^d(x)\} = \hat{\mathbf{A}}^I \cdot \hat{\mathbf{E}}^*(x), \tag{A2.6}$$

by introducing a new variable $\hat{\mathbf{A}}^I \equiv (\hat{\mathbf{C}} - \hat{\mathbf{C}}^I)^{-1} \cdot \hat{\mathbf{C}}$. The eigenstrain $\hat{\mathbf{E}}^*(x)$ and the disturbance strain $\hat{\mathbf{E}}^d(x)$ are no longer a function of x. Eq. (A2.6) is rearranged for $\hat{\mathbf{E}}^*(x)$, or $\hat{\mathbf{E}}^*$, from Eqs. (A2.1) and (A2.4) as

$$\hat{\mathbf{E}}^* = (\hat{\mathbf{A}}^I - \hat{\mathbf{S}}^E)^{-1}\hat{\mathbf{E}}^0. \tag{A2.7}$$

Substituting Eq. (A2.7), into Eq. (A2.6) gives

$$\hat{\mathbf{E}}^0 + \hat{\mathbf{E}}^d(x) = \hat{\mathbf{A}}^I(\hat{\mathbf{A}}^I - \hat{\mathbf{S}}^E)^{-1}\hat{\mathbf{E}}^0, \tag{A2.8}$$

or

$$\hat{\mathbf{E}}^0 + \hat{\mathbf{E}}^d = \hat{\mathbf{A}}^I(\hat{\mathbf{A}}^I - \hat{\mathbf{S}}^E)^{-1}\hat{\mathbf{E}}^0. \tag{A2.9}$$

Appendix 3.

The relationship between Voigt notation and Kelvin notation

The traditional notation for the anisotropic Hooke's law is the representation of the fourth rank tensor, which is given in indical notation by

$$T_{ij} = C_{ijkm} E_{km} \quad \text{or} \quad E_{ij} = S_{ijkm} T_{km}, \tag{A3.1}$$

where T_{ij}, E_{ij}, C_{ijkm}, and S_{ijkm} are the stress tensor, the strain tensor, the elasticity tensor, and the compliance tensor, respectively. Voigt (1910) employed the matrix notation as the coefficients of linearity in the relation between stress and strain,

$$\mathbf{T} = \mathbf{cE} \quad \text{or} \quad \mathbf{E} = \mathbf{sT}, \tag{A3.2}$$

where $\mathbf{T}$ and $\mathbf{E}$ are one-by-six column matrices representing stress and strain. $\mathbf{c}$ and $\mathbf{s}$ are the elasticity matrix and the compliance matrix, respectively. The double index notation (or Voigt matrix notation) is important because most of the data on the mechanical properties of anisotropic elastic materials are reported in the double index notation (Hearmon 1961; Cowin and Mehrabadi 1987, 1989, 1995). The relation between the fourth rank tensor involves factors of 1, 2, and 4. The elements in the upper left hand 3-by-3 matrix have the proportionality factor one, eg, $S_{1111} = s_{11}$; the elements in the upper right hand 3-by-3 matrix (and lower left hand 3-by-3 matrix) have the proportionality factor two, eg, $2S_{2311} = s_{41}$; and the elements in the lower

right hand 3-by-3 sub matrix have the proportionality factor four, eg, $4S_{1212} = s_{66}$ (Hearmon 1961; Cowin and Mehrabadi, 1987, 1989, 1995). However, for the elasticity tensor, no proportionality factors are involved. The proportionality factors do not occur between the Kelvin notation (1856) and the Voigt fourth rank tensor. Kelvin notation equivalent to Eq. (A3.2) is

$$\hat{\mathbf{T}} = \hat{\mathbf{C}}\hat{\mathbf{E}} \quad \text{or} \quad \hat{\mathbf{E}} = \hat{\mathbf{S}}\hat{\mathbf{T}}, \tag{A3.3}$$

where the stress vector $\hat{\mathbf{T}}$ has components $\{\hat{T}_1, \hat{T}_2, \hat{T}_3, \hat{T}_4, \hat{T}_5, \hat{T}_6\}$, the strain vector $\hat{\mathbf{E}}$ has components $\{\hat{E}_1, \hat{E}_2, \hat{E}_3, \hat{E}_4, \hat{E}_5, \hat{E}_6\}$, $\hat{\mathbf{C}}$ is the elasticity tensor for the orthotropic symmetry and is given as a 6-by-6 matrix of the second rank tensor components in 6 dimensions,

$$\hat{\mathbf{C}} = \begin{Bmatrix} \hat{c}_{11} & \hat{c}_{12} & \hat{c}_{13} & 0 & 0 & 0 \\ \hat{c}_{12} & \hat{c}_{22} & \hat{c}_{23} & 0 & 0 & 0 \\ \hat{c}_{13} & \hat{c}_{23} & \hat{c}_{33} & 0 & 0 & 0 \\ 0 & 0 & 0 & \hat{c}_{44} & 0 & 0 \\ 0 & 0 & 0 & 0 & \hat{c}_{55} & 0 \\ 0 & 0 & 0 & 0 & 0 & \hat{c}_{66} \end{Bmatrix}, \tag{A3.4}$$

and $\hat{\mathbf{S}} = \hat{\mathbf{C}}^{-1}$ is the compliance tensor with the same structure. The relationship between the components of the Voigt fourth rank tensor and the components of the Kelvin second rank tensor is as follows: $C_{1111} = \hat{c}_{11}$, $C_{2222} = \hat{c}_{22}$, $C_{3333} = \hat{c}_{33}$, $C_{1122} = \hat{c}_{12}$, $C_{1133} = \hat{c}_{13}$, $C_{2233} = \hat{c}_{23}$, $C_{2323} = \frac{1}{2}\hat{c}_{44}$, $C_{1313} = \frac{1}{2}\hat{c}_{55}$, and $C_{1212} = \frac{1}{2}\hat{c}_{66}$. Similarly, the compliance tensor has the relationship between the components of the Voigt fourth rank tensor and the components of the Kelvin second rank tensor as

$S_{1111} = \hat{s}_{11}$, $S_{2222} = \hat{s}_{22}$, $S_{3333} = \hat{s}_{33}$, $S_{1122} = \hat{s}_{12}$, $S_{1133} = \hat{s}_{13}$, $S_{2233} = \hat{s}_{23}$, $S_{2323} = \frac{1}{2}\hat{s}_{44}$, $S_{1313} = \frac{1}{2}\hat{s}_{55}$, and $S_{1212} = \frac{1}{2}\hat{s}_{66}$, respectively.

References

Chapter 1

Ajubi NE, Klein-Nulend J, Nijweide PJ, Vrijheid-Lammers T, Alblas MJ, Burger EH (1996) Pulsating fluid flow increases prostaglandin productivity by cultured chicken osteocytes – a cytoskeleton-dependent process, Biochem. Biophys. Res. Commun., 225: 62-68

Ascenzi A, Bonucci E (1967) The tensile properties of single osteons. Anatomical Record. 158: 375-386

Ascenzi A, Bonucci E (1968) The compressive properties of single osteons. Anatomical Record. 161: 377-391

Ascenzi A, Bonucci E (1972)The shearing properties of single osteons. Anatomical Record 172: 499-510

Ashman RB, Cowin SC, Van Buskirk WC, Rice JC (1984) A continuous wave technique for the measurement of the elastic properties of bone. Journal of Biomechanics 17; 349-361

Bassett CAL (1965) Electrical effects in bone. Scientific American 213: 18-25

Beatty MF (1966) Kinematics of finite rigid body displacements. Am J. Phys. 34: 949-956

Beatty MF (1997) Vector analysis of rigid rotations. J Appl. Mech. 44: 501-507

Biot MA (1941) General theory of three-dimensional consolidation. J. Appl. Phys. 12: 155-164

Biot MA (1955) Theory of elasticity and consolidation for a porous anisotropic solid. J. Appl. Phys. 26: 182-185

Bonfield W, Li CH (1967) Anisotropy of non-elastic flow in bone. Journal of Applied Physiology 38: 2450

Choi K, Goldstein SA (1992) A comparison of the fatigue behavior of human trabecular and cortical bone tissue. J. Biomech. 25: 1371-1381

Chow CL, Wang J (1987) An anisotropic theory of elasticity for continuum damage mechanics. Int. J. Fracture 33:2 1987

Cowin SC, Mehrabadi MM (1995) Anisotropic symmetries of linear elasticity, Appl. Mech. Rev. 48: 247-285

Cowin SC, Weinbaum S, Zeng Y (1995) A case for bone canaliculi as the anatomic site of strain generated potentials. Journal of Biomechanics 28: 1281-1297

Cowin SC (1999) Bone poroelasticity, Journal of Biomechanics 32: 217-238

Cowin SC, Mehrabadi MM (1989) Identification of the elastic symmetry of bone and other materials. J. Biomech. 22: 503-515

Cowin SC, Mehrabadi MM (1992) On the structure of the linear anisotropic elastic symmetries. J. Mech. Phys. Solids. 40:1459-1472

Cowin SC, Mehrabadi MM (1995) Anisotropic symmetries of linear elasticity. Appl. Mech. Rev. 48: 247-285

Crolet JM, Aoubiza B, Meunier A (1993) Compact bone: numerical simulation of mechanical characteristics. Journal of Biomechanics 26: 677-687

Currey JD (1969) The mechanical consequences of variation in the mineral content of bone. Journal of Biomechanics. 2: 1-11

Currey JD (1969) The relationship between the stiffness and the mineral content of bone. Journal of Biomechanics 2: 477-480

Currey JD (1988) Effects of porosity and mineral content on the Young's modulus of elasticity of compact bone. Journal of Biomechanics 21: 131-139

Detournay E, Cheng HDA (1993) Fundamentals of poroelasticity. In: Hudson JA (ed.), Comprehensive Rock Engineering: Principles, Practice, and Projects, Pergamon, 113-171

Fan Z, Swadener JG, Rho JY, Roy ME, Pharr GM (2002) Anisotropic properties of human tibial cortical bone as measured by nanoindentation. Journal of Orthopaedic Research 20: 806-810

Fondrk MT, Bahniuk EH, Davy DT (1999) A damage model for non-linear tensile behavior of cortical bone. J Biomech. Eng. 121: 533

Forwood MR (1996) inducible cyclooxygenase (COX-2) mediates the induction of

bone formation by mechanical loading in vivo. J. Bone. Miner. Res. 11: 1688-1693

Frost HM (1960) Presence of microscopic cracks in vivo in bone. Henry Ford Hospital Medical Bulletin 8: 25-35

Frost HM (1962) Specific surface and specific volume of normal human lamellar bone. Henry Ford Hospital Medical Bulletin 10: 35-41

Frost HM (1964) The laws of bone structure. Thomas, Springfield.

Frost HM (1986) Intermediary Organization of the skeleton. CRC Press, Boca Raton.

Hearmon RFS (1961) An introduction to applied anisotropic elasticity. Oxford university press, Oxford.

Katz JL (1981) Composite material models for cortical bone, in Mechanical Properties of Bone (Edited by SC Cowin), American Society of Mechanical Engineers, New York, 1981

Knets I, Malmeisters A (1977) Deformability and strength of human compact bone tissue. In: Brankov G (Ed.), Mechanics of Biological Solids: Proc. Euromech Colloquium 68, Bulgarian Academy of Sciences, Sofia 133

Li G, Bronk JT, An KN, Kelly PJ (1987) Permeability of cortical bone of canine tibiae. Microcirculation Research 34: 302-310

Liebschner MAK (2004) Biomechanical considerations of animal models used in

tissue engineering of bone. Biomaterials, 25: 1697-1714

Love AEH (1944) A treatise on the mathematical theory of elasticity. Dover, New York

Martin RB, Ishida J (1989) The relative effects of collagen fiber orientation, porosity,density, and mineralization on bone strength. Journal of Biomechanics 22: 419-426

Martin RB, Burr DB, Sharkey NA (1998) Skeletal Tissue Mechanics, Springer-Verlag, New York

Mehrabadi MM, Cowin SC (1990) Eigentensors of linear anisotropic elastic materials. Quart. J. Mech. Appl. Math. 43: 15-41

Mehrabadi MM, Cowin SC, Jaric J (1994) Six dimensional orthogonal tensor representation of the rotation about an axis in three dimensions. Int. J. Solids Struct. 32: 439-449

Mori S, Harruff R, Ambrosius W, Burr DB (1997) Trabecular bone volume and microdamage accumulation in the femoral heads of woven with and without femoral neck fractures. Bone 21: 521-526

Norman TL, Wang Z (1997) Microdamage of human cortical bone: incidence and morphology in long bones. Bone 20: 375-379

Norris AN (1989) On the acoustic determination of the elastic moduli of anisotropic

solids and acoustic conditions for the existence of symmetry planes, Quart J. Mech. Appl. Math. 42: 413-426

Morris MA, Lopez-Curato JA, Hughes SPF, An KN, Bassingthwaighte JB, Kelly PJ (1982) Fluid spaces in canine bone and marrow. Microvascular Research 23: 188-200

Otter MW, Palmieri VR, Wu DD, Seiz KG, MAcGinitie LA, Cochran GVB (1992) A comparative analysis of streaming potentials in vivo and in vitro. Journal of Orthopaedic Research 10: 710-719

Owan I, Burr DB, Turner CH, Qui J, Tu Y, Onyia JE, Duncan RL (1997) Mechanotransduction in bone: osteoblasts are more responsive to fluid forces than mechanical strain. American Journal of Physiology 273: C810-C815

Piekaski K(1973) Analysis of bone as a composite material. Journal of Biomechanics 11: 557-565

Pitsillides AA, Rawlinson SCF, Suswillo RFL, Bourrin S, Zaman G, Lanyon LE (1995) Mechanical strain-induced NO production by bone cells – a possible role in adaptive bone (re)modeling. FASEB J. 9: 1614-1622

Reilly DT, Burstein AH (1975) The elastic and ultimate properties of compact bone tissue. Journal of Biomechanics 8; 393

Rho JY, Kuhnspearing L, Zioupos P (1998) Mechanical properties and the

hierarchical structure of bone, Med. Eng. Phys., 20: 92

Rice JR, Cleary MP (1976) Some basic stress diffusion solutions for fluid-saturated elastic porous media with compressible constituents. Rev. Geophys. Space. Phys. 14: 227-241

Rogers HJ, Weidmann SM, Parkinson A (1952) Studies on the skeletal tissues – II. The collagen content of bones from rabbits, oxen, and humans. Biochem J. 50: 537~

Rubin CT, Lanyon LE (1984) Regulation of bone mass by mechanical strain magnitude. Calcified Tissue International 37: 411-417

Schaffler MB, Burr DB (1988) Stiffness of compact bone:effects of porosity and density. Journal of Biomechanics 21:13-16

Schaffler MB, Choi K, Milgrom C (1995) Aging and matrix microdamage accumulation in human compact bone. Bone 17: 521-525

Siperko LM, Landis WJ (2001) Aspects of mineral structure in normally calcifying avian tendon. J. Struct. Biol. 135: 313-320

Smit TH, Huyghe JM, Cowin SC (2002) Estimation of the poroelastic parameters. Journal of Biomechanics.35:829-835

Smith JW (1960) Collagen fiber patterns in mammalian bone. J. Anat. 94: 329~

Starkebaum W, Pollack SR, Korostoff E (1979) Microeletrode studies of stress-

generated potentials in four point bending of bone. Journal of Biomedical Material Research 13: 729-751

Thompson M, Willis JR (1991) A reformation of the equations of anisotropic poroelasticity. J. Appl. Mech. 58: 612-616

Thompson M, Willis JR (1991) A reformation of the equations of anisotropic poroelasticity. Journal of Applied Mechanics 58: 612-616

Torrance AG, Mosley JR, Suswillo RFL, Lanyon LE (1994) Noninvasive loading of the rat ulna in vivo induces a strain-related modeling response uncomplicated by trauma or periosteal pressure. Calcified Tissue International 54: 241-247

Uhthoff HK, Jaworski ZFG (1978) Bone loss in response to long-term immobilization. Journal of Bone and Joint Surgery 60B: 420-429

Wagner HD, Weiner S (1992) On the relationship between the microstructure of bone and its mechanical stiffness. J. Biomechanics 25: 1311

Wang L, Fritton SP, Cowin SC, Weinbaum S (1999) Fluid pressure relaxation depends upon osteonal microstructure: modeling an oscillatory bending experiment. Journal of Biomechanics 32: 663-672

Weinbaum S, Cowin SC, Zeng Y (1994) A model for the excitation of osteocytes by mechanical loading-induced bone fluid shear stresses. Journal of Biomechanics 27; 339-360

Weiner S, Arad T, Traub W (1991) Crystal organization in rat bone lamellae, FEBS Lett. 285: 49

Weiner S, Arad T, Sabanay I, Traub W (1997) Rotated plywood structure of primary lamellar bone in the rat: orientations of the collagen fibril arrays. Bone 20: 509

Weiner S, Wagner HD (1998) The material bone: structure-mechanical function relations, Annu. Rev. Mater. Sci. 28: 271

Woo SL, Kuei SC, Amiel D, Gomez MA, Hayes WC, White FC, Akeson WH (1981) The effect of prolonged physical training on the properties of long bone: a study of Wolff's law. Journal of Bone and Joint Surgery 63A: 780-787

Yoon HS, Katz JL (1976a) Ultrasonic wave propagation in human cortical bone. I. Theoretical consideration for hexagonal symmetry. J. Biomechanics 9; 407-411

Yoon HS, Katz JL (1976b) Ultrasonic wave propagation in human cortical bone. II. Measurements of elastic properties and micro-hardness. Journal of Biomechanics 9; 459-

Zysset PK, Curnier A (1996) A 3D damage model for trabecular bone based on fabric tensors. J. Biomech. 29: 1549

Zeng Y, Cowin SC, Weinbaum S (1994) A fiber matrix model for fluid flow and streaming potentials in the canaliculi of an osteon. Annals of Biomedical Engineering 22: 280-292

Zhang D, Weinbaum S, Cowin SC (1998) On the calculation of bone pore water pressure due to mechanical loading. International Journal of Solids Structures 35: 4881-4897

Ziv V, Sabanay I, Arad T, Traub W, Weiner S (1996) Transitional structures in lamellar bone. Microsc.Res. Tech., 33:203

Zysset PK, et al. (1998) Mechanical properties of human trabecular bone lamellae quantified by nanoindentation. Technol. Health Care 6: 429-432

Zysset PK, Guo XE, Hoffler CE, Moore KE, Goldstein SA (1999) Elastic modulus and hardness of cortical and trabecular bone lamellae measured by nanoindentation in the human femur. Journal of Biomechanics 32:1005-1012

Chapter 2

Aboudi J (1991) Mechanics of composite materials – a unified micromechanical approach, Elsevier

Berryman JG (1980a) Long-wavelength propagation in composite media. I. Spherical inclusions, J. Acoust. Soc. Am. 68. 1809-1819

Berryman JG (1980b) Long-wavelength propagation in composite media. II. Ellipsoidal inclusions, J. Acoust. Soc. Am. 68. 1820-1831

Budiansky B (1965) On the elastic moduli of some heterogeneous materials, J. Mech.

Phys. Solids 13, 223

Cowin SC, Yang G, Mehrabadi MM (1999) Bounds on the effective anisotropic elastic constants. Journal of elasticity 57: 1-24

Eshelby JD (1957) The determination of the elastic field of an ellipsoidal inclusion and the related problems. Proc. R. Soc. London. Ser. A, 241: 376-396

Hill R (1952) The elastic behavior of a crystalline aggregate, Proc. Phys. Soc A65, 349

Hill R (1963) Elastic properties of reinforced solids: some theoretical principles. J. Mech. Phys. Solids. 11: 357-372

Hill R (1965a) Theory of mechanical properties of fibre-strengthened materials III. Self-consistent model. J. Mech. Phys. Solids. 13: 189-198

Hill R (1965b) A self-consistent mechanics of composite materials. J. Mech. Phys. Solids. 13: 213-222

Iwakuma T, Nemat-Nasser S (1983) Composites with periodic microstructure, Computers and Structures. 16: 13-19

McLaughlin R (1977) A study of the differential scheme for composite materials, Int. J. Eng. Sci. 15: 237-244

Mori T, Tanaka K (1973) Average stress in matrix and average elastic energy of materials with misfitting inclusions, Acta. Metal. 21, 571

Mura T (1987) Micromechanics of defects in solids (2nd edition), Martinus Nijhoff Publishers, Dordrecht.

Nemat-Nasser S, Iwakuma T, Hejazi M (1982) On composites with periodic structure. Mech. Mater. 1: 239-267

Nemat-Nasser S, Taya M (1981) On effective moduli of an elastic body containing periodically distributed voids. Quarterly of Applied Mathematics, 39: 43-59

Nemat-Nasser S, Taya M (1985) On effective moduli of an elastic body containing periodically distributed voids: Comments and correction. Quarterly of Applied Mathematics 43: 187-188

Nemat-Nasser S, Hori M (1999) Micromechanics: overall properties of heterogeneous materials (2nd Edition) Elsevier. The Netherlands

Reuss A (1929) Berechnung der Fliessgrenze von Mischkristallen auf Grund der Plastizitatsbedingung fur Einkristalle. Z. Angrew. Math. Mech. 9, 49-58

Torquato S (2000) Random heterogeneous materials, Springer-Verlag, New York.

Voigt W (1889) Uber die Beziehung zwischen den beiden Elastizitatskonstanten isotroper Korper. Wied. Ann. 38, 573-587

Willis JR (1964) Anisotropic elastic inclusion problems. Q. J. Mech. Appl. Math., 17: 157-174

Willis JR (1977) Bounds and self-consistent estimates for the overall properties of

composites of anisotropic composites. J. Mech. Phys. Solids. 25: 185-202

Chapter 3

Akiva U, Itzhak E, Wagner HD (1997) Elastic constants of three-dimensional orthotropic composites with platelet/ribbon reinforcement. Composite Science and Technology. 57: 173-184

Akiva U, Wagner HD, Weiner S (1998) Modelling the three-dimensional elastic constants of parallel-fibred and lamellar bone. Journal of Materials Science. 33: 1497-1509

Arnold JS, Tont SA (1967) Bone water studied by differential centrifugation. Calcif. Tissue. Res. 1:68

Ascenzi, A.; Bonucci, E.: The tensile properties of single osteons. Anatomical Record 158 (1967) 375-386

Ascenzi, A.; Bonucci, E.: The compressive properties of single osteons. Anat. Rec. 161 (1968) 377-391

Ashman RB (1989) Experimental Techniques. In: Bone Mechanics (Edited by S.C.Cowin), CRC Press

Biltz RM, Pellegrino ED (1969) The chemical anatomy of bone. J. Bone Joint Surg. 51A. 456-466

Bonfield W, Li CH (1966) Deformation and fracture in bone. J. appl. Phys. 38: 3181-3184

Cowin SC, Mehrabadi MM (1987) On the identification of material symmetry for anisotropic elastic materials. Quart J. Mech. Appl. Math. 40: 451-476

Cowin SC, Mehrabadi MM (1989) Identification of material symmetry of bone and other materials. J. Biomech. 22: 503-515

Cowin SC (1989) The mechanical properties of cortical bone tissue. In: Bone Mechanics (Edited by S.C.Cowin), CRC Press

Cowin SC; Mehrabadi MM (1995) Anisotropic symmetries of linear elasticity. Applied Mechanics Review 48: 247-285

Cowin SC (1999) Bone poroelasticity. Journal of Biomechanics 32: 217-238

Crolet, J.M.; Aoubiza, B.; Meunier, A: Compact bone: numerical simulation of mechanical characteristics. J. Biomechanics 26 (1993) 677-687

Currey JD (1964) Three analogies to explain the mechanical properties of bone. Biorheology 2:1-10

Currey JD (1969) The mechanical consequences of variation in the mineral content of bone. Journal of Biomechanics. 2: 1-11

Currey JD (1974) Mechanical properties of bone tissues with greatly differing functions. J. Biomechanics 12:313-319

Eppell SJ, Tong W, Katz JL, Kuhn L, Glimcher MJ (2001) Shape and size of isolated bone mineralites measured using atomic force microscopy. J Orthop. Res. 19:1027-1034

Fan Z, Swadener JG, Rho JY, Roy ME, Pharr GM (2002) Anisotropic properties of human tibial cortical bone as measured by nanoindentation. Journal of Orthopaedic Research. 20: 806-810

Fernandez-Seara MA, Wehrli SL, Wehrli FW (2002) Diffusion of exchangeable water in cortical bone studied by nuclear magnetic resonance. Biophysical Journal 82: 522-529

Fernandez-Seara MA, Wehrili SL, Takahashi M, Wehrili W (2004) Water content measured by proton-deuteron exchange NMR predicts bone mineral density and mechanical properties. Journal of bone and mineral research. 19: 289-296

Gong JK, Arnold JS, Cohn S"H (1964) Composition of trabecular and cortical bone. Anat. Rec. 149: 325-332

Halpin JC, Tsai SW (1967) Environmental factors in composite design. Air Force Materials Laboratory Technical Report. AFML-TR 67-423

Hearmon, R.F.S.: An introduction to applied anisotropic elasticity. Oxford University Press, Oxford (1961)

Hellmich C, Ulm FJ (2002) Micromechanical Model for ultrastructural stiffness of

mineralized tisues. Journal of Engineering Mechanics. 128: 898-908

Hellmich C, Barthelemy JF, Dormieux L (2004) Mineral-collagen interactions in elasticity of bone ultrastructure – a continuum micromechanics approach. European Journal of Mechanics- A/Solids 23: 783-810

Iwakuma, T.; Nemat-Nasser, S.: Composites with periodic microstructure. Computers and Structures 16 (1983) 13-19

Katz LJ (1971) Hard tissue as a composite material – 1. Bounds on elastic behavior. J. Biomech. 4: 455-173

Kelvin, Lord [W. Thompson] Elements of a mathematical theory of elasticity. Phil. Trans. R. Soc 166 (1856) 481-498

Ladis W, Moradian-Oldak J, Weiner S (1991) Topographic imaging of mineral and collagen in the calcifying turkey tendon. Connect Tissue Res. 25: 217-222

Landis W, Song M (1993) Mineral and organic matrix interaction in normally calcifying tendon visualized in three dimensions by high voltage electron microscopic tomography and graphic image reconstructure. J. Struct. Biol. 110: 39-54

Landis W, Hodgens K, Arena J, Song M, McEwen B (1996) Structural relations between collagen and mineral in bone as determined by high voltage electron microscopic tomography. Microsc. Res. Tech. 33:192-202

Lucchinetti E (2001) Composite models of bone properties. In: Bone Mechanics Handbook (Edited by S.C.Cowin) (2nd Edition), CRC Press

Martin RB, Burr DB, Sharkey NA (1998) Skeletal Tissue Mechanics, Springer-Verlag, New York

Nemat-Nasser S, Iwakuma T, Hejazi M, (1982) On composites with periodic structure. Mechanics of Materials 1 239-267

Nemat-Nasser S, Yu N, Hori M (1993) Bounds and estimates of overall moduli of composites with periodic microstructure. Mechanics of Materials. 15: 163-181

Nemat-Nasser, S.; Hori, M.: Micromechanics: overall properties of heterogeneous materials. 2nd revised edition, Elsevier. (1999)

Neuman WF, Toribara TY, Mulrvan BJ (1953) The surface chemistry of bone. VII. The hydration shell. Journal of the American Chemical Society 75: 4239-4242

Neuman WF, Neuman MW (1958) The chemical dynamics of bone. University of Chicago Press, Chicago.

Pidaparti RMV, Chandran A, Takano Y, Turner CH (1996) Bone mineral lies mainly outside collagen fibrils: predictions of a composite model for osteonal bone. J. Biomech. 29: 909-916

Piekaski K(1973) Analysis of bone as a composite material. Journal of Biomechanics 11: 557-565

Rho JY, Ashman RB, Turner CH (1993) Young's modulus of trabecular and cortical bone material: ultrasonic and microtensile measurements. J. Biomech. 26: 111-119

Rho JY, Tsui TY, Pharr GM (1997) Elastic properties of human cortical and trabecular lamellar bone measured by nanoindentation. Biomater. 18: 1325-1330

Rho JY, Kuhn-Spearing L, Zioupos P (1998) Mechanical properties and the hierarchical structure of bone. Medical Engineering and physics, 20: 92-102

Rho JY, Zioupos P, Currey JD, Pharr GM (1999a) Variations in the individual thick lamellar properties within osteons by nanoindentation. Bone 25: 295-300

Rho JY, Pharr GM (1999b) Effects of drying on the mechanical properties of bovine femur measured by nanoindentation. J. Mater. Sci. Mater. Med. 10: 485-488

Rho JY, Roy ME, Tsui TY, Pharr GM (1999c) Elastic properties of microstructural components of human bone tissue as measured by nanoindentation. J. Biomed. Mater. Res. 45: 48-54

Rho JY, Zioupos P, Currey JD, Pharr GM (2002) Microstructural elasticity and regional heterogeneity in aging human bone examined by nano-indentation. J. Biomech. 35: 161-165

Sasaki N, Ikawa T, Fukuda A (1991) Orientation of mineral in bovine bone and the anisotropic mechanical properties of plexform bone. J. Biomech. 24: 57-61

Siperko LM, Landis WJ (2001) Aspects of mineral structure in normally calcifying

avian tendon. J. Struct. Biol. 135: 313-320

Swandener JG, Rho JY, Pharr GM (2001) Anisotropic effects on elastic moduli measured by nanoindentation in human tibial cortical bone. J. Biomed. Mater. Res. 57: 108-112

Traub W, Arad T, Weiner S (1989) Three-dimensional ordered distribution of crystals in turkey in tendon collagen fibers. Proc. Natl. Acad. Sci. USA 86: 9822-6

Turner CH, Cowin SC (1988) Error induced by off-axis measurement of the elastic properties of bone. Journal of Biomechanical Engineering. 110: 213-215

Voigt, W.: Lehrbuch der Kristallphysik, Leipzig (1910)

Wagner HD, Weiner S (1992) On the relationship between the microstructure of bone and its mechanical stiffness. J. Biomech. 25: 1311-1320

Weiner S, Price P (1986) Disaggregation of bone into crystals. Calcif. Tissue Int. 39:365-375

Weiner S, Arad T, Traub W (1991) Crystal organization in rat bone lamellae. FEBS 285: 49-54

Weiner S, Traub W (1992) Bone structure: from angstroms to microns. FASEB 6: 879-885

Zysset PK, Guo XE, Hoffler CE, Moore KE, Goldstein SA (1999) Elastic modulus and hardness of cortical bone and trabecular bone lamellae measured by

nanoindentation in the human femur. Journal of Biomechanics 32: 1005-1012

Chapter 4

Ascenzi, A.; Bonucci, E.: The tensile properties of single osteons. Anatomical Record 158 (1967) 375-386

Ascenzi, A.; Bonucci, E.: The compressive properties of single osteons. Anat. Rec. 161 (1968) 377-391

Ascenzi, M.G.; Ascenzi, A.; Benvenuti, A.; Burghammer, M.; Panzavolta, S.; Bigi, A.: (2003) Structural differences between "dark" and "bright" isolated human osteonic lamellae. J. Struct. Biol. 141 (2003) 22-33

Burger, E.H.; Veldhuijzen, J.P.: Influence of mechanical factors on bone formation, resorption, and growth in vitro. In: Hall, BK (ed.), Bone vol.7, CRC Press, Boca Raton, Florida, 37–56. (1993)

Cheng, A.H.D: Material coefficients of anisotropic poroelasticity. Int. J. Rock. Mech. Min. Sci 34 (1997) 199-205

Cowin, S.C.; Moss-Salentijin, L.; Moss, M.L.: Candidates for the mechanosensory system in bone. Journal Biomechanical Engineering 113 (1991) 191-197

Cowin, S.C.; Mehrabadi, M.M.: Anisotropic symmetries of linear elasticity. Applied Mechanics Review 48; (1995) 247-285

Cowin, S.C.; Weinbaum, S.; Zeng, Y.: A case for bone canaliculi as the anatomical site of strain generated potentials. Journal of Biomechanics 28 (1995) 1281-1297

Cowin, S.C.: Remarks on the paper entitled "Fabric and elastic principal directions of cancellous bone are closely related," Journal of Biomechanics 30 (1997) 1191-1192

Cowin, S.C. Bone poroelasticity. Journal of Biomechanics 32 (1999) 217-238

Cowin, S.C.; Yang, G.; Mehrabadi, M.M.: Bounds on the effective anisotropic elastic constants. Journal of Elasticity 57; (1999) 1-24

Cowin, S.C., Moss, M.L.: Mechanosensory mechanisms in bone, In: Cowin SC (ed.), Bone mechanics handbook (2nd edition), CRC press (2001)

Cowin, S.C.: A recasting of anisotropic poroelasticity in matrices of tensor components. Transport in porous media 50 (2003) 35-56

Cowin, S.C.: Anisotropic poroelasticity: Fabric tensor formulation, Mechanics of Materials 36 (2004) 665-677

Crolet, J.M.; Aoubiza, B.; Meunier, A: Compact bone: numerical simulation of mechanical characteristics. J. Biomechanics 26 (1993) 677-687

Currey, J.D.: The relationship between the stiffness and the mineral content of bone. Journal of Biomechanics 2 (1969) 477-480

Detournay, E.; Cheng, A.D.H.: Fundamentals of poroelasticity. In: Hudson JA (Ed.),

Compressive Rock Engineering: Principles, Practices & Projects. Pergamon, Oxford (1993) 113-171

Gay, D.; Hoa S.V.; Tsai, S.W.: Composite Materials: Design and Applications, CRC Press. (2003)

Gibson, R.F.: Principles of composite material mechanics. McGraw-Hill, Inc. (1994)

Hashin, Z.; Shtrikman, S.: A variational approach to the theory of the elastic behavior of multiphase materials, J. Mech. Phys. Solids 11 (1963) 127

Hearmon, R.F.S.: An introduction to applied anisotropic elasticity. Oxford University Press, Oxford (1961)

Iwakuma, T.; Nemat-Nasser, S.: Composites with periodic microstructure. Computers and Structures 16 (1983) 13-19

Kelvin, Lord [W. Thompson] Elements of a mathematical theory of elasticity. Phil. Trans. R. Soc 166 (1856) 481-498

Manfredini, P.; Cocchetti, G.; Maier, G; Redaelli, A.; Montevecchi, F.M.: Poroelastic finite element analysis of a bone specimen under cyclic loading. Journal of Biomechanics 32 (1999) 135-144

Marotti, G., Muglia, M.A.: A scanning electron microscope study of human bony lamellae proposal for a new model of collagen lamellar organization. Archivio Italiano di Anatomia e di Embryologia 93 (1988) 163-175

Marotti, G.; Muglia, M.A.; Palumbo, C.: Collagen texture and osteocyte distribution in lamellar bone. It. J. Anat. Embryol. 100 (1995) 95-102

Martin, R.B.; Burr, D.B.; Sharkey, N.A.: Skeletal Tissue Mechanics, Springer-Verlag, New York (1998)

Nemat-Nasser, S.; Iwakuma, T.; Hejazi, M.: On composites with periodic structure. Mechanics of Materials 1 (1982) 239-267

Nemat-Nasser, S.; Hori, M.: Micromechanics: overall properties of heterogeneous materials. 2nd revised edition, Elsevier. (1999)

Odgaard,A.; Kabel, J.; van Rietbergen, B.; Dalstra, M.; Huiskes, R.: Fabric and elastic principal directions of cancellous bone are closely related. Journal of Biomechanics 30 (1997) 487-495

Piekarski, K.; Munro, M.: Transport mechanism operating between blood supply and osteocytes in long bones. Nature 269 (1977) 80–82.

Remaggi, F.; Cane, V.; Palumbo, C.; Ferretti, M.: Histomorphometric study on the osteocyte lacuno-canalicular network in animals of different species. I. Woven-fibered and parallel fibered bones. It. J. Anat. Embryol. 103 (1998) 145-155

Smit, T.H.; Hyughe, J.M.; Cowin, S.C.: Estimation of the poroelastic parameters of cortical bone. Journal of Biomechanics 35 (2002) 829-835

Thompson, M.; Willis, J.R.: A reformation of the equations of anisotropic

poroelasticity. Journal of Applied Mechanics 58; (1991) 612-616

Turner, C.H.; Chandran, A.; Pidaparti, R.M.V.: The anisotropy of osteonal bone and its ultrastructural implication. Bone17; (1995) 85-89

Voigt, W.: Lehrbuch der Kristallphysik, Leipzig (1910)

Wang, L.; Fritton, S.; Cowin, S.C.; Weinbaum, S.: Fluid pressure relaxation depends upon osteonal microstructure: modeling of an oscillatory bending experiment. Journal of Biomechanics 32: (1999) 663-672

Wang, L.; Cowin, S.C.; Weinbaum, S.; Fritton, S.: Modeling tracer transport in an osteon under cyclic loading. Annals of Biomedical Engineering 28 (2000) 1200-1209

Weinbaum, S.; Cowin, S.C.; Zeng, Y.: A model for the excitation of osteocytes by mechanical loading-induced bone fluid shear stresses, Journal of Biomechanics 27 (1994) 339-360

Weiner, S; Traub, W: Bone structure: from angstroms to microns. FASEB 6 (1992) 879-885

Williams, J.L.; Iannotti, J.P.; Ham, A.; Bleuit, J.; Chen, J.H.: Effects of fluid shear stress on bone cells. Biorheology 31 (1994) 163-170

Yoon, Y.J.; Yang, G.; Cowin, S.C.: Estimation of the effective transversely isotropic elastic constants of a material from known values of the material's orthotropic

elastic constants. Biomechan. Model. Mechanobiol 1 (2002) 83-93

Yoon, Y.J.; Cowin, S.C.: A calculation of elastic constants for the normal bone matrix. (in preparation)

You, J.; Yellowley, C.E.; Donahue, H.J.; Zhang, Y.; Chen, Q.; Jacobs, C.R.: Substrate deformation levels associated with routine physical activity are less stimulatory to bone cells relative to loading-induced oscillatory fluid flow. Journal of Biomechanical Engineering, 122 (2000) 387-393

You, L.; Cowin, S.C.; Schaffler, M.B.; Weinbaum, S.: A model for strain amplification in the actin cytoskeleton of osteocytes due to fluid drag on pericellular matrix. Journal of Biomechanics 34: (2001)1375-1386

Zeng, Y.; Cowin, S.C.; Weinbaum, S.: A fiber matrix model for fluid flow and streaming potentials in the canaliculi of an osteon. Annals of Biomedical Engineering, 22 (1994) 280-292

Zhang, D.; Cowin, S.C.: Oscillatory bending of a poroelastic beam. Journal of the Mechanics and Physics of Solids 42 (1994) 1575-1599

Zhang, D.; Cowin, S.C.: Load carrying capacity of the pore pressure in a poroelastic beam subject to oscillatory excitations. In: Selvaduri APS (Ed.), Mechanics of Poroelastic Media. Wolters Kluwer Academic Publishers, Solid Mechanics and its applications Series 35: (1996) 273-298

Zhang, D.; Weinbaum, S.; Cowin, S.C.: Estimates of the peak pressure in bone pore water. Journal of Biomechanical Engineering 120 (1998) 697-703

Chapter 5

Ashman RB, Cowin SC., Van Buskirk WC, Rice JC (1984) A continuous wave technique for the measurement of the elastic properties of cortical bone. Journal of Biomechanics 17: 349-361

Cowin, SC, Sadegh AM (1991) Non-interacting modes for stress, strain and energy in hard tissue. Journal of Biomechanics 24: 859-867

Cowin SC, Mehrabadi MM (1995) Anisotropic symmetries of linear elasticity. Applied Mechanics Review 48: 247-285

Cowin SC, Yang G, Mehrabadi MM (1999) Bounds on the effective anisotropic elastic constants. Journal of Elasticity 57: 1-24

Cowin SC (1999) Bone Poroelasticity. Journal of Biomechanics 32: 218-238

Hearmon RFS (1946) The elastic constants of anisotropic materials. Rev. Mod. Phys. 18: 409-440

Hearmon RFS (1948) The elasticity of wood and plywood. Forest Products Research Special Report #9, Dept. Sci. Inds. Res., HMSO, London

Hearmon RFS (1961) An Introduction to Applied anisotropic Elasticity. Oxford

University Press, Oxford

Hill R (1952) The elastic behavior of crystalline aggregate. Proceedings of the Physical Society, *London* A65: 349-354

Hill R (1963) Elastic properties of reinforced solids: some theoretical principles, Journal of the Mechanics and Physics of Solids 11: 357-372

Kabel J, van Bietbergen B, Dalstra M, Odgaard A, Huiskes R (1999a) The role of an effective isotropic tissue modulus in the elastic properties of cancellous bone. Journal of Biomechanics 32: 673-680

Kabel J, van Rietbergen B, Odgaard A, Huiskes R (1999b) Constitutive relationships of fabric, density, and elastic properties in cancellous bone architecture. Bone 25: 481-486

Mehrabadi MM, Cowin SC (1990) Eigentensors of linear anisotropic elastic materials. Quart J. Mech. Appl. Math. 43: 15-41

Reuss A (1929) Berechnung der Fließgrenze von Mischkristallen auf Grund der Plastizitätsbedingung für Einkristalle. *ZAMM* 9: 49-58

Smit TH, Huyghe JM and Cowin SC, A double poroelastic model of cortical bone: estimation of the linear isotropic parameters, Journal of Biomechanics: *in press*

van Buskirk WC, Ashman RB (1981) The elastic moduli of bone. In: Cowin SC (ed.) The Mechanical Properties of Bone. ASME AMD 45: 131-143

van Rietbergen B, Odgaard A, Kabel J, Huiskes R (1996) Direct mechanical assessment of elastic symmetries and properties of trabecular bone architecture. Journal of Biomechanics 29: 1653-1657

van Rietbergen B, Odgaard A, Kabel J, Huiskes R (1998) Relationships between bone morphology and bone elastic properties can be accurately quantified using high-resolution computer reconstructions. Journal of Orthopaedic Research 16: 23-28

Voigt W (1928) Lehrbuch der Kristallphysik. Teubner

Yang G, Kabel J, van Bietbergen. B, Odgaard A, Huiskes R, Cowin SC (1999) The anisotropic Hooke's law for cancellous bone and wood. Journal of Elasticity 53:125-146

Chapter 6

Ascenzi A, Improta S, Portigliatti Barbos, Carando S, Boyde A (1987) Distribution of lamellae in human femoral shafts deformed by bending with interfaces on mechanical properties. Bone 8: 319-325

Cowin SC (1999) Bone Poroelasticity. Journal of Biomechanics 32: 218-238

Hill R (1965) Theory of mechanical properties of fibre-strengthened materials III. Self-consistent model. J. Mech. Phys. Solids. 13: 189-198

Suvorov AP, Dvorak GJ (2002) Rate form of the Eshelby and Hill tensors. International Journal of Solids and Structures 39: 5659-5678